An investigation of the iron-cyanide mineralization in gold mine dumps

by

MD Welman-Purchase

2005115189

Submitted in Fulfilment of the

Requirements for a Degree in

Ph.D. Geochemistry

under the supervision of

Dr. RN Hansen

Department of Geology

University of the Free State

Bloemfontein

Nov 2022

Declaration

I, MD Welman-Purchase, declare that this document is my own work, that it has not been submitted for any degree or examination in any other university, and that all the sources I have used or quoted have been indicated and acknowledged by complete reference.

MD Welman Purchase

2005115189

Acknowledgements

“It is our choices that show what we truly are, far more than our abilities”

Albus Percival Wulfric Brian Dumbledore

First of all, the author would like to thank God for always supplying the answers to my questions and her spouse, Jani, especially for the support and patience through this roller coaster.

Thank you to her supervisor, Dr. Robert Hansen, for great guidance and for sharing his passion for this science. Marike Stander, soon to be a Ph.D. holder, for the moral support and walking with the author through this journey.

Financial support was supplied by Iphakade and the CMBG – Biogrip, for which the author is very grateful.

Thank you to Liesl van der Westhuizen for assisting in the submission of my papers to journals and the moral support connected to it.

Abstract

Cyanide, in the form of NaCN/KCN, is still widely used world-wide in the gold extraction process. Success of this extraction is owed to the high affinity that cyanide has for gold. Post extraction, waste material is added to tailings dam facilities in the form of a slurry. This slurry is likely to contain cyanide, which is hazardous if it is not managed. Another element that cyanide has a high affinity for, is iron. Iron-cyanide compounds (such as Prussian and Turnbull's blue) are CN_{SAD} (strong acid dissociable cyanide), meaning that they are stable compounds that only dissociate at pH conditions that are very low (<1). UV-radiation also dissociates these compounds. The potential determination of iron-cyanide compounds to form in the environment and their subsequent dissociation, is an area that requires more investigation.

The main aims of the study include the modelling of Prussian/Turnbull's blue in the goldmine tailings environment. To determine in a lab investigation whether or not iron-cyanide are able to form in different samples associated with such environments. Different analysis of the different samples and the analysis of a blue sample found on a tailings dam close to Welkom. Further modelling the affects that pH and the presence of other complexes has on the production of Prussian blue. The last aim was to determine if there are bacteria present that are able to degrade cyanide.

The research approach consisted of two branches, namely modelling and the analysis of samples. Modelling was preformed using PHREEQC. The samples mentioned in this research consist of two branches, namely the laboratory study of adding cyanide to different samples and analysing them, and analysing tailings samples. Methods used in the laborarory study include XRD, FT-IR, XPS and total cyanide analysis. 9 samples were collected from a tailings dam close to Welkom, which forms apart of the Free State goldfields. XRF, ICP-OES, total cyanide, CNS analyzer (LECO) and metagenome analysis were performed on these samples.

The main findings show that Prussian and Turnbull's blue are able to form in such tailings environments. Prussian blue forms in an oxic environment and Turnbull's blue forms in both an oxic and anoxic environment. The main variables that affect the formation of these iron-cyanide compounds is oxygen, the pH and concentrations of cyanide and iron available in solution. A NaCN solution was added to a pyrite sample, a Witwatersrand reference material and a tailings sample, where pyrite and the

Witwatersrand reference material produced a blue substance. The analysis of these two samples and a blue sample from a tailings dam were analysed with FT-IR, revealing the presence of an iron-cyanide bond. The cyanide concentrations of the 9 tailings samples ranged from 0.6 – 10 ppm, where the highest concentration was found in a sample containing a blue substance (2.1) and the lowest is deeper into the tailings below the blue sample (2.3), suggesting that iron-cyanide compounds/complexes immobilize cyanide. The metagenome analysis revealed that the naturally occurring bacteria in the tailings are able to degrade or assimilate cyanide in the oligotrophic tailings environment. Cyanide is a source of carbon for the bacteria and an energy source.

In conclusion, iron-cyanide compounds/complexes are able to form in the goldmine tailings environment, where a blue sample from a tailings dam was analysed and determined to be an iron-cyanide compound. It was also determined that these compounds/complexes immobilize cyanide, which are naturally degraded by the bacteria on the tailings dam. Ultimately, geochemical risk assessments for mining projects may benefit from including a microbiological aspect, which has not previously been considered.

It is recommended that the following options be followed for remediation of cyanide:

1) The addition of an iron-source for iron-cyanide formation, immobilizing the cyanide
2) Burial of the material, possible burial in a mine void (anoxic environments result in higher pH conditions and zero UV radiation) or the addition of a pH buffer e.g., dolomite
3) Determine which microbes are present in the environment
4) Nurture the bacteria colonies, if found to be necessary

Contents

List of figures

List of tables

Chapter 1 - Introduction

Cyanide, that consists of a carbon and a nitrogen ion, is used in numerous industries (plastics, photography, mining/ metallurgy, electroplating, paints, agriculture, textile, medicine and food industries) as a crucial raw material (Kuyucak and Akcil, 2003). In the metallurgical industry, cyanide is used due to its high affinity for metals such as gold and silver, where cyanide selectively leaches the mentioned metals from their ores (Kuyucak and Akcil, 2003).

Gold in South Africa is mostly mined from the Witwatersrand Supergroup, in Gauteng and the Free State. The gold is found in sedimentary sequences associated with pyrite and carbon-rich layers (Tucker et al., 2016). The extraction of the gold from their host rocks involves the cyanidation process (known as the Elsner equation), which used a solution of NaCN/KCN to leach the gold from crushed ore, producing a gold-cyanide compound (Kyle, 1997) ("compound" is used in this thesis to describe precipitates, and "complex" used to describe aqueous complexes). The gold is then released from the cyanide and attaches to activated carbon in the Carbon-In-Pulp (CIP) process. Gold is then precipitated, producing ingots after the Merrill-Crowe process/electrowinning (Acheampong et al., 2010).

Cyanide used in this extraction process can be recycled and reused in the cyanidation process, but cyanide has been found on the gold tailings dams with the waste material (Bakatula and Tutu, 2016). The presence of cyanide in tailings dams and cyanide speciation has been previously studied (Donato et al., 2007; Bakatula and Tutu, 2016; Anning et al., 2019; Dong et al., 2021; among others). Where the results revealed that cyanide is in the tailings material and in the run-off water sources, including in the South Africa, mostly in the Central, East and West rand gold fields, at concentrations of <200 $mg.kg^{-1}$ (Bakatula and Tutu, 2016). Speciation of the cyanide compounds include free cyanide/volatile hydrogen cyanide (HCN and CN-), simple inorganic salts/readily soluble cyanide (KCN, NaCN), weak acid dissociable cyanide (CN_{WAD} – cyanide bonded to nickel, copper, zinc and cadmium) and strong acid dissociable cyanide (CN_{SAD} – cyanide bonded to silver, gold, cobalt and iron), thiocyanate (SCN^-), cyanates (OCN^-) and organic cyanides (cyanohydrins and nitriles) (Zagury et al., 2004; Baxter and Cummings, 2006; Kumar et al., 2013, Luque-Almagro et al., 2016).

Iron-cyanide compounds (CN_{SAD} type compounds) are the most stable of the compounds, where Prussian and Turnbull's blue are examples of CN_{SAD} compounds. Precipitating iron-cyanide compounds can possibly be an in-situ treatment preventing cyanide from contaminating groundwater reservoirs and the migration of cyanide into the surrounding environment (Ghosh et al., 1999). The proposal by Kyle (1997) involved the dissolution of CN_{WAD} compounds, followed by the addition of an $FeSO_4$ solution to promote the precipitation of the cyanide as Prussian blue.

There are numerous methods that have been explored to remediate cyanide, one being the production of an iron-cyanide compounds, mentioned above. Other methods include natural remediation, chemical remediation and biological remediation. Natural remediation, involves the disposal of the waste material and believing that the cyanide will degrade naturally, not affecting the environment (Bakatula and Tutu, 2016). It includes volatilization, photo-degradation, hydrolysis, chemical/bacterial oxidation, dissociation of cyanide, producing cyanate (Misra et al., 2003). Chemical remediation involves the addition of chemicals to cyanide waste to produce less toxic compounds (Anning et al., 2019). This remediation process incurs additional costs and as such are not the most popular. Biological remediation involves the determination of microorganisms in a tailings dam and adding or promoting the reproduction of microorganisms that are able to degrade cyanide. Where some bacteria are able to use cyanide as a nitrogen and/or carbon requiring no further nutrition (Razanamahandry et al., 2017).

This study delves into the modelling and production of Prussian and Turnbull's blue, the conditions that they are stable in have been studied previously, yet not specifically in a gold tailings environment. An empirical study will also be employed where a cyanide solution will be added to different materials and the production of reference iron-cyanide compounds to use for comparison purposes. Finally, metagenome analysis on tailings samples will be completed in order to determine the indigenous bacteria that occur on the tailings dams and the possibility for the bacteria present to degrade cyanide.

Chapter 2 – Thesis outline

This thesis is an article-based thesis, including 4 articles. The aims and objective investigated in this thesis are displayed in Table 2.1. Included in Table 2.1 is the journal of submission.

Table 2.1: The aims and objectives of this study. Included is the Journal, current status and authors contributions.

Aim	Objective	Chapter	Journal for submission	Status of the submission	Contribution of authors
Investigate the formation and the behaviour of Prussian and Turnbull's blue in a gold tailings dam environment.	By using PHREEQC modelling software, this project explores the possibility for Prussian and Turnbull's blue to form in a goldmine tailings environment. Additionally altering parameters to see how the precipitation of the two complexes' is affected.	6	Environmental Pollution	Accepted 2023	Megan Welman-Purchase: conceptualization, visualization, data curation, investigation, writing the original draft; Robert Hansen: conceptualization, writing in terms of review and editing, supervision
Reconstruction of pH vs Eh diagrams with varying cyanide and iron concentrations. Comparing it to previous studies	Production of pH vs pE diagrams using PREEPLOT	7	Environmental Processes	Submitted	Megan Welman-Purchase: conceptualization, methodology, formal analysis, investigation, data curation, writing the original draft; Robert Hansen: conceptualization, validation, methodology, resources, writing in terms of review and editing, supervision
An empirical study on lab grown Prussian and Turnbull's blue complexes. Exploring the ability for them to form in different samples.	Producing a reference material by mixing the chemicals required to produce Prussian and Turnbull's blue. Adding cyanide to other samples such as a gold ore sample, pyrite and tailings samples to observe if a blue substance (Prussian and Turnbull's blue) will form. The analysis of the different samples using different methods.	7			
Discuss the possibility of Prussian or Turnbull's blue to be used as a remediation solution for cyanide contamination.	Involve the search for a blue sample (Prussian or Turnbull's blue) on a gold mine tailings dam in the Free State goldfields. Analysing the cyanide content of it and the surrounding material.	7			
Determine which iron complexes had an affect on the formation of Prussian /Turnbull's blue at different pH conditions	This involved PHREEQC modelling	8	IMWA conference	Submitted and accepted for IMWA 2022, due to visa constrains, will be presented at IMWA 2023	Megan Welman-Purchase: conceptualization, visualization, data curation, investigation, writing the original draft; Robert Hansen: conceptualization, writing in terms of review and editing, supervision
Determine the microbial diversity of goldmine tailings dam as well as their metabolisms to determine if natural bioremediation of cyanide may occur.	Metagenomic data will be obtained from tailings sediment samples. Investigating the microbes and metabolisms that are present in the samples.	9	Science of the Total Environment	Submitted	Megan Welman-Purchase: Sample collection, DNA extraction, pH and Eh analysis, SO_3 analysis, writing of the article; Julio Castillo Hernandez: assisted with the interpretation of the metagenomic results; A Matu: assisted with DNA extraction; A Gomez-Arias: analysis - bioavailable chemical; RN Hansen: supervision

Chapter 3 - Literature review

3.1 Cyanide

Cyanide is a cyano-moiety, consisting of a carbon atom that is triple bonded to a nitrogen atom (C≡N) (Dzombak et al., 2006). It occurs in the environment in many forms, occurring naturally in sources such as plants (over 2000 variants) as cyanogenic glycoside or produced for and in anthropogenic processes such as mining, sewage, fires, tobacco smoke and exhaust gas from vehicles (Jaszczak et al., 2017) (Figure 3.1). The natural sources (cyanogenic glycoside) are generally derived from amino acids, which are used as a defence mechanism in plants (Nyirenda, 2020). These natural sources are most often non-problematic, unless poorly processed that results in the presence of HCN in the plant (Nyirenda, 2020). The anthropogenic sources have the potential to increase the cyanide concentration in water and soil surrounding environment (Mansfeldt and Höhener, 2016). The presence of cyanide in soil and water is most often from an anthropogenic source (Dzombak et al., 2006; Anning et al., 2019), where numerous active and decommissioned mines' tailings dams contain cyanide (Anning et al., 2019).

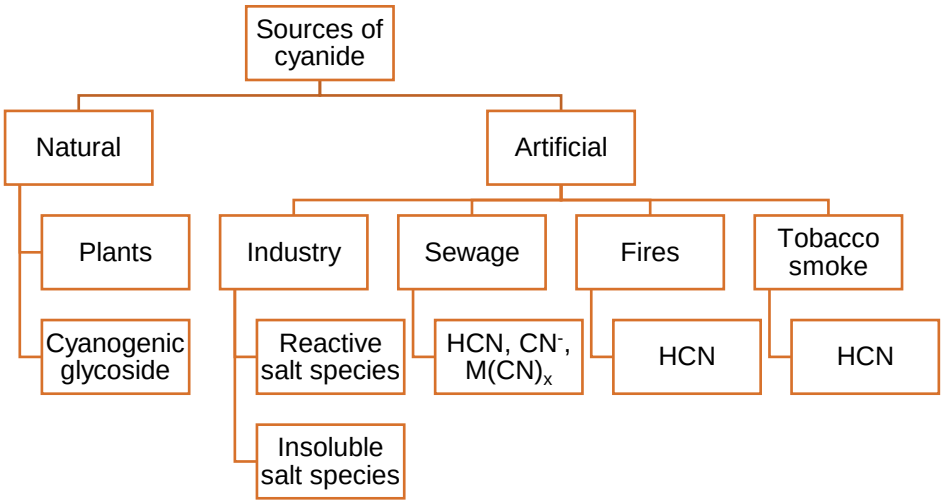

Figure 3.1: Graphical display of the different sources of cyanide (taken from Jaszczak et al., 2017). This diagram also displays the forms in which the cyanide occurs in each of the sources.

3.2 Uses of cyanide

The benefits of the usage of cyanide are numerous and cyanide products are safely used worldwide daily by a large amount of people and industries (Mudder and Botz,

2004). These uses include processes and products such as metal extraction, pesticides, electroplating, metal hardening, printing, photography, dyeing, cosmetics, computer electronics, adhesives, plexiglass, paints, road and table salts, rocket propellant, pharmaceuticals, among others (Razanamahandry et al., 2017, Mudder and Botz, 2004). Approximately 1.1 million tons of HCN is produced worldwide every year, of which 50% is used in the production of different organic chemicals (Mudder and Botz, 2004), namely acrylic plastics, nitrile and nylon (Akcil, 2003). $K_4Fe(CN)_6$ and $Na_4Fe(CN)_6$, at concentrations of less than 200 $mg.kg^{-1}$, is used in road salts as an anti-caking agent facilitating the distribution process (Razanamahandry et al., 2017). Cyanide has also been used in chemical warfare, such as in World War I by the French and in the Holocaust in World War II to execute criminals and innocents alike (Razanamahandry et al., 2017).

Only 6 % of all production of cyanide is used in the mining industry (Mudder and Botz, 2004). An example of such a mining industry is in the extraction of gold, where KCN or NaCN, or a combination of these compounds, are used (Bakatula and Tutu, 2016). This is an effective process, as cyanide has the ability to form an extremely strong complex with heavy metals, in this case gold (Wang and Forssberg, 1990). The process of extraction follows the Elsner equation (also referred to as the alkaline cyanidation process) coupled with processes such as carbon-in-pulp, the Merrill-Crowe process/electrowinning and resin-in-pulp, which will be discussed in detail later in this thesis. These processes use large amounts of cyanide, which amount to approximately a ratio of one part gold to six parts NaCN/KCN. Although there is an option to recycle the cyanide into the extraction process, this is not always possible as the cyanide may form a part of the solid and liquid residues that are disposed of onto the tailings dams.

3.3 Classes of cyanide

CN^- solutions can be fairly complex, as cyanide has the ability to form a number of complexes (Smith and Struhsacker, 1988). Cyanide compounds/complexes in goldmine effluents are classified into four classes, namely free cyanide (HCN and CN^-), readily soluble cyanide (simple inorganic salts - $Ca(CN)_2$, KCN and NaCN), weak acid dissociable cyanides (referred to as CN_{WAD} – compounds of cyanide and transition metals cadmium, copper, nickel, zinc) and strong acid dissociable cyanide

(referred to as CN_{SAD} – compounds cyanide and iron, copper, silver and gold) (Zagury et al., 2004). CN_{WAD} are moderately unstable compounds and tend to dissociate in neutral to slightly acidic conditions, forming CN^- and whichever metal present in the compound (Zagury et al., 2004). CN_{SAD} are relatively stable, dissociating only in the utmost acidic conditions. All compounds/species/forms can be found in Figure 3.2. In the interest of this study, it is important to note that if an environment is iron-rich, the cyanide tends to form iron-cyanide complexes (Zagury et al., 2004).

3.4 Cyanide toxicity

Cyanide does not accumulate in the body but its hazardous nature originates from its high attraction to iron, which is present in blood (Alvillo-Rivera et al., 2021). Exposure to cyanide via inhalation, oral or dermatological contact results in the inability for cells to uptake O_2 (causing hypoxia), thus respiration does not occur (Anning et al., 2019). Most other animals are vulnerable to cyanide poisoning, including reptiles, mammals, amphibians, waterfowl, migratory birds and aquatic animals (Mudder and Botz, 2004). These animals can be exposed to cyanide when they interact with waste facilities of industries that make use of cyanide in their production line, disposing of waste onto waste/tailings dams (Donato et al., 2017). An example where cyanide had an effect on animals, involved the death of ~9500 animals (amphibians, birds, mammals and reptiles) between 1986 and 1991 originating from a goldmine tailings after exposure to elevated concentrations of cyanide (Henny et al., 1994).

Cyanide has an adverse effect on aquatic life in aquatic environments when precautions are not executed to control cyanide exposure (Eisler, 1991; Henny et al., 1994; Eisler, 2000; Anning et al., 2019). Fish are highly vulnerable to cyanide poisoning (Anning et al., 2019), where exposure to concentrations of 1 – 50 $mg.L^{-1}$ can cause damage to kidneys, liver and their brain tissue (Rubec and Soundararajan, 1990). Exposure to concentrations from 5 – 7.2 $\mu g.L^{-1}$ have an effect on the fertility and mobility of fish (Eisler, 1991; Eisler, 2000).

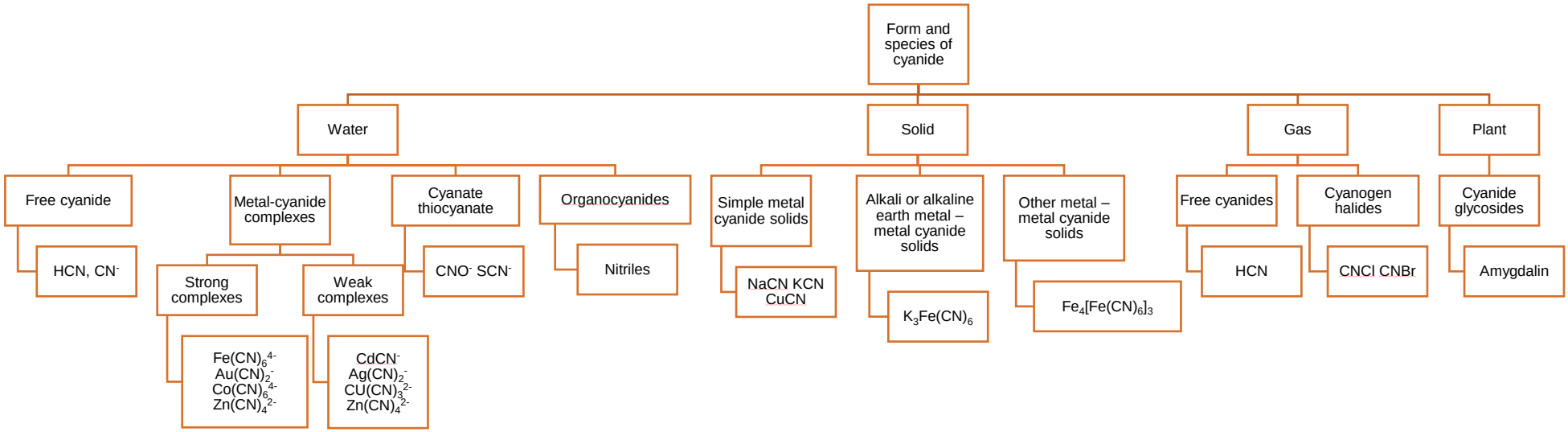

Figure 3.2: Diagram displaying the various species that cyanide may occur in and their states (modified after Jaszczak et al., 2017).

3.5 Cyanide concentrations and speciation in environments of interest

Bakatula and Tutu (2016) conducted a study on the tailings environment in the Nasrec area of the Central Rand goldfields. They analysed the cyanide content in water samples, crusts on the water and algae samples. The results are displayed in Table 3.1. From this study, it can be observed that cyanide is present in the tailings dam environment and that the concentrations are above that which is required by regulations (Department of Health – South Africa: 0.07 $mg.L^{-1}$).

Table 3.1: Cyanide results from Bakatula and Tutu (2016), from a tailings dam in Central Rand goldfields.

Sample type	CN_{free} ($mg.L^{-1}$)	CN_{WAD} ($mg.L^{-1}$)	CN_{SAD} ($mg.L^{-1}$)	CN_T ($mg.L^{-1}$)	SCN^- ($mg.L^{-1}$)	CNO^- ($mg.L^{-1}$)
Water	7.18	13.17	4.19	24.54	97.43	112.35
Crust	15.73	85.92	96.75	198.4	247.9	333.2
Algae	10.45	14.24	0.47	25.16	213.4	301.6

Figure 3.3 is a representation of the different cyanide species and the natural degradation or attenuation of the species in the tailings dam environment (Smith and Mudder, 1991). Within the Figure 3.3, it can be observed that there are numerous geochemical, chemical and biochemical reactions within this cycle (Smith and Mudder, 1991). Only 20 % of the HCN in the tailings dam environment is present in the gaseous phase, due to the boiling point of HCN being 27 °C (Kyoseva et al., 2009). Resulting in the presence of both CN^- and HCN in the system. Note that some of the reactions are reversable and will favour the reaction depending on the conditions of the environment. In the tailings pond, volatilisation of cyanide into the atmosphere is the greatest mechanism by which cyanide is removed from aqueous solution (cannot be reversed) (Smith and Mudder, 1991). Complexes of cyanide may form in the tailings ponds, where the reactions are reversible, remain in solution (Huiatt et al., 1983). Although ferro- and ferricyanides are able to adsorb onto sediments and soils (Theis and West, 1986).

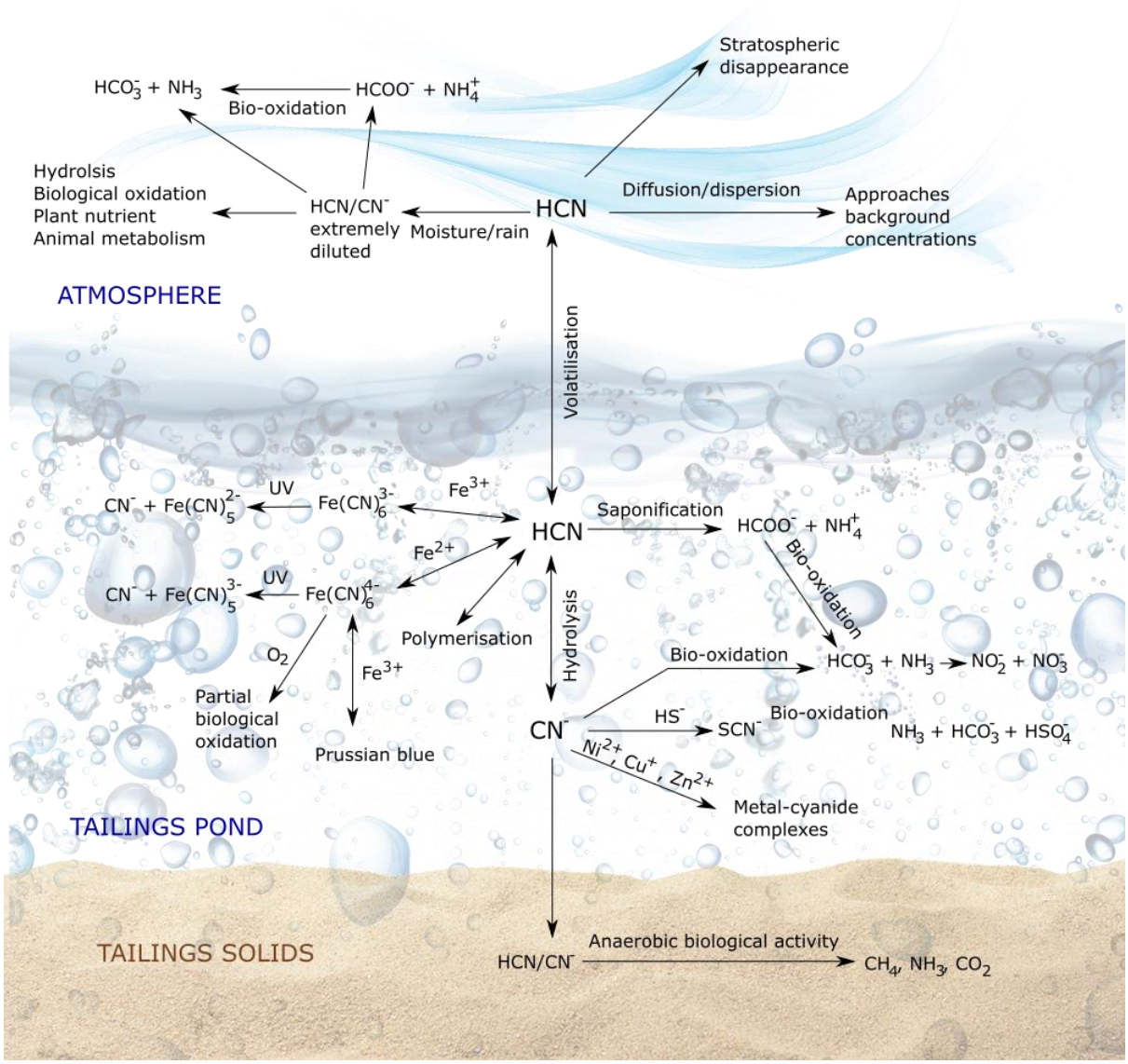

Figure 3.3: The life cycle of different cyanides. The natural processes of cyanide degradation.

3.6 Prussian blue and other iron-cyanide compounds

Prussian and Turnbull's blue are blue pigments consisting of iron and cyanide. In gas purifying and coke ovens, blast furnace waste, road salts, waste from the production of aluminium, NaCN used in gold and silver extraction, NaCN and KCN used for electroplating (and more) may produce Prussian blue (Mansfeldt and Höhener, 2016). In soils, the anthropogenic presence of CN^- from the metallurgical industrial forms iron-cyanide compounds (Jaszczak et al., 2017). The compounds are typically as the aqueous complexes $Fe(CN)_6^{4-}$ and $Fe(CN)_6^{3-}$ (Jaszczak et al., 2017) which have a high probability to attach to other metals in the environment. Prussian blue forms when

Fe^{3+} reacts with $[Fe(CN)_6^{4-}]$, forming Fe^{3+}/Fe^{2+}-cyanide compounds (Bakatula and Tutu, 2016). According to Ghosh et al. (1999), depending on the pH and Eh condition of the system, the Fe^{2+} and Fe^{3+} may switch positions in the crystal structure and form Turnbull's blue. Prussian blue forms according to equations 1 and 2 and Turnbull's blue according to equation 3 (Ghosh et al., 1999).

$$4Fe^{3+} + 3Fe(CN)_6^{4-} \leftrightarrow Fe_4[Fe(CN)_6]_3(s) \quad (1)$$

$$3Fe^{2+} + Fe^{3+} + 3Fe(CN)_6^{3-} \leftrightarrow Fe_4[Fe(CN)_6]_3(s) \quad (2)$$

$$3Fe^{2+} + 2Fe(CN)_6^{3-} \leftrightarrow Fe_3[Fe(CN)_6]_2(s) \quad (3)$$

Other iron-cyanide compounds include Berlin white ($Fe_2[Fe(CN)_6]$), which alters to Prussian blue in an oxic environment and Prussian brown/Berlin green, where the colour can vary from brown (more Fe^{3+}-rich) to green depending on the Fe^{2+} to Fe^{3+} ratio (Ghosh et al., 1999a). Both Berlin white and Prussian brown/Berlin green alter to a blue product over time. Thus, the two stable iron-cyanide compounds (in solid form) are Prussian blue and Turnbull's blue (Ghosh et al., 1999a).

Prussian blue has previously been found in gold mine tailings or the surrounding areas. Bakatula and Tutu (2016), completed a study on cyanide in a tailings dam of the Central Rand goldfields, where a bluish-green colour crust was found, believed to be Prussian blue. Jambor et al. (2009) completed studies on the Balmer lake in Canada, which is a source for gold mining discharge, finding the presence of a blueish green material where X-Ray Diffraction (XRD) determined that it was Prussian blue. These studies determined that other (excluding the blue samples) soil and water samples from the tailings dams contain between 0 and 1300 $mg.kg^{-1}$ total cyanide concentrations.

3.7 Cyanide remediation

Cyanide polluting the environment can be avoided by treating the waste prior to discharge onto tailings dams (Monsser and Adhoum, 2002; Acheampong et al., 2010). Numerous cyanide detoxification methods for slurries and solutions have been documented (Acheampong et al., 2010; Akcil, 2003; Akcil et al., 2003; Anning et al., 2019; Botz, 2001; Botz et al., 2005). The motivation for these processes can be considered as either for destructive purposes or recovery purposes and are classified

into natural, chemical and biological remediation (Anning et al., 2019). The process used for detoxification is dependent on the concentration of cyanide in slurries or solution (Demopoulos and Cheng, 2004). The different methods are mentioned below.

3.7.1 Natural remediation

A portion of the gold mining industry suggest that the cyanide in the tailings dams degrade naturally and thus cannot affect the environment (Bakatula and Tutu, 2016). The natural degradation involves the processes, volatilization, photo-degradation, hydrolysis, chemical/bacterial oxidation, dissociation, and the conversion of cyanide to cyanate (Misra et al., 2003) and involves the deposition of waste water and slurries into a tailings storage facility (Botz et al., 2005; Anning et al., 2019). One of the advantages of this is that it incurs no additional funds, but the cyanide is able combine with metals forming metal cyanides. The disadvantage to letting the cyanide in tailings naturally degrade, is that the cyanide has the potential through seepage to contaminate the groundwater before the natural degradation occurs (Acheampong et al., 2010).

3.7.2 Chemical remediation

All chemical equations involved in chemical remediation of cyanide have been summarised in Table 3.2. The volatilization method occurs naturally, as cyanide volatilizes to HCN when the pH decreases below 9 (Anning et al., 2019).

Alkaline chlorination along with oxygen, can successfully remove cyanide in the system to an acceptable limit (Acheampong et al., 2010). This process consists of two stages, seen in Table 3.2, where the first stage involves the production of CNCl and the second involves the hydrolysis of CNCl to cyanate (Anning et al., 2019). An additional step involves the continued hydrolysis of OCN^- in an alkaline pH, producing ammonium (Anning et al., 2019). During the process of chlorination, toxic compounds may form intermittently such as CNCl, other organo-chlorines and the remaining chlorine, producing a sludge, which may create additional environmental issues (Acheampong et al., 2010). The other disadvantage to this method is it is moderately expensive.

The ozonation process involves adding ozone to the cyanide-rich waste. This is due to the concept that ozone is a strong oxidizing agent, thus having the ability to oxidize

free cyanide and CN_{WAD} to cyanate (OCN^-), NH_3 and NO_3 (Carillo-Pedroza and Soria-Aguilar, 2001). A catalyst is not required as the reaction is rapid and is only limited by the absorption rate of ozone into solution (Botz et al., 2005). Ozone is generally expensive to produce and is better applied to smaller volumes to recover the cyanide (Botz et al., 2005).

The sulphur dioxide and air process was developed by INCO limited in the 1980's (Anning et al., 2019), which according to Botz et al. (2005), is used by over 30 mining operations, worldwide, to assist in prevention of contaminating the environment with cyanide. This process makes use of the chemicals, SO_2, O_2 and a soluble Cu^{2+} (usually $CuSO_4.5H_2O$) catalyst, to oxidize cyanide to OCN^-, which is less harmful (Acheampong et al., 2010). In alkaline pH conditions, 3.5 - 5.0 g SO_2 is required to oxidize a gram of cyanide, where the forms of SO_2 can be one of the following, compressed liquid SO_2, a sulfur salt (such as $Na_2S_2O_5$), Na_2SO_3 or NH_4HSO_3 (Botz et al., 2005). A concentration of 50 $mg.L^{-1}$ of the Cu^{2+} catalyst is added in order to accelerate the chemical reaction (Anning et al., 2019). The mixing of all chemicals occurs in a tank, where lime is added to neutralize acidity, as H_2SO_4 is a by-product of the reaction (see Table 3.2) (Botz et al. 2005). Metals (such as copper, zinc and nickel) that are complexed with cyanide, precipitate as metal-hydroxides and iron-cyanide complexes precipitate copper-iron-cyanide compounds and the process doesn't decrease thiocyanate concentrations below the legislation limits (Botz et al., 2005). This process is effective and profitable for the treatment of cyanide waste below 200 ppm (CN_{WAD}) (Demopoulos and Cheng, 2004),

The hydrogen peroxide treatment process, is similar to the INCO/sulfur dioxide process, except H_2O_2 is the chemical used instead of SO_2/air (Acheampong et al., 2010). Soluble copper as $CuSO_4.5H_2O$ (Botz et al., 2005) is added as a catalyst, producing OCN^-, equations are displayed in Table 3.2 (Ackil, 2003). This process effectively oxidizes free cyanide complexes and CN_{WAD} compounds, where iron-cyanide compounds precipitate as insoluble copper-iron-cyanide compounds (Botz et al., 2005). This process is applicable over wide pH conditions, to create effluents suitable for discharge (Akcil, 2005), without increasing the TDS (Total Dissolved Solids) of the effluent (Botz et al., 2005). 50 to 70 % concentration of liquid H_2O_2 in quantities of 2 to 8 g is needed to oxidize a gram of cyanide (Botz et al., 2005). The

constant presence of H_2O_2 will eventually result in the dissociation of cyanide to CO_2 and NO_3 (see Table 3.2). Similar studies involved the addition of H_2O_2 along with $Ca(OCl)_2$ to the waste water to ensure that the cyanide content is within appropriate limits before discarding (Muntasir et al., 2016). The study showed that at a pH of 8, the cyanide was removed, using a ratio of 1:1 of H_2O_2 and $Ca(OCl)_2$ (Anning et al., 2019). This will unfortunately introduce extra total dissolved salts (TDS) and chlorine to the system, thus also potentially adding it to the natural systems.

The CARO acid process, involves the usage of H_2SO_5 (known as Caro's acid), which is produced on site as it is not stable by reacting 1:1.5-3 mols of 70 % H_2O_2 to 98 % H_2SO_4, while controlling the temperature of the reaction (Norcross, 1996). This process does not require a catalyst. Acid may be produced which is generally neutralized with lime (not always necessary) and the pH is kept at a range of ~7-10 (Botz et al., 2005). This process is best for tailings slurries that initially contain low-moderate levels of cyanide and that require a product of concentrations of 10-50 $mg.L^{-1}$ (Botz et al., 2005).

A possible detoxification option of cyanide (Prussian blue method in Table 3.2) involves the oxidation of free cyanide to cyanate in order to dissociate weak and moderately strong cyanide compound (including zinc, copper and silver compounds) (Kyle, 1997). The goal is then to precipitate the metals as hydroxides and to form CN_{SAD} compounds, specifically iron-cyanide compounds. Alternatively, cyanide can be precipitated by adding $FeSO_4$ to the solution, forming iron-cyanide compounds. The precipitation of iron-cyanide compounds can potentially be an in-situ treatment for the contamination of cyanide in groundwater, preventing the migration of cyanide in this environment (Ghosh et al., 1999).

The issue with producing iron-cyanide compounds to remediate cyanide, is although they have a low toxicity, when exposed to light they decompose into toxic components, such as free cyanide (Jaszczak et al., 2017). This decomposition is shown in equations 4 and 5 (Jaszczak et al., 2017). Where equation 4 represents the decomposition of ferrocyanide to ferricyanide.

$$Fe(CN)_6^{4-} + UV - radiation \rightarrow Fe(CN)_6^{3-} + e^- \quad (4)$$

$$Fe(CN)_6^{3-} + 6H_2O + 3H^+ \rightarrow Fe(OH)_3 + 6HCN(aq) \quad (5)$$

Using iron-cyanide production as a remediation process has a few environmental drawbacks, including the production of cyanide waste products and stable iron-cyanide compounds that may remain stable for many years (Botz et al., 2005).

Table 3.2: Summary of the different chemical remediation methods.

Method	Reactions	Disadvantage
Volatilization	$HCN \leftrightarrow H^+ + CN^-$	Toxic product.
Alkaline chlorination	$CN^- + Cl_2 \rightarrow CNCl + Cl^-$ $CNCl + H_2O \rightarrow OCN^- + 2H^+ + Cl^-$ $OCN^- + 3H_2O \rightarrow NH_4^+ + HCO_3^- + OH^-$	Additional chemicals produced are toxic. Expensive.
Ozonation	$CN^- + O_3 \rightarrow OCN^- + O_2$ $2OCN^- + 3O_3 + H_2O \rightarrow 2HCO_3^- + N_2 + 3O_2$	Ozone is expensive.
Sulfur dioxide (INCO)	$CN^- + SO_2 + O_2 + H_2O \leftrightarrow OCN^- + SO_4^{2-} + 2H^+$ $M(CN)_4^{2-} + 4SO_2 + 4O_2 + 4H_2O \leftrightarrow 4OCN^- + 8H^+ + 4SO_4^{2-} + M^{2+}$	Decrease in pH, due to production of H_2SO_4, incurs extra costs
Hydrogen peroxide	$CN^- + H_2O_2 \leftrightarrow CNO^- + H_2O$ $OCN^- + 3H_2O_2 \leftrightarrow NO_2^- + CO_3^{2-} + 2H_2O + 2H^+$ $NO_2^- + H_2O_2 \leftrightarrow NO_3^- + H_2O$	Possible decrease in pH as H^+ is produced.
CARO acid	$CN^- + H_2SO_5 + 2OH^- \leftrightarrow OCN^- + 2H_2O + 4SO_4^{2-}$ $M(CN)_4^{2-} + 4H_2SO_5 + 10OH^- \leftrightarrow M(OH)_2 + 4OCN^- + 8H_2O + 4SO_4^{2-}$	Has a limit as to the concentration of cyanide can remediate.
Prussian blue	$4Fe^{2+} + 24CN^- + O_2 + 4H^+ \rightarrow 4Fe(CN)_6^{3-} + 2H_2O$ $16Fe^{2+} + 12Fe(CN)_6^{3-} + O_2 + 4H^+ \rightarrow 4Fe_4[Fe(CN)_6]_3 + 2H_2O$	UV-radiation decomposition. Production of cyanide compounds, that may affect the environment.

3.7.3 Biological remediation

Biological remediation involves a treatment process that promotes the growth of large colonies of essential bacteria (Botz et al., 2005). These essential bacteria along with other plants and fungi, have the ability to use the contaminant present in the environment as a source of nitrogen for their own metabolic activities where some bacteria can metabolize both nitrogen and carbon requiring no further nutrition (Razanamahandry et al., 2017). The optimal pH conditions for the degradation to occur are, for bacteria - 5.2 to 10.5, for fungi - 6 to 8.5 and for plants – 12 and the temperatures can range from 25 to 50 °C but optimally, for bacteria - 30 °C, for fungi - 43 °C and for plants - 40 °C (Alvillo-Rivera et al. 2021; Razanamahandry et al., 2017).

In the biological remediation of cyanide, free cyanide and cyanide complexed with metals are converted with use of bacteria into HCO_3 and NH_3, releasing metals that are either precipitated (as carbonates, hydroxides or sulphides) or adsorbed into the biofilm (Ackil, 2003). Free cyanide is the easiest to biodegrade, whereas iron-cyanide compounds are the most rigid; zinc > nickel > copper are intermediately difficult to

remediate (Ackil, 2003). In aerobic processes the compounds CN^-, SCN^-, NO_2^- and NH_3 are oxidized to NO_3^- and in anaerobic processes, the NO_3^- and NO_2^- are converted to $N_2(g)$ (Ackil, 2003).

Alvillo-Rivera et al. (2021) classifies the cyanide biodegradation pathways into four sections (Figure 3.4), whereas Luque-Almagro et al. (2018) classifies then into six sections. The four pathways are referred to as hydrolysis, oxidation, reduction, and substitution/transfer (see Table 3.3), whereas the two additional sections included in Luque-Almagro et al. (2018) are subsections of the hydrolysis/oxidation pathway (namely, hydrolytic nitrile degradation and hydrolytic/oxidative thiocyanate degradation). The pathway used is dependent on the enzymes that are produced by the organisms themselves (Alvillo-Rivera et al., 2021), where a combination of these pathways can be used simultaneously with a combination of different microorganisms. The factors that affect which process and which microorganisms should be used are pH, O_2 and cyanide concentration, bioavailability and solubility in water and/or soil (Ibrahim et al., 2015).

The hydrolytic, oxidative and reductive pathways result in the formation of simple inorganic compounds which are then converted to NH_3, CH_4, CO_2, HCO_2H or carboxylic acid, whereas the substitution and biosynthesis pathways use the cyanide as a carbon and nitrogen source (Ibrahim et al., 2015).

Hydrolytic pathways are catalysed by the enzymes cyanide hydratase, cyanide dihydratase (cyanidase), nitrile hydratase and nitrilase (Alvillo-Rivera et al., 2021; Luque-Almagro et al., 2018; Park et al., 2017 and Dash et al., 2009). Where cyanide hydratase/cyanidase enzymes dissociate HCN and nitrile hydratase/nitrilase dissociate nitriles. Cyanide hydratase, usually found in fungi, produces formamide from cyanide according to the reaction in equation 6 (Alvillo-Rivera et al., 2021). Cyanidase directly converts cyanide to NH_3 and formate, see equation 7 (Alvillo-Rivera et al., 2021). Equation 8 shows the process of nitrile hydratase, where organic nitriles/aliphatic nitriles are degraded. The last of the enzymes in this process is nitrilase, viewed in equation 9, involving the conversion of nitriles to carboxylic acid (Alvillo-Rivera et al., 2021).

$$HCN + H_2O \rightarrow HCONH_2 \quad (6)$$

$$HCN + 2H_2O \rightarrow HCOOH + NH_3 \quad (7)$$

$$R - CN + H_2O \rightarrow R - CONH_2 \quad (8)$$

$$R - CN + H_2O \rightarrow R - COOH_2 + NH_3 \quad (9)$$

In the oxidative pathways, NH_3 and CO_2 are the final products. In the first of two pathways, the enzymes cyanide monooxygenase and cyanase (both enzymes are required) are required and in the second the cyanide dioxygenase enzyme (Alvillo-Rivera et al., 2021; Park et al., 2017; Parmar et al., 2013 and Dash et al., 2009). Equation 10 demonstrated the breakdown of cyanide with use of cyanide monooxygenase (converts cyanide into cyanate) and 11 with the use of cyanase (converts cyanate to NH_3 and CO_2). Equation 12, shows the second pathway, mentioned above.

$$HCN + O_2 + H^+ + NAD(P)H\ (enzyme) \rightarrow HOCN + NAD(P)^+ + H_2O \quad (10)$$

$$HOCN + HCO_3^- + H_2O \rightarrow 2CO_2 + NH_3 + OH^- \quad (11)$$

$$HCN + O_2 + 2H^+ + NAD(P)H\ (enzyme) \rightarrow CO_2 + NH_3 + NAD(P)^+ \quad (12)$$

The reductive pathway uses the enzyme nitrogenase to form CH_4 and NH_3. This is is not common and involves two steps that are present in equations 13 and 14 (Alvillo-Rivera et al., 2021; Park et al., 2017 and Dash et al., 2009).

$$HCN + 2H^+ + 2e^- \rightarrow CH_2 = NH + H_2O \rightarrow CH_2 = O \quad (13)$$

$$CH_2 = NH + 2H^+ + 2e^- \rightarrow CH_3 - NH + 2H^+ + 2e^- \rightarrow CH_4 + NH_3 \quad (14)$$

The last of the pathways is referred to as substitution and amino acid synthesis (Park et al., 2017). The substitution pathways make use of two enzymes, namely β-cyanoalanine synthase (CAS) and nitrile hydratase/nitrilase, which producing asparagine/aspartate and ammonium from aminonitrile (Dash et al., 2009). CAS catalyses the degradation of cysteine into β-cyanoalanine and sulfide, seen in equation 15 (Alvillo-Rivera et al., 2021). Equation 16 involves the enzyme thiosulfate sulfurtransferase (known as Rhodanase), converts cyanide into SCN^- and SO_3 (Alvillo-Rivera et al., 2021). Rhodanase is found in the liver and kidneys of animals.

$$HCN + HSCH_2CHNH_2CO_2H \rightarrow NCCH_2CHNH_2CO_2H + H_2S \quad (15)$$

$$CN^- + S_2O_3^{2-} \rightarrow SCN^- + SO_3^{2-} \quad (16)$$

Using bacteria to remediate waste that contains cyanide is cost-effective, fast and environmentally safe, as opposed to the use of chemical methods for treatment (Gurbuz et al., 2009).

Table 3.3: The different cyanide degradation pathways and examples of microorganisms that preform such degradations (Alvillo-Rivera et al., 2021).

	Degradation pathway	**Microorganism**
Hydrolytic	Cyanide hydratase	Fungal species (*Fusarium sp.*) and bacterium (*Pseudomonas fluorescens*)
	Cyanidase	*Alcaligenes xylosooxidans, Alcaligenes xylosoxidans, Bacillus pumillus, Pseudomonas stutzeri.*
	Nitrile hydratase	*Pseudomonas (marginales, putida), Corynebacterium, Brevibacterium, Rhodococcus rhodochrous, Pseudonocardia thermophila*
	Nitrilase	*Klebsiella, Arthrobacter, Pseudomonas, Nocardia Rhodococcus rhodochrous, Klebsiella ozaenae, Arthrobacter sp., Alcaligenes faecalis, Acinetobacter sp., Fusarium solani, F. oxysporum, Nocardia sp.*
Oxidative	Cyanide monoxygenase	*Pseudomonas sp.*
	Cyanase	*Escherichia coli, Rhodococcus, Pseudomonas pseudoalcaligenes*
	Cyanide dioxygenase	*Pseudomonas fluorescens, Pseudomonas cereus, Bacillus pumillus, Escherichia coli*
Reductive	Nitrogenase	*Klebsiella oxytoca, Rhodopseudomonas gelatinosa, Streptomyces thermoautotrophicus, Herbaspirillum seropedicae, Azotobacter sp., Azospirillum sp., Rhodospirillum rubrum*
Substitution	Cyanoalanine synthase	*Chromobacterium violoaceum, Bacillus megaterium, Enterobacter sp., E. coli, Pseudomonas sp.*
	Thiosulfate sulfurtransferase (Rhodanase)	*Azotobacter vinelandii, E. coli, Pseudomonas aeruginosa, Ferrobacillus ferroxidans, Thermobacillus denitrificans, Desulfotomaculum nitrifican, Fusarium sp.*

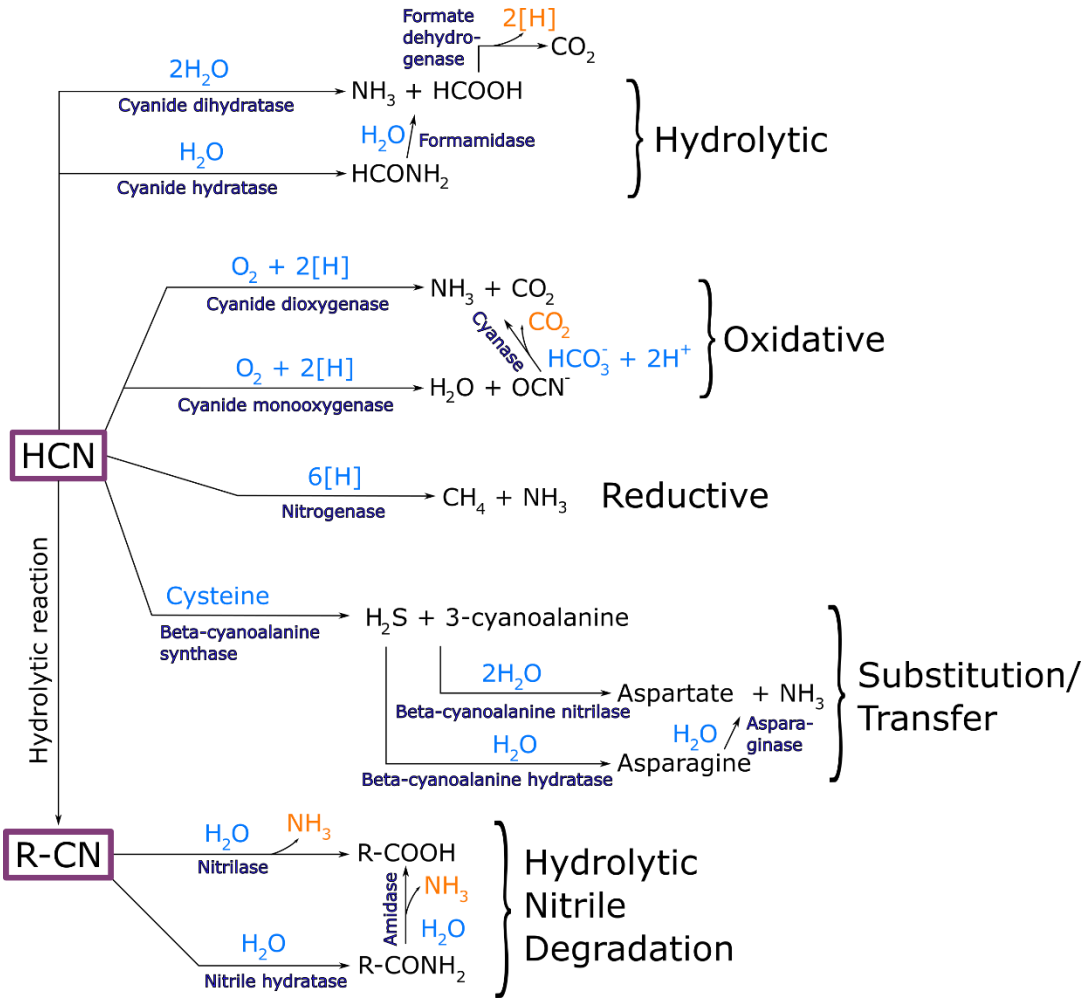

Figure 3.4: The different processes involved in the biodegradation of cyanide (modified after Luque-Almagro et al., 2018). [H] refers to a hydrogen atom (H^+ and an e^-), compounds in blue are added to the reaction and orange are produced. Enzymes were also added to the diagram.

3.8 Microbial diversity in gold mine dumps and potential cyanide degraders

Factors that determine a microbial profile in an environment, in this case tailings dams, are metal content, pH, temperature, total organic carbon and concentration of dissolved O_2 (Sajjad et al., 2018). The presence of organic carbon in the Witwatersrand gold mine tailings environment (any tailings that contain sulfides) has been noted in numerous studies to be low as they are barren of the growth of vegetation and plant nutrients as the soils are rather acidic (Sibanda et al., 2019; Ngole-Jeme and Fantke, 2017; Callender et al., 2016; Dhal and Sar, 2014; Huang et al., 2012; Navarro-Noya et al., 2010). This is also the scenario with the total nitrogen in the soils.

Sibanda et al. (2019) studied the microbial diversity of gold mine tailings dams from five sites in the West rand in Johannesburg, South Africa. They concluded that these tailings dams are locations that host unique and diverse microbial assemblages, where *Actinobacteria* were the most dominant and others present include *Firmicutes*, *Proteobacteria, Cyanobacteria, Chloroflexi, Bacteroidetes, Planctomycetes and Acidobacteria* (Sibanda et al., 2019). Previous studies on similar sulfide-rich tailings environments in different countries found microbial communities consisting of the phyla *Acidobacteria*, *Actinobacteria*, *Bacteroidetes*, *Firmicutes*, *Nitrospirae* and *Proteobacteria* (Yang et al., 2014; Gupta et al., 2017; Sajjad et al., 2018). Several studies report the phylum *Proteobacteria* as the most abundant in tailings and acid mine drainage (AMD) (Keshri et al., 2015; Dhal and Sar, 2014; Rastogi et al., 2010; Winch et al., 2009), but Sibanda et al. (2019) reports *Actinobacteria* as the most abundant.

Gschwendtner et al. (2016), studied the possible cyanide degraders of Prussian blue in de-icing salt. They concluded that *Acidobacteria* (Gp3, Gp4, Gp6), *Gammaproteobacteria* (*Thermomonas* and *Xanthomonadaceae*) and *Gemmatimonadetes* (*Gemmatimonas*) are able to use iron-cyanide compounds as a carbon source. Overtime, they concluded that *Actinomycetales* surpass the usage of other microorganisms in the usage of iron-cyanide as a carbon source (Gschwendtner et al., 2016). *Pseudomonas putida* and *Pseudomonas stutzer*, have been used in batch tests to degrade cyanide and phenol in the waste products from coke-ovens (Singh et al., 2018). These microbes were able to degrade up to 80.6 % of the cyanide present, but can tolerate a concentration of cyanide of <360 $mg.L^{-1}$ (Singh et al. 2018). Where Luque-Almagro et al. (2016) studied the ability for *Pseudomonas pseudoalcaligenes* CECT5344 to use cyanide and its derivatives as a nitrogen source. In bioreactor studies to investigate the bioremediation of SCN^- and CN^-, Kantor et al. (2015), determined that their microorganism community was dominated by the microbe, *Thiobacillus spp*. Other microbes present include, *Comamonas, Mesorhizobium, Microbacterium, Rhodanobacter Sphingomonas* and *Sphingopyxis*. Their study showed that the microbes can tolerate/dissociate the SCN^- and CN^- and have the capacity to use the produced compounds (Kantor et al., 2015). References to studies on various other microbes can be found in Table 3.4.

Table 3.4: List of microorganisms that have been reported that are able to biodegrade cyanide. Included is the sources of sample as medium (taken from Bhalla et al., 2017).

Microorganism	Medium	Reference
Stemphylium loti	Soil	Fry and Miller (1972)
Fusarium lateritium	Soil	Fry and Miller (1972); Cluness et al. (1993)
Achromobactor	Soil	Knowles (1976)
Bacillus cereus	Soil	Knowles (1976)
Chromobacterium violaceum	Soil	Knowles (1976)
Tetrahymena pyriformis	Soil	Knowles (1976)
Pseudomonas sp.	Activated sludge	White et al. (1988)
Pseudomonas fluorescens NCIMB 11764		Kunz et al. (1992)
Alcaligenes xylosoxidans	Soil	Ingvoresen et al. (1991)
Bacillus pumulis	Waste water	Meyers et al. (1991)
Fusarium solani	Alkaline waste water	Dumestre et al. (1997)
Pseudomonas stutzeri AK 61	Metal plating waste	Watanabe et al. (1998)
Burkholderia cepacia	Soil	Adjei and Ohta (1999)
Fusarium solani	Soil	Barclay and Day (2002)
Pseudomonas flourescens NCIMB 11764	Waste water	Fernadez et al. (2004)
Trichoderma sp.	Soil	Ezzi and Lynch (2005)
Fusarium sp.	Soil	Ezzi and Lynch (2005)
Ascophyllum sp	Soil	Ezzi and Lynch (2005)
Rhizopus oryzae	Soil	Ezzi and Lynch (2005)
Rhizobium daejeonense		Quan et al. (2005)
Saragassum sp	Soil	Igwe and Abia (2006)
Ecklonia radiata	Soil	Igwe and Abia (2006)
Pseudomonas aeuroginosa	Soil	Cipollone et al. (2006)
Cryptococcus humicolus	Full scale coke wastewater	Park et al. (2008)
Klebesiella oxyotoca	Soil	Chen et al. (2008)
Rhizopus oryzae (MTCC 2541)	Waste water	Dash et al. (2009a)
Agrobacterium tumefaciens SUTS 1	Cassava wastewater	Potivichayanon and Kitleartpornpairoat (2010)
Pseudomonas pseudoalcaligens	Waste water	Luque-Almagro et al. (2011)
Micromonospora braunna	Garden soil	Shete and Kapdnis (2012)
Bacillus sp. CN-22	Soil	Wu et al. (2013)
Serratia marcescens RL2b	Soil	Kumar et al. (2013)
Aspergillus niger K10	Soil	Rinagelova et al. (2014)
Trichoderma harzianum VSL291 Jorge		Rodriguez and Ramirez-Lepe (2015)

Chapter 4 - Geological setting, gold extraction and disposal/composition of waste

The Witwatersrand Supergroup hosts the largest gold deposit in the world. It consists of a series of sedimentary deposits that have generated to date over a third of all of the world's gold ever produced (Tucker et al., 2016). The deposition of the supergroup occurs in what is known as the Witwatersrand basin, where the initial deposition was shallow marine quartzites and shales forming the West Rand Group (Tucker et al., 2016). This was overlain with the arenaceous Central Rand Group, where deposition was in a basin environment (Tucker et al., 2016). Fluvial deposits became the main type of deposition towards the top of the sequence (Tucker et al., 2016). The gold deposits are found on braided fluvial plains and at the base of the Central Rand Group in a reworked marine environment (Tucker et al., 2016). Majority of the gold deposits are found within the Central Rand group.

Tucker et al. (2016) mentions that the lithologies (reefs included) are mostly consistent across the entire basin except for separate channels and shoots of reef material. The Witwatersrand basin extends from North of Johannesburg to south of Welkom, consisting of nine goldfields, where gold is extracted. The goldfields are the Evander, East Rand, Central Rand, West Rand, South Deep, Western Areas, Carletonville, Far West Rand and Free State Rand goldfields, see Figure 4.1 (Frimmel et al., 2005). The gold found in the Witwatersrand goldfields, is generally associated with the pyrite-rich units of the deposit and occurs primarily as micron-sized inclusions and veinlets (De Wet et al., 1995).

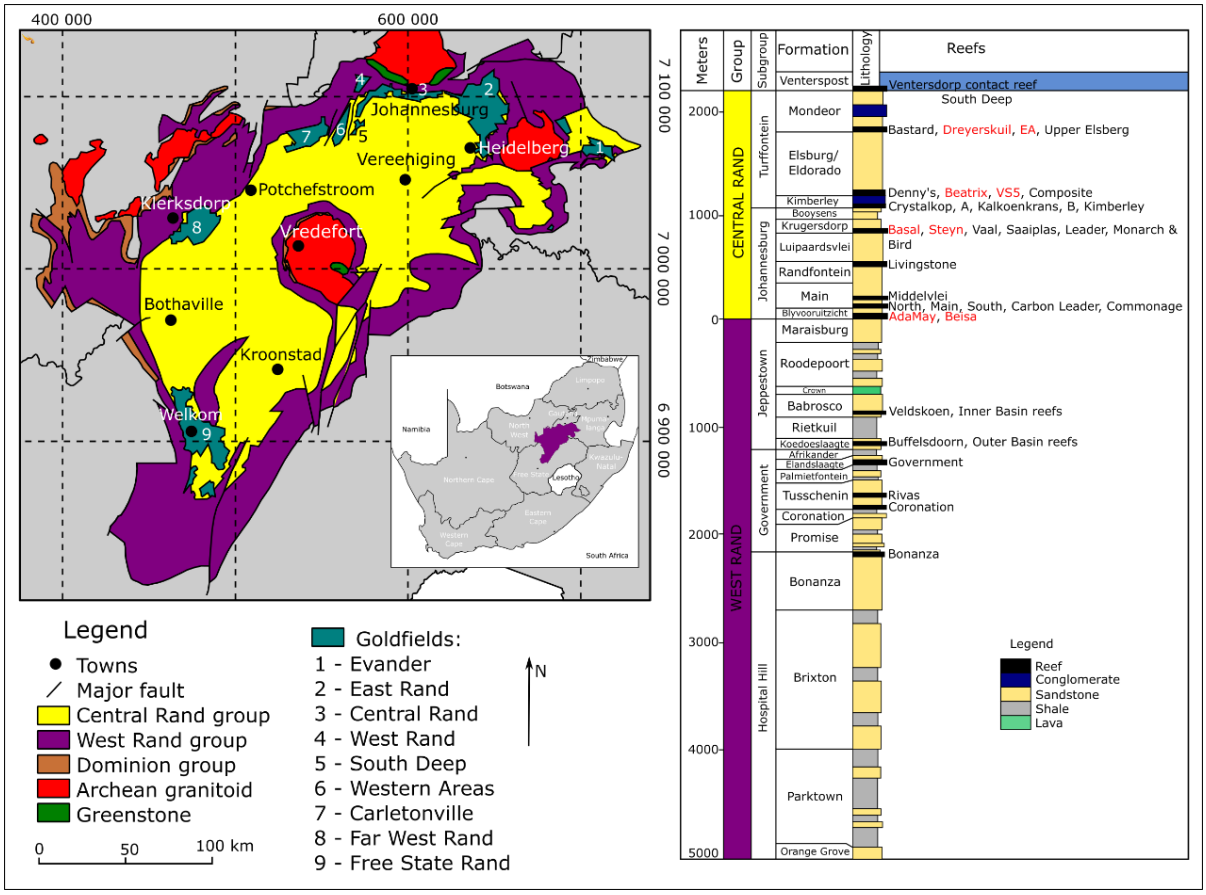

Figure 4.1: Geological map of the Witwatersrand basin, including the positions of the goldfields (Modified after Hansen, 2018 and Frimmel et al., 2005). To the right is the general stratigraphy of the Witwatersrand basin which consists of conglomerates, sandstones, shales and lavas. The names of reefs in red are the most important reefs in mining in the Free State Rand basin (Tucker et al., 2016).

During the gold extraction process, the gold-bearing material is crushed and milled to grain sizes of approximately 100 µm (Acheampong et al., 2010). This material is then added to a mixture of cyanide, lime and oxygen at the leaching plant. Lime increases the pH of the slurry, while cyanide and oxygen complex and oxidize the gold according to the equation 17 (Acheampong et al., 2010). This equation is known as the Elsner equation.

$$4Au(s) + 8NaCN(aq) + O_2(g) + 2H_2O(l) \rightarrow 4Na[Au(CN)_2](aq) + 4NaOH(aq) \quad (17)$$

The Elsner equation shows that the cyanide solution dissolves the gold present in the initial crushed material. The products of this process are collected and the gold in solution is precipitated (Acheampong et al., 2010). Gold precipitation occurs using a combination of carbon-in-pulp (CIP), the Merrill-Crowe process/electrowinning and resin-in-pulp processes (Acheampong et al., 2010). CIP involves the addition of

activated carbon to the solution where the gold-cyanide complex adsorbs onto the activated carbon (Acheampong et al., 2010). The particle size of the carbon is larger than that of the slurry and thus can be easily filtered using wire mesh. The gold-cyanide coated carbon is removed and washed, after which it desorbed from the carbon at high pH and high temperatures (Acheampong et al., 2010). The carbon is then reactivated and reused. The Merrill-Crowe process, also referred to as zinc cementation (lead can also be used), is a method by which the gold is dissociated from the cyanide compound. It involves the addition of zinc and NaCN to the gold-cyanide in a reducing environment, according to equation 18 (Kyle, 1997).

$$Zn + 4NaCN + NaAu(CN)_2 \rightarrow Au + Na_2Zn(CN)_4 + 2NaCN \quad (18)$$

In equation 18, the main difference that occurs is the exchange of zinc and gold. Smelting of this material refines the gold and ingots are produced (Acheampong et al., 2010).

The waste material produced during this gold-extraction process is discarded of on tailings dams. The waste material consists of the gangue minerals (quartz, mica, clay minerals, etc.), (Vermeulen et al., 2002) as well as possible contaminants used in the extraction process (cyanide, heavy metals, etc). Depending on the mining company's protocol, carbonates may be added to this material to increase the pH of the material and assist in the prevention of acid mine drainage (AMD) (Yibas et al,. 2010). The zones of the tailing's dams, seen in Figure 4.2, are not horizontal but rather like that of an onion (Hansen, 2018). According to Hansen (2018), the outer zone is the oxidation zone, adjacent to the transition zone and the core is the reducing zone.

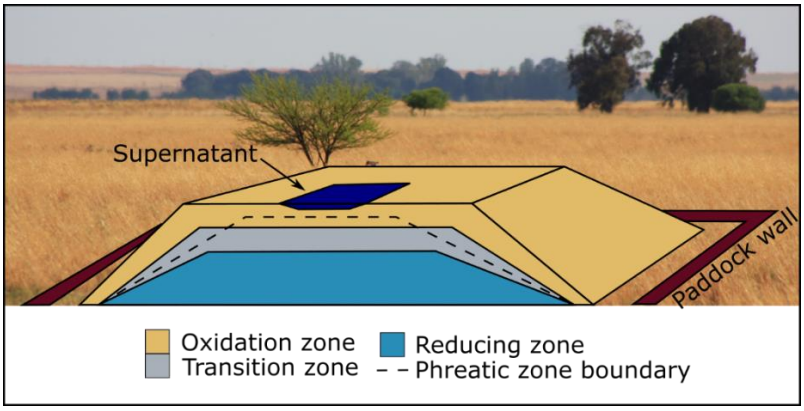

Figure 4.2: A simplified graphical depiction of the geochemical structure of a tailings dam, modified after Hansen (2018).

The oxidation zone is the outer layer that is in contact with the atmosphere, being the zone where oxidation of pyrite occurs according to the equation 19 (Williamson and Rimstidt, 1994).

$$FeS_2(s) + \frac{7}{2}O_2 + H_2O(l) \leftrightarrow Fe^{2+} + 2SO_4^{2-} + 2H^+ \quad (19)$$

The boundary between this oxidation zone and the adjacent zone, namely the transition zone, is known as the oxidation front (Hansen, 2018). This boundary separates the oxidized sulfide minerals from the unoxidized sulfide minerals. Within the transition zone, the acid front can be found, which represents the boundary where neutralisation ceases as there is depletion in carbonate minerals (Hansen, 2018).

Chapter 5 - Methodology

The extended methodology of Chapter 7

For the production of Prussian and Turnbull's blue powders, the following procedure was followed. A cyanide source, either $K_3[Fe(CN)_6]$ (Merck AR chemical) or $K_4[Fe(CN)_6]$ (ACE CP chemical) was added to an iron source, either $FeSO_4$ (ACE CP chemical) or $Fe_2(SO_4)_3$ (ACE CP chemical). Each powder was created in triplicate, where the Prussian blue samples were named PBS1-3 and the Turnbull's blue samples named TBS1-3. The chemicals used and their masses (calculated to produce 15 g of product) can be found in Table 5.1. The chemicals were dissolved in 200 ml of 18.25 MΩ deionized H_2O, where the cyanide source was mixed in a volumetric flask and the iron source in a beaker. The iron source was then added to the cyanide source. The production of Prussian and Turnbull's blue is instantaneous and was filtered immediately after production, an additional 100ml 18.25 MΩ deionized water was used to rinse the last of the volumetric flask. The powders were dried in a fume hood. Volumetric flasks and beakers that were used are from Lasec borosilicate, grade A.

Table 5.1: The chemicals used and their masses used in the experiments for this study.

Sample	CN source	CN mass (g)	Fe source	Fe mass (g)
PBS1	$K_4[Fe(CN)_6]$	20.77	$Fe_2(SO_4)_3$	14.16
PBS2	$K_4[Fe(CN)_6]$	19.47	$Fe_2(SO_4)_3$	14.00
PBS3	$K_4[Fe(CN)_6]$	19.83	$Fe_2(SO_4)_3$	13.83
TBS1	$K_3[Fe(CN)_6]$	16.63	$FeSO_4$	11.60
TBS2	$K_3[Fe(CN)_6]$	16.66	$FeSO_4$	11.62
TBS3	$K_3[Fe(CN)_6]$	16.93	$FeSO_4$	11.12

The extended methodology of Chapter 9

Sample collection

A tailings dam facility of the Free State goldfields was visited to collect samples for this study. Three sets of samples were collected (sample names being Profile 1 – 3), two sets originated from the top plateau of the dam and two sets from the side slopes of the dam. Three samples were taken at each site totalling nine samples collected (sample names being Profile 1.1, 1.2, 1.3, 2.1, etc.). Samples were collected on slopes

according to Figure 5.1. The top surface of material was removed and blocks of sample were collected at each point that were ~10-20 x 10 x 8 cm in order to preserve an uncontaminated sample within. Samples were stored in sterile bags bought from Lasec and stored at -4 ºC in a fridge.

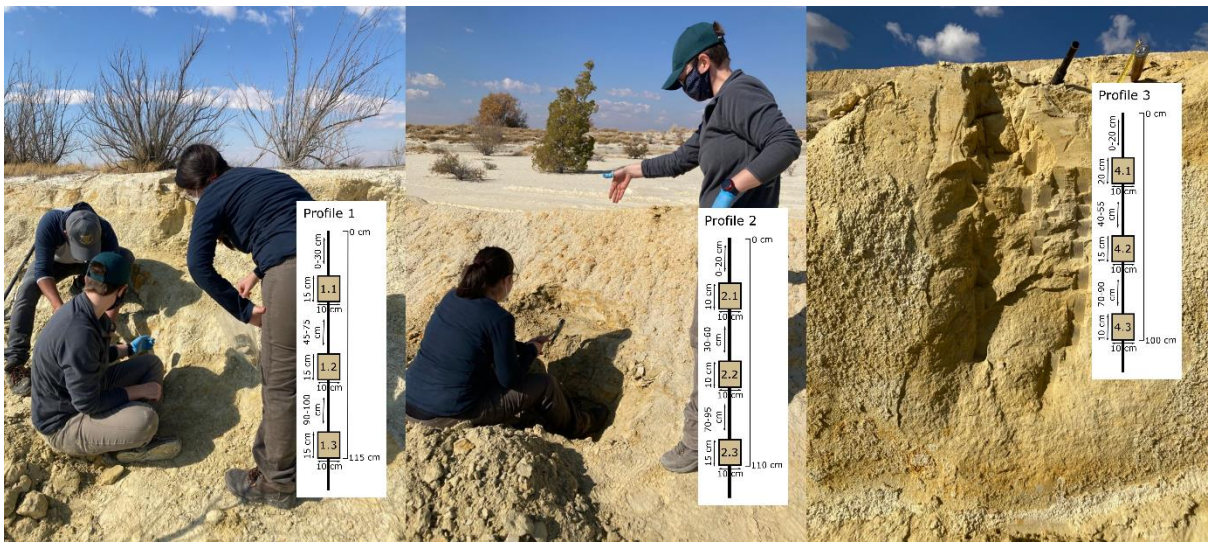

Figure 5.1: Graphic depiction of the profiles (vertical profiles) of sample collection from a tailings dam in the Free State goldfields. Each block represents a sample that was extracted from a slope at 3 positions on the tailings dam, 2 from slopes on top of the facility and 2 from the side of the facility.

Bio-available fraction determination/Exchangeable fraction – sequential extraction

The first step of the sequential extraction process (Dold, 2003) was performed in order to determine elements available for the consumption of microbes. This was done by adding 40 ml of 0.11 M acetic acid (ACE product) to 0.5 g of sample. This was performed on the nine samples collected, a control was added (deionized water was added instead of acetic acid) and a blank which consisted of acetic acid only. This was then mixed for 16 hours, centrifuged for 20 min at 4 ºC at a speed of 5000 rpm. The supernatant was then removed using a syringe and 2 µm filter.

The supernatant was then analysed using a Prodigy7 ICP-OES. 2 ml of 65 % Merck nitric acid was added to each sample before analysis. Calibrations were created using the reference material ICP multi-element standard solution IV from Merck at concentrations: 0, 0.1, 0.5, 1, 5 and 10 ppm (Ag, Al, B, Ba, Bi, Ca, Cd, Co, Cr, Cu, Fe, Ga, In, K, Li, Mg, Mn, Na, Ni, Pb, Sr, Tl and Zn). Merck V standard was also added to each at the same concentrations.

Total C and N analysis

0.4 g of each sample was air-dried in an aluminium cup and weighed. A thermal conductivity detector in a CNS analyzer (LECO Trupsec CN) was used to determine the gas released as the sample is heated to 950 °C. Synthetic Carbon L certified reference material was used and the detection limit is 0.0001 g.

DNA extraction

The DNA extraction occurred on all three profiles' samples for metagenome analysis. It required 4 g of sample and 8x the reagents for each sample in the profile and then the three samples per profile were added together to produce one sample per profile (12 g of sample in total). A DNA extraction kit used for extraction was the QIAGEN – DNeasy PowerLyster PowerSoil kit. The kit was mostly used for the lysis and washing process, binding was performed using CTAB (10 g N-cetyl-n n-trimethylammonium-bromide in 100 ml deionized H_2O) and SEVAG (24 chloroform:1 Isoamyl alcohol). Below is the process followed for the 4 samples for metagenome analysis.

CTAB/SEVAG binding process and DNA extraction process according to the DNeasy PowerLyster PowerSoil kit:

- A sterile surgical blade was used to remove the outer surface of the sample in order to extract DNA on uncontaminated sample within the sample blocks
- 4 g of sample from the nine samples were added to 8x beads, 6000 µL of Power bead solution and 480 µL of C1 in a 50 ml falcon tube
- Vortexed for 15 min
- Centrifuge for 3 min at 10000 x g at room temperature
- 10 min in an ice bucket
- Added 8 µL of Proteinase K
- Vortex for 5 s
- Placed in a water bath at 60 ºC for 60 min
- 1120 µL of 5 M NaCl solution was added and 520 µL of CTAB
- Samples were vortexed for 5 s
- Placed in a water bath at 60 ºC for 10 min
- Added 5600 µL SEVAG

- Vortex for 5 s
- Added to an ice bucket for 30 min
- Centrifuged for 10 min at 4 ºC at ~10000 x g
- Supernatant was transferred to a new falcon tube
- 4080 µL of ice-cold isopropanol was added
- Centrifuged for 10 min at 4 ºC at 12000 rpm
- Supernatant was then discarded and the pellet was washed with 2000 µL of cold 70% ethanol
- Ethanol is then discarded and pellet was dried
- 9400 µL of C4 was added
- Vortexed for 5 s
- 675 µL of the fluid was filtered through an MB spin column and centrifuged for 1 min at 10000 x g, this was repeated till all the fluid was filtered
- Added 500 µL of C5 and centrifuged for 30 s at 10000 x g
- Flow through was discarded
- The filter was then placed in a 2 ml collection tube
- DNA was then eluded with 60 µL deionized H_2O and centrifuged for 30 s at 10000 x g

The eluded DNA from samples Profile 1.1, 1.2 and 1.3 were then added together using a pipette and then added to the speedy vac (Eppendorf – Concentrator 5301) at 45 ºC till approximately 80 µL of sample were left. This was completed for each of the profiles. The concentration of DNA and the purity were analysed using 2 µL of sample in the Thermo- Scientific NanoDrop OneC UV-vis spectrophotometer.

Chapter 6

This chapter is based on the article Welman-Purchase MD and Hansen RN, 2023, Cyanide within gold mine waste of the free state goldfields: A geochemical modelling approach, Environmental Pollution, 120825. 10.1016/j.envpol.2022.120825

Cyanide within gold mine waste of the Free State goldfields: A geochemical modelling approach

Megan D. Welman-Purchase[a,*], Robert N. Hansen[b]

[a] University of the Free State, Department of Geology, Bloemfontein, South Africa

[b] University of the Free State, Centre for Mineral Biogeochemistry, Bloemfontein, South Africa

*Corresponding author.

Email address: purchasemd@ufs.ac.za (MD Welman-Purchase).

Abstract

Cyanide, which remains the preferred chemical used in the gold extraction process, has the potential to be disposed of on goldmine tailings. South Africa has nine goldfields, producing approximately a third of the world's gold to date. The cyanide interacts with metals in the tailings environment, where Prussian blue $Fe_4^{3+}[Fe^{2+}(CN)_6]_3$ and Turnbull's blue $Fe_3^{2+}[Fe^{3+}(CN)_6]_2$ are among these. In previous studies, Prussian blue or Turnbull's blue have been found as a blue substance in tailings material. PHREEQC modelling software was used adding the mineralogical data from 16 tailings samples from the Free State goldfield. The results revealed that Prussian blue prefers to precipitate in an oxic environment and Turnbull's blue prefers an anoxic environment. It was also determined that their precipitation is affected by the availability of iron in solution. As soon as all of the iron is consumed in solution, all excess cyanide produces HCN, which is a free cyanide which volatilizes. Contrarily, Prussian and Turnbull's blue are CN_{SAD} compounds, only dissociating in extremely low pH condition in the absence of photolysis. Ultimately, these iron-cyanide compounds are able to immobilize cyanide, preventing seepage into environments such as the ground water. This along with an anoxic environment such as mine void, keeping the pH high, may be a possible solution for cyanide remediation.

Key words: Geochemical modelling, goldmine tailings, Prussian blue, Turnbull's blue, Witwatersrand

6.1 Introduction

The Witwatersrand basin in South Africa is unique and is regarded as the largest goldfield worldwide with conglomerate beds having already yielded approximately 52000 t of gold (Tucker et al., 2016; Frimmel et al., 2005). This is in excess of a third of the gold ever produced and the basin is estimated to contain a further ~30000 t in reserves (Tucker et al., 2016). This deposit also contains 84 % of South Africa's in-situ uranium resources, which total about 679310 t U_3O_8 (Kenan and Chirenje, 2016). Industrial scale extraction of gold generates a huge quantity of waste, which is disposed of into the environment (Anning et al., 2019). This waste may consist of cyanide, transition metals, radioactive metals, sulphide minerals and metalloids (Roche et al., 2017). Anning et al. (2019) mentions that the waste is dependent on the type of ore, the processing technique, and the milled particle size.

Mined material from gold-bearing reefs is crushed to approximately 100 µm and transferred to a leaching plant where lime (used to increase the pH of the system), oxygen and cyanide are added (Acheampong et al., 2010). The extraction of gold (Figure 6.1) from ore is based on the formation of a strong complex that develops between gold and cyanide (Kyle, 1997). This is described by the Elsner's equations (1) and (2) (Kyle, 1997). Either NaCN, KCN or an amalgamation of the two chemicals can be used in this process (Bakatula and Tutu, 2016).

$$4Au + 8NaCN + O_2 + 2H_2O \rightarrow 4NaAu(CN)_2 + 4NaOH \quad (1)$$

$$4Au + 8KCN + O_2 + H_2O \rightarrow 4KAu(CN)_2 + KOH \quad (2)$$

This is followed by the carbon-in-leach process (CIL) (Figure 6.1), which involves the absorption of the gold-cyanide complex onto activated carbon (Acheampong et al., 2010). Activated carbon is added to the last of the leaching drums of the process while the pulp is added to the first leaching drum. The gold-coated carbon particles are removed, washed and then undergo an elution process at high temperatures and high pH conditions (Acheampong et al., 2010). The gold is then recovered from solution using the Merrill-Crowe process (also known as zinc cementation). This process involves the chemical reaction between the gold-cyanide complex and a zinc powder in a reducing environment, according to equation (3) (Kyle, 1997), where gold replaces

zinc in the NaCN complex. The gold is then transported to the smelter to produce ingots (Acheampong et al., 2010).

$$Zn + 4NaCN + NaAu(CN)_2 \rightarrow Au + Na_2Zn(CN)_4 + 2NaCN \quad (3)$$

Cyanide is used in the leaching process and in the Merrill-Crowe method. Kruger (2019) mentions that four companies in South Africa produce over 100 t of gold annually. In order for this production to occur, the leaching process will use 50 t of NaCN (equation 1) and the Merrill-Crowe process will use 100 t (equation 3). Thus, a total of 150 t of NaCN is used to extract 100 t of gold annually if no recycling of NaCN occurs.

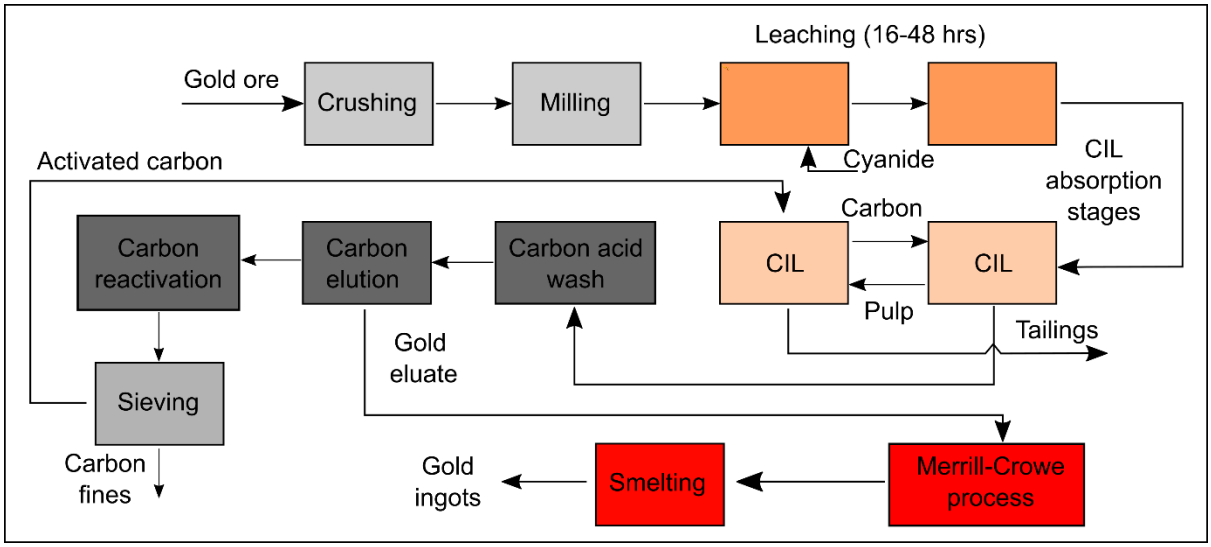

Figure 6.1: A simplified schematic diagram of the gold extraction process (modified after Acheampong et al., 2010). (CIL - carbon-in-leach).

In the same scenario, the waste produced in the Merrill-Crowe method is 50 t of NaCN and 109 t of $Na_2Zn(CN)_4$ (lead can be used instead of zinc). NaCN is highly soluble in H_2O, releasing 26 t of CN^- annually into the tailings environment, which is free to produce a large variety of compounds depending on the dissolved constituents present. $Na_2Zn(CN)_4$ is a weak acid dissociable cyanide (CN_{WAD}), dissociating in neutral to slightly acidic pH conditions, similar to ambient Earth surface conditions (Zagury et al., 2004). Therefore, the $Na_2Zn(CN)_4$ produced in the gold extraction process has the potential to additionally release 53 t CN^- and 33 t Zn^{2+} into the tailings environment annually, thus posing a significant environmental risk. According to Anning et al. (2019), large amounts of the cyanide used in the extraction process

environment remains in solution or in the waste slurries (i.e., tailings) where 50 % of the slurry is water and 50 % is solids, which is then pumped into a tailings dam (Bakatula and Tutu, 2016). Bakatula and Tutu (2016) indicate that the “Best Practice” limit of cyanide is 0.5 $mg.L^{-1}$ in tailings dams, which is iterated by the WHO (World Health Organization) cyanide limit (Anning et al., 2019). When the effluent is recycled into the plant, the impact of cyanide on humans, aquatic life and terrestrial life is lowered.

Tailings dams, that contain cyanide, are a suitable environment for the interaction of cyanide with other mineral residues (Bakatula and Tutu, 2016). It creates an environment to form compounds with metals such as copper, iron, mercury, nickel and zinc, depending on the composition of the original ore material (Kyle, 1997). There are several publications on the goldmine tailings dam environment that focus on acid mine drainage, heavy metals and uranium (Rösner and van Schalkwyk, 2000; Naicker et al., 2003; Schonfeld et al., 2014; among others). When iron and cyanide interact, blue compounds (occasionally green/brown) form, which has been mentioned with no additional research was completed on them, according to the authors best knowledge (Jambor et al., 2009; and Bakatula and Tutu, 2016).

There are four main iron-cyanide compounds, namely Prussian blue, Prussian brown/green, Berlin white and Turnbull’s blue. Prussian brown/green only contains Fe^{3+} ions, but in the tailings environment both Fe^{3+} and Fe^{2+} ion is present, diminishing its’ probability to precipitate. Berlin white is only stable in an anoxic environment, altering to Prussian blue in an oxic environment (Ghosh et al., 1999). Thus, it was decided that Prussian brown/green and Berlin white be excluded from this study. The main focus is thus on Prussian and Turnbull’s blue with the chemical formulas $Fe_4^{3+}[Fe^{2+}(CN)_6]_3$ and $Fe_3^{2+}[Fe^{3+}(CN)_6]_2$, respectively. This study delves into the interaction of iron with cyanide in the tailings dam environment of the Free State goldfields and modelling the behaviour of these species. Additionally, the authors considered the possibility that iron-cyanide compounds may be a solution to cyanide remediation or a means to immobilize cyanide and prevent it from contaminating the environment further, such as ground water studies.

6.2 Geological context

The Witwatersrand intracratonic basin consists of a sedimentary succession and occupies a central position on the Kaapvaal Craton (Tucker et al., 2016). Within this geological succession, the West Rand group comprises iron rich shales and quartzites (shale to quartzite ratio 1:1), whereas the arenaceous Central Rand group consists of quartzites, quartzwackes, quartz-pebble conglomerates and shales (shale to quartzite ratio 1:12.6) (Tucker et al., 2016). The Central Rand group contains the majority of the gold mineralisation (Tucker at al., 2016) and accounts for ~95 % of gold production (Frimmel et al., 2005) (Figure 6.2). The reefs are generally composed of a variety of lithofacies of different fluvial origin that range from "clast-supported oligomictic conglomerate to loosely packed conglomerate, pebbly arenite, or pebble lag surfaces associated with trough cross-bedded quartz arenite" (Frimmel et al., 2005, p. 777).

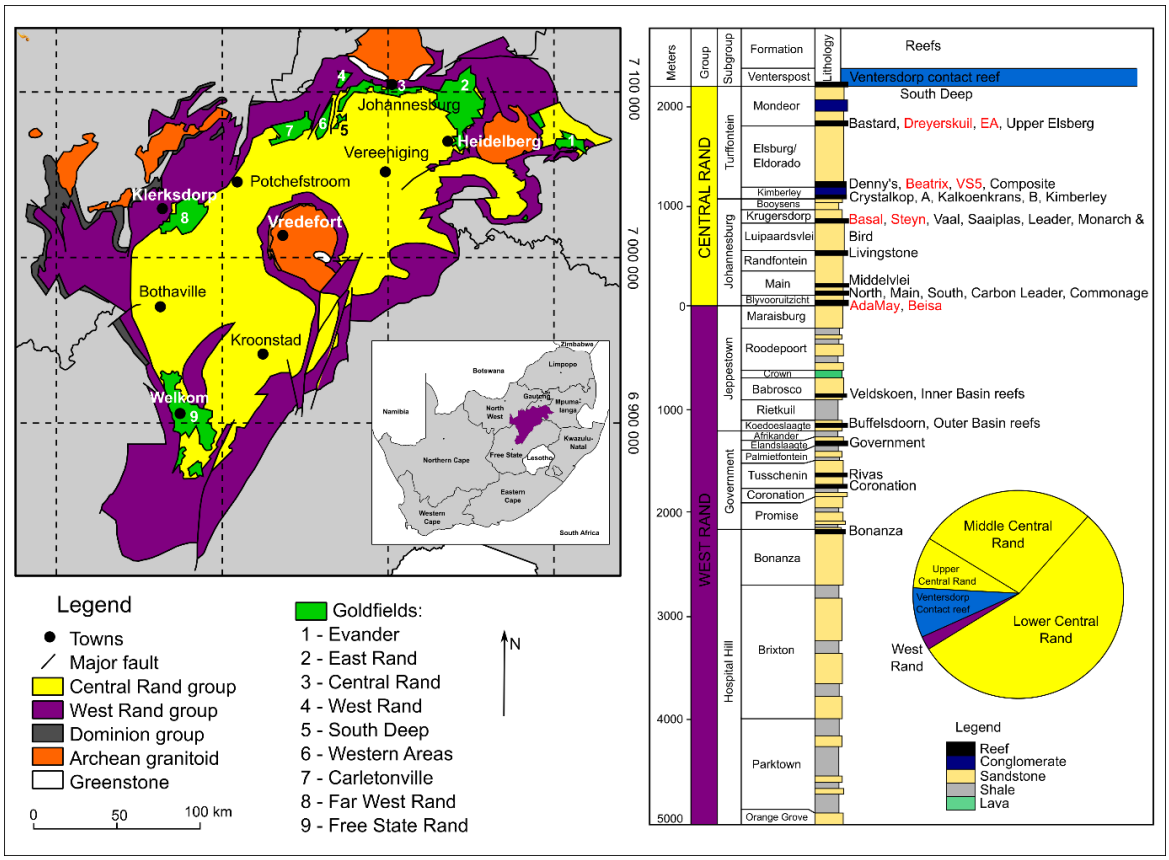

Figure 6.2: Map of the Witwatersrand basin displaying the position of the goldfields (Modified after Hansen, 2018 and Frimmel et al., 2005). Included is the general stratigraphy of the Witwatersrand basin, which consists of conglomerates, sandstones, shales and lavas, and a pie chart displaying which groups produce the most gold (modified after Frimmel et al., 2005). Reefs in red are the most important for mining in the Free State Rand basin, mentioned by Tucker et al. (2016).

6.3 Methodology

Mineralogical data was acquired from tailings dams of goldmines in the Free State goldfield. A total of 16 samples were collected from the tailings thickener underflow just before being pumped to the tailings facility. The geochemical modelling was completed using PHREEQC, which is a United States Geological Survey project developed by Parkhurst and Appelo (2013). PHREEQC was used for this study due to it having the capabilities needed for this study and that it is a freeware. The thermodynamic data of Prussian blue and Turnbull's blue had to be added to the PHREEQC database; the reactions and $logK_{eq}$ values are displayed in Table 6.1.

Table 6.1: Thermodynamic data added to the PHREEQC database for the study

Reaction	$logK_{eq}$	Proposed $logK_{eq}$ for this study	Reference
$Fe^{2+}(CN)_6^{4-} = Fe^{2+} + 6CN^-$	-45.61		Sehmel (1989)
$Fe^{3+}(CN)_6^{3-} = Fe^{3+} + 6CN^-$	-52.63		Sehmel (1989)
$Fe_3^{2+}[Fe^{3+}(CN)_6]_2 = 3Fe^{2+} + 2Fe^{3+} + 12CN^-$	-173.00	-181.45	Ghosh et al. (1999a)
$Fe_4^{3+}[Fe^{2+}(CN)_6]_3 = 4Fe^{3+} + 3Fe^{2+} + 18CN^-$	-257.00	-263.01	Ghosh et al. (1999a)

Quantitative Evaluation of Materials by Scanning Electron Microscopy (QEMSCAN) mineralogical data of the 16 samples was produced at the SGS laboratory in Bryanston, South Africa. A Zeiss Evo QEMSCAN was used with Imeasure and Idiscover software packages. The instrument settings were 25 kV acceleration voltage, beam spot-size between 520 to 550 and beam current of 5 nA.

Model setup

Three models were completed for this study (summary of the input parameters in Table S6.1), namely Speciation model 1, Speciation model 2 and a Sensitivity analysis. The two Speciation models differed only by their gaseous phase input. Speciation model 1's gas composition equal to that of the atmosphere and Speciation model 2 was oxygen free. This was orchestrated to mimic the outer most layer (<2 m from the surface) of a tailings dam and inner portion (>2 m from the surface) of a tailings dam, respectively. The Sensitivity analysis model involved the increase the concentrations of cyanide, pyrite, calcite and gypsum. Mineralogical inputs (QEMSCAN data) were able to dissolve and precipitate without restrictions. The

composition of the solution was pure water, with the addition of only dissolved cyanide. The purpose of the speciation models was to determine whether the cyanide produced iron-cyanide compounds in an oxic environment and an anoxic environment. The sensitivity analysis determined if the precipitation of Prussian and/or Turnbull's blue was affected by varying parameters.

6.4 Results

6.4.1 Mineralogical results (QEMSCAN results)

The average QEMSCAN data (mineralogical data) is displayed in Table 6.2 (full mineralogical results can be found in Table S6.2). The 16 samples were dominated by silicate minerals, mainly quartz (64.61 – 82.84 wt%), pyrophyllite (2.9 – 11.86 wt%), mica (3.76 – 16.66 wt%) and chlorite (0.52 – 4.49 wt%). Other minerals of importance in this study were pyrite (0.25 to 4.4 wt%), carbonate minerals (0.01 to 0.45 wt%) and gypsum (0.1 to 0.47 wt%).

Table 6.2: Average mineralogical QEMSCAN results. Full results are displayed in Table S6.2.

Mineral	Mineral Ideal Formula	Concentration (wt%)
Quartz	SiO_2	76,96±3,67
Pyrophyllite	$Al_2Si_4O10(OH)_2$	8,01±2,77
Mica	$KAl_2(AlSi_3O_{10})(OH)_2$	7,71±2,66
Chlorite	$(Mg,Fe)_6(Si,Al)_4O_{10}(OH)_8$	1,39±1,09
Plagioclase	$(Na,Ca)(Al,Si)_4O_8$	0,61±0,32
Chloritoid	$(Fe,Mg,Mn)_2(Al,Fe)(OH)_4Al_3O_2(SiO_4)_2$	1,07±0,49
Amphibole	$(Ca,Na)_{2-3}(Mg,Fe,Al)_5Si_6(Si,Al)_2O_{22}(OH)_2$	0,18±0,12
Pyroxene/Olivine	$(Ca,Mg,Fe)SiO_3/(Mg,Fe)SiO_4$	0,41±0,14
Zircon	$ZrSiO_4$	0,05±0,03
Other silicates		0,24±0,23
Pyrite	FeS_2	2,30±0,84
Other sulphides		0,05±0,03
Fe-oxides		0,27±0,21
Rutile/Ilmenite	$TiO_2/FeTiO_3$	0,18±0,05
Other oxides		0,08±0,08
Dolomite	$CaMg(CO_3)_2$	0,02±0,02
Calcite	$CaCO_3$	0,15±0,03
Ankerite	$CaFe(CO_3)_2$	0,01±0,01
Apatite	$Ca_5(PO_4)_3(F,Cl,OH)$	0,03±0,03
Alunite	$KAl_3(SO_4)_2(OH)_6$	0,08±0,05
Gypsum	$CaSO_4.2H_2O$	0,13±0,14
Other		0,06±0,07

6.4.2 Modelling results

Initial modelling with the thermodynamic data from Ghosh et al. (1999a) and Sehmel (1989) revealed that Prussian and Turnbull's blue do not precipitate. This reoccurred when the modelling forced the precipitation of the two cyanide minerals. This initiated an investigation into the thermodynamic data in the database. It was calculated that in order for Prussian blue to form, the $\log K_{eq}$ value needed to be -263.01 instead of -257.00 as taken from literature. The same occurred with Turnbull's blue, the $\log K_{eq}$ value had to be -181.45 instead of -173.00. These values were added to the PHREEQC database prior to the modelling of this study.

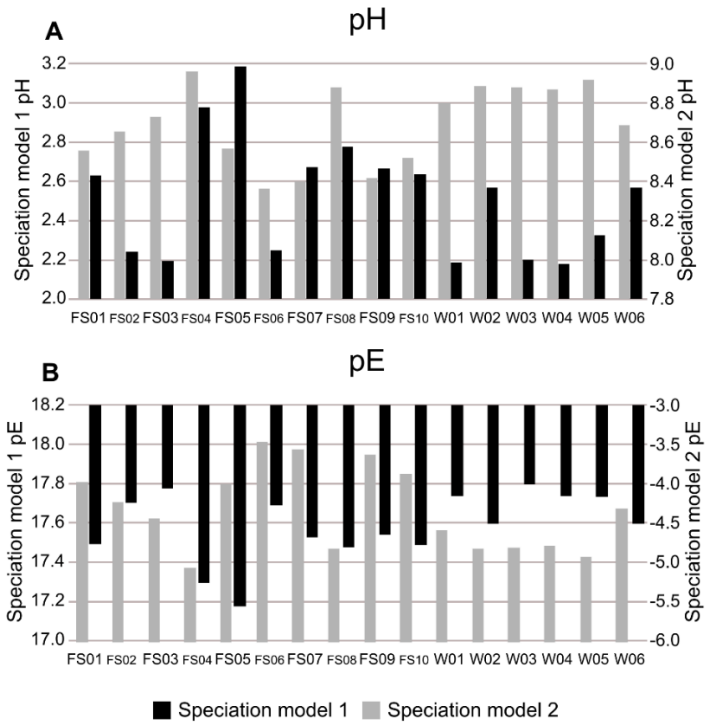

Figure 6.3: Graphs displaying the pH and pE conditions of the models for each of the localities. A) is a display of the pH results of Speciation model 1 and 2 and B) is a graph displaying the pE results of Speciation model 1 and 2.

The pH and pE results from the Speciation models 1 and 2 is displayed in Figure 6.3 A and B, respectively. The median pH and pE for Speciation model 1 are 2.9 and 17.7, respectively and for Speciation model 2, 8.3 and -4.5, respectively. The samples FS04, FS08 and W05 produced the highest pH conditions compared to the other samples as well as the highest Turnbull's blue concentrations (Figure 6.4A). FS04 and FS08 contain the highest percentage of total carbonates (0.44 and 0.45 %, respectively),

which was not the case with W05. The total carbonate concentration may have caused the increase in the pH in sample FS04 and FS08. W05 contained the least amount of quartz and elevated concentrations of sheet silicate minerals and elevated amounts of iron-rich minerals.

Speciation model 1

The modelling revealed that goethite, hematite, jarosite, Prussian and Turnbull's blue are able to precipitate in these sample. Other minerals also precipitated (Table S6.3), but are not of interest for this study (do not consume iron). Fe^{3+} (average concentration 9149 mg.L^{-1}) is the prominent iron ion in an oxic environment, yet Fe^{2+} (average concentration 0.17 mg.L^{-1}) is not absent (Figure 6.4A). The concentration of the Fe^{2+} remains almost constant between the samples, yet the Fe^{3+} composition varies greatly from 2120 (W02) and 21483 (FS09) mg.L^{-1}.

Figure 6.4B is a display of the distribution of cyanide into different compounds that may have formed in the model and the values are percentages of the cyanide total concentration of 0.5 mg.L^{-1}. The majority of the cyanide formed part of $Fe_4^{3+}[Fe^{2+}(CN)_6]_3$ (Prussian blue) with a mean of 93 %, the second constituent was HCN with a mean constituent of 6 % and $Fe_3^{2+}[Fe^{3+}(CN)_6]_2$ (Turnbull's blue) constituted a minor mean portion of 0.3 %. Other constituents included CN^-, $Fe(CN)_6^{3-}$, $Fe_2(CN)_6$ and $Fe(CN)_6^{4-}$, which in total comprised a total of 7.18x10^{-7} % (mean). Increases in Turnbull's concentrations results in the decrease in HCN concentration.

The Fe^{2+} compounds that formed is observed Figure 6.4C as percentages of the total 0.17 mg.L^{-1}. The mean Fe^{2+} consumed included $Fe_4^{3+}[Fe^{2+}(CN)_6]_3$ (Prussian blue) at 99 %, Fe^{2+} at 0.4 % and $Fe_3^{2+}[Fe^{3+}(CN)_6]_2$ (Turnbull's blue) at 0.5 %. Other constituents included $FeSO_4$, $FeHCO_3^+$, $FeHPO_4$, $FeOH^+$, $FeCO_3$, $FeH_2PO_4^+$, $FePO_4^-$, $Fe(OH)_2$, $Fe(OH)_3^-$, $Fe(CN)_6^{4-}$ and $Fe(OH)_4^{2-}$ with a mean total of 2x10^{-7} %.

Figure 6.4D displays the Fe^{3+} compounds that formed in the model as percentages of the total 9149 mg.L^{-1} (average). Contrasting to the cyanide and Fe^{2+} results, which mostly produced cyanide minerals, the majority of the compounds contained form hydroxide compounds. The mean total concentration of Fe^{3+} that formed included $Fe_3(OH)_4^{5+}$ at 51 %, $Fe_2(OH)_2^{4+}$ at 29 %, $FeNO_3^{2+}$ at 12 %, $Fe(OH)^{2+}$at 3 %, Fe^{3+} at 1

%, $FeHPO_4^+$ at 0.5 % and $Fe(OH)_2^+$ at 0.1 %. $Fe_4^{3+}[Fe^{2+}(CN)_6]_3$ (Prussian blue) only consumed 3x10^{-3} %. Other constituents included $FeSO_4^+$, $FeCO_3^+$, $Fe(OH)_3$, $Fe(SO_4)_2^-$, $Fe_3^{2+}[Fe^{3+}(CN)_6]_2$ (Turnbull's blue), $FeH_2PO_4^{2+}$, $FeNO_2^{2+}$, $Fe(OH)_4^-$, $Fe(CN)_6^{3-}$ and $Fe_2(CN)_6$, consisting of a mean of 3x10^{-5} %. Not all compounds were present in each of the samples.

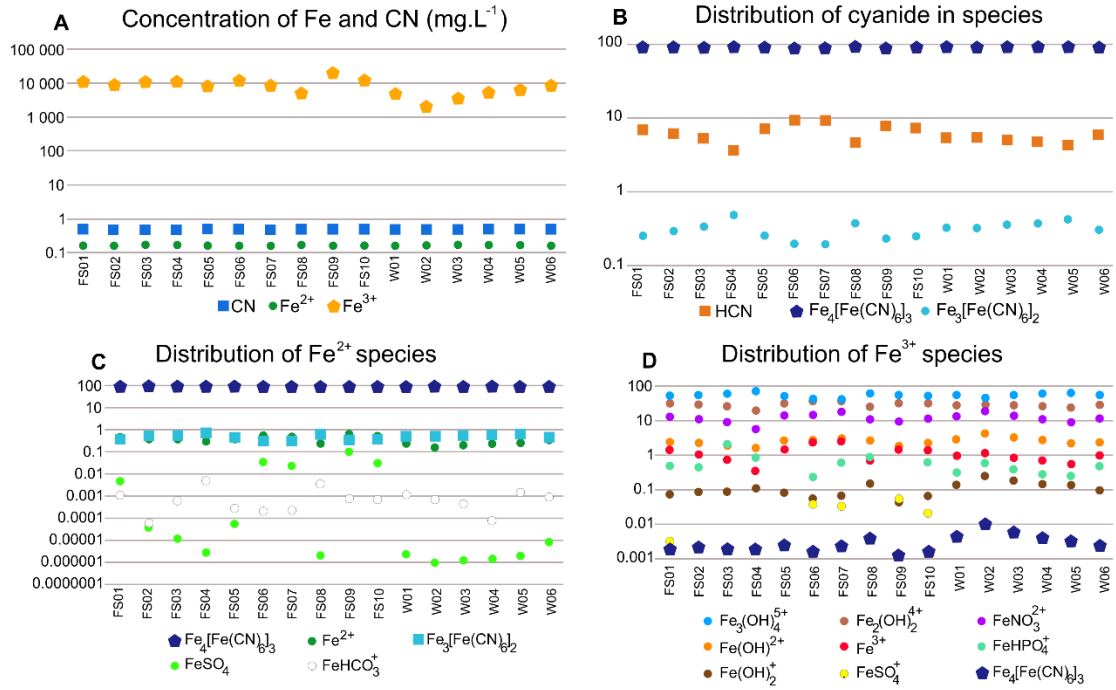

Figure 6.4: A) Concentrations of cyanide and iron available in solution according to the Speciation model 1 in mg.L^{-1}. B), C) and D) display the constituent percentile split of each of the concentrations displayed in A.

Speciation model 2

In the Speciation model 2, the minerals that form are different to those in an oxic environment, most minerals are alteration minerals/clay minerals, no iron minerals precipitate (Table S6.4). The other difference is the total iron available in the solution, which is available to precipitate iron-rich minerals. Fe^{2+} is the dominant iron ion amounting 0.27 mg.L^{-1}, yet Fe^{3+} trails slightly at 0.18 mg.L^{-1} (Figure 6.5A). Prussian blue does not form in the absence of oxygen and Turnbull's blue is the main consumer of available iron.

Figure 6.5B displays the distribution of the cyanide into compounds. 99 % (mean) of the cyanide forms $Fe_3^{2+}[Fe^{3+}(CN)_6]_2$ (Turnbull's blue), 0.7 % (mean) forms HCN, 0.1 % (mean) forms CN^- and 0.3 % (mean) forms $Fe(CN)_6^{4-}$.

Fe^{2+} distribution into compounds, is presented in Figure 6.5C. The main portion of the Fe^{2+} concentration (mean) formed $Fe_3^{2+}[Fe^{3+}(CN)_6]_2$ (Turnbull's blue) at 99.5 %. The remaining 0.5 % $Fe(CN)_6^{4-}$, Fe^{2+}, $FeSO_4$, $FeCO_3$, $FeHCO_3^+$, $FeOH^+$, $FePO_4^-$, $FeHPO_4$, $Fe(OH)_2$, $Fe(OH)_3^-$, $Fe(OH)_4^{2-}$, $FeH_2PO_4^+$ and finally $Fe_4^{3+}[Fe^{2+}(CN)_6]_3$ (Prussian blue constituting 1x10^{-15} %). The distribution of the Fe^{3+} was not included in Figure 6.5 due to its complete consumption by $Fe_3^{2+}[Fe^{3+}(CN)_6]_2$ (Turnbull's blue). Table S6.5 displays the results produced from the Speciation models 1 and 2 using the mineralogical data in Table 6.2.

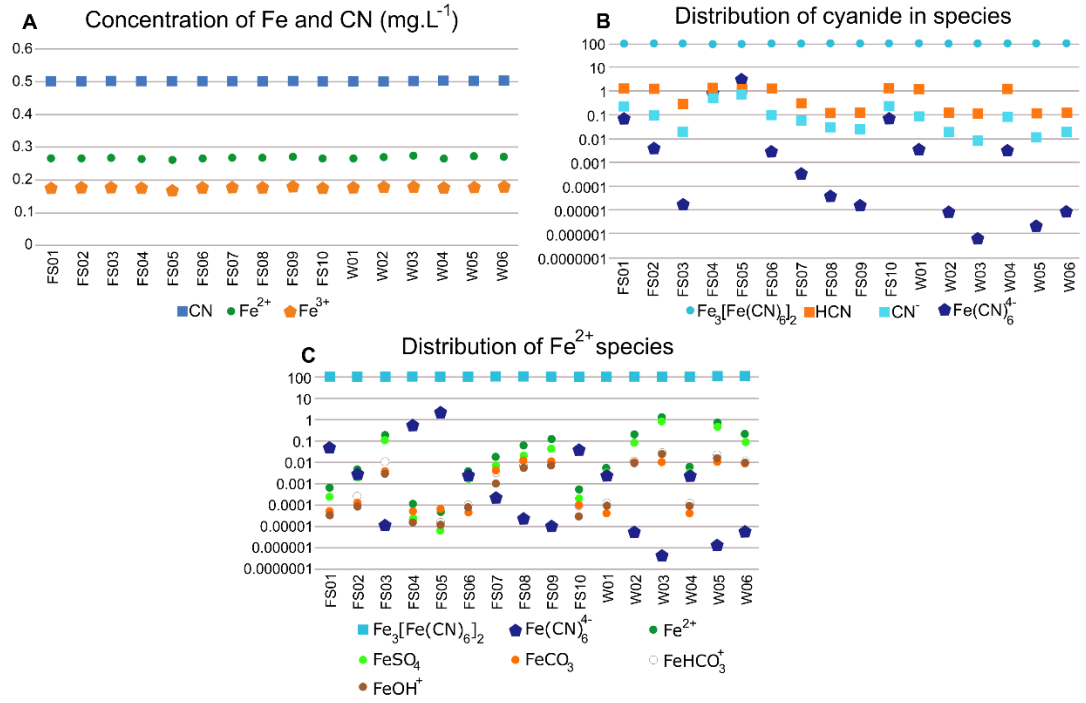

Figure 6.5: A) A graph displaying the cyanide and iron concentrations of the anoxic Speciation model 2. The concentrations were split into the proportions of different compounds with B) representing cyanide distribution, and C) Fe^{2+} distribution.

Sensitivity analysis

In the sensitivity analysis the input parameters of Speciation models 1 and 2 were altered. This included altering the cyanide concentration in solution, as well as the pyrite, calcite and gypsum concentrations. This was completed on the average

concentrations of the mineralogy of the 16 samples in an oxic and anoxic environment. Other conditions remained were the same as the other models.

Increasing the cyanide concentration in solution from 0.5 (Best Practice limit) to 15000 $mg.L^{-1}$, resulted in a gradual decreased in the Fe^{3+} from 9140 gradually to 5190 $mg.L^{-1}$ where it stabilized (Figure 6.6A). The Fe^{2+} contrarily increased from $1.71x10^{-4}$ to 3.89 $mg.L^{-1}$ where it stabilized (Figure 6.6A). At a cyanide concentration of 0.5 $mg.L^{-1}$, HCN and Prussian blue utilized the most cyanide, Fe^{2+} is mostly consumed by Prussian blue and Fe^{3+} is consumed by $Fe_3(OH)_4^{5+}$. Cyanide concentrations >5761 $mg.L^{-1}$, Prussian blue utilized most of the cyanide and iron. From concentrations >11394 $mg.L^{-1}$, HCN utilized the most cyanide. The pH slightly decreased from 2.97 to 2.89 at stabilization in this model (Figure 6.6C).

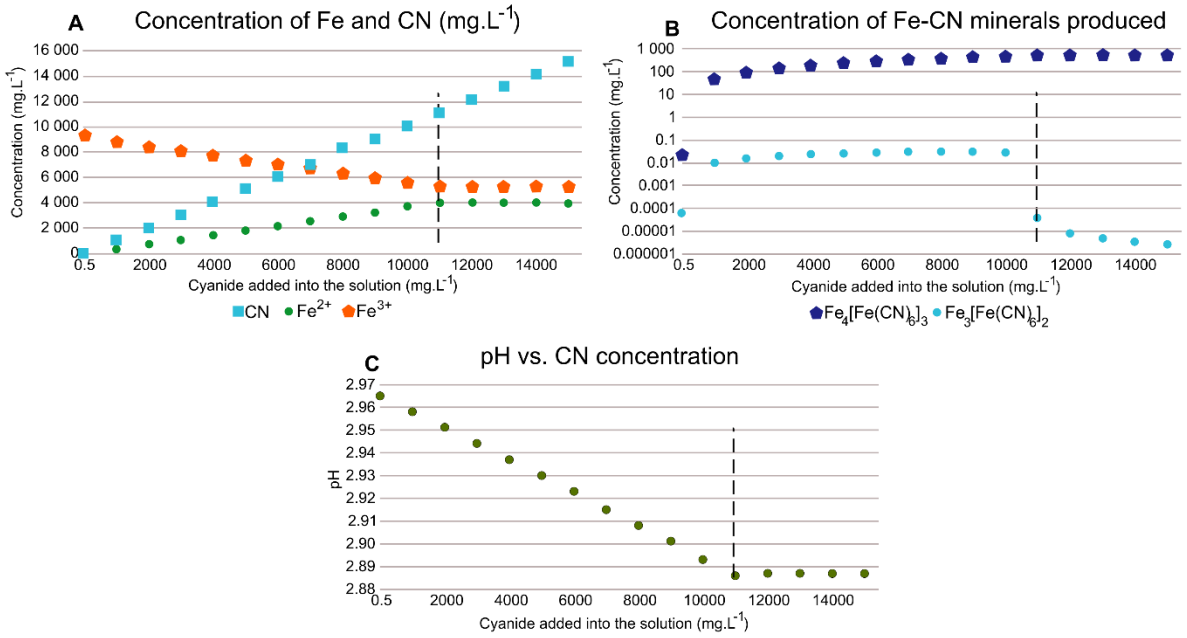

Figure 6.6: Graphs displaying the evolution of the sensitivity analysis model as the cyanide in solution increased with A) Fe^{2+} and Fe^{3+} progression, B) Prussian blue and Turnbull's blue precipitation, and C) pH. The dashed line in each of the graphs represents the point where Turnbull's blue ceased precipitation.

Changes were more drastic in an anoxic environment than an oxic environment (Figure 6.7). The cyanide in solution was increased from 0.5 $mg.L^{-1}$ to 3000 $mg.L^{-1}$. Initially, both Fe^{2+} and Fe^{3+} increase with an increase in cyanide, yet the changes for Fe^{3+}, which decreases >1000 $mg.L^{-1}$ (Figure 6.7A). Turnbull's blue used the highest concentration of cyanide and iron in this model, which changed to $Fe(CN)_6^{4-}$. The

change in concentration of Prussian and Turnbull's blue with an increase in cyanide in solution can be viewed in Figure 6.7B. The maximum Turnbull's blue produced was 24.25 mg.L^{-1}. The pH slightly decreased from 8.17 (0,5 mg.L^{-1} cyanide in solution) to 7.78 (3000 mg.L^{-1} cyanide in solution) (Figure 6.7C). The same occurred with the pE, decreasing from -4.63 to -4.58.

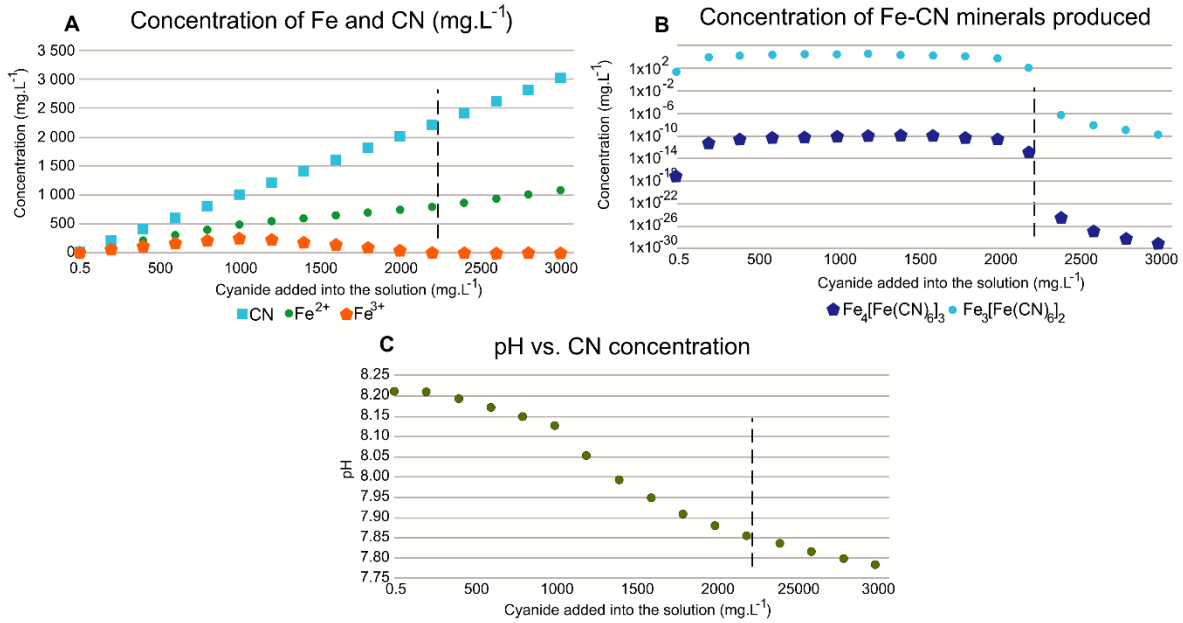

Figure 6.7: The evolution of concentrations and pH with an increase in cyanide concentration in solution with A) Fe^{2+} and Fe^{3+} progression, B) Prussian blue and Turnbull's blue precipitation, and C) pH. The dashed line in each of the graphs represents the point where Prussian and Turnbull's blue ceased precipitation.

With an increase in pyrite concentration in an oxic environment, the pH decreased, Prussian and Turnbull's blue concentrations increased followed by a decrease till Prussian blue ceased precipitating and Turnbull's blue sharply increased. At this point the concentration of Fe^{2+} increased immensely and Fe^{3+} dropped immensely at ~2.5 mol. Increase in calcite in an oxic environment increased the pH and this decreased the production of HCN, expected as the calcite buffers the pH. The precipitation of Prussian blue remained constant, contrarily the precipitation of Turnbull's blue increased. An increase in gypsum did not affect the model.

6.5 Discussion

The lack of precipitation of Prussian blue or Turnbull's blue according to the modelling with data from Ghosh et al. (1999a) and Sehmel (1989) was unexpected as literature

mentions that there is a high probability for iron-cyanide compounds to form in the tailings environment. According to Wei et al. (2018), cyanide in soils in an oxic environment, thermodynamically prefer species such as ferricyanide $[Fe(CN)_6]^{3-}$ and ferrocyanide $[Fe(CN)_6]^{4-}$. Ghosh et al. (1999a) iterates this by mentioning that there is a high possibility that iron-cyanide compounds and Fe^{3+} hydroxides will form in a tailings dam environment. Mansfeldt and Höhener (2016) state that the majority of cyanide released into the environment is chemically connected to iron as iron-cyanide compounds. Evidence of a blue precipitate, thought to be Prussian blue, has been found in tailing samples (Jambor et al., 2009; Bakatula and Tutu, 2016). $logK_{eq}$ values are sensitive to the specific environment, thus being the reason for the different $logK_{eq}$ values added to the database in this study compared to values available in literature. The $logK_{eq}$ values are sensitive to aqueous complexation and to the high salinity of the environment. The authors thus proposed these $logK_{eq}$ values for goldmine tailings dam environments.

Zagury et al. (2004) mentions that cyanide is able to form the following species: free cyanide (CN^- and HCN), readily soluble cyanide (KCN, NaCN), Weak Acid Dissociable cyanide (CN_{WAD} - contain nickel, copper, zinc and cadmium) and Strong Acid Dissociable cyanide (CN_{SAD} – contain silver, gold, copper and iron). CN_{WAD} dissociates at neutral to slightly acid pH conditions to free cyanide and CN_{SAD} dissociates in extreme acidic environments. According to the modelling in this study, in an oxic environment Prussian blue starts forming at a cyanide concentration in solution of $7.67x10^{-3}$ $mg.L^{-1}$ and at concentrations of 0.5 $mg.L^{-1}$ (Best Practice limit), Prussian blue consumed ~0.47 $mg.L^{-1}$ and Turnbull's blue consumed ~$1.61x10^{-3}$ $mg.L^{-1}$ cyanide. 94% of the cyanide that was added to the system formed part of CN_{SAD} compounds. The remaining 6% of the cyanide formed HCN and CN^-, which are free cyanide compounds.

Reasons for the preference of Prussian blue over Turnbull's blue can be explained by the theory of Kyle (1997), which states that in the Merrill-Crowe process, all ferricyanide $[Fe(CN)_6]^{3-}(aq)$ compounds will reduce to ferrocyanide $[Fe(CN)_6]^{4-}(aq)$. This method is performed in an oxic environment, which is the same environment of this model. Another reason is that Fe^{3+} hydroxides (such as goethite) form in tailings environments, mentioned by Ghosh et al. (1999a). According to the modelling,

goethite and hematite will form, consuming the Fe^{3+} ions, preventing the production of Turnbull's blue.

The average pH (2.9) is relatively acidic, which can be attributed to the dissociation of pyrite, mentioned in Hansen (2018). Pyrite along with O_2 and H_2O (equation 4) produces Fe^{3+} hydroxides, which agrees with the hypothesis above, along with H^+ ions (Hansen, 2018). The production of H^+ ions will then decrease the pH, which is the same effect that occurs in acid mine drainage.

$$FeS_2(s) + \frac{15}{4}O_2(aq) + \frac{7}{2}H_2O \rightarrow Fe(OH)_3(s) + 2SO_4^- + 4H^+ \quad (4)$$

The samples FS04, FS08, W02, W03, W04 and W05 had decreased amounts of HCN and increased amounts of Turnbull's blue produced, believed to be the effect of pH which is above 3. According to the modelling, an increase in cyanide in solution results in an increase in Prussian and Turnbull's blue till the available iron is consumed. At this point they plateau, at 20 $mg.L^{-1}$. Excess cyanide then forms HCN.

Iron−cyanide compounds are not predominantly toxic, but they have the ability to release toxic free cyanide compounds. This release may occur, according to Rader et al. (1993), when iron−cyanide compounds decompose by photolysis, see equations (5) and (6) (taken from Jaszczak et al., 2017), which will not be an issue in an anoxic environment.

$$Fe(CN)_6^{4-} + UVrad \rightarrow Fe(CN)_6^{3-} + CN^- \quad (5)$$

$$Fe(CN)_6^{3-} + 3H_2O + 3H^+ \leftrightarrow Fe(OH)_3(s) + 6HCN(aq) \quad (6)$$

An anoxic environment was included in this study due to this ability to dissociate, and in exploring other possible means for waste disposal (such as in a in a mine void). Turnbull's blue is the main cyanide compound that forms in the gold-tailings anoxic environment, consuming ~99 % of all cyanide. This is a CN_{SAD} compound, in addition to this, the pH is ~8.3 (average), assisting in the preservation of dissociation of iron-cyanide compounds. Only minuscule amounts of Prussian blue form, but the remaining 1 % forms HCN, CN^- and $Fe(CN)_6^{4-}$.

The concentration of Prussian and Turnbull's blue production in the system is dependent on the cyanide concentration and the available iron in solution. An anoxic

environment was determined to be a great environment for remediation over an oxic environment, as the pH is more basic and a larger percentage of cyanide produces iron-cyanide compounds. There is also less probability of being exposed to UV-radiation, preventing photolysis.

6.6 Conclusion

This study comprised an in-depth modelling investigation into the possibility of iron-cyanide compounds to form in gold-tailings environments. Modelling was completed using PHREEQC, adding the mineralogy of 16 tailings samples from the Free State goldfields tailings and 0.5 $mg.L^{-1}$ (Best Practice) of cyanide in solution. In an oxic environment, Prussian blue was the preferred compound, followed by HCN then Turnbull's blue. An oxic environment, along with the presence of pyrite, is perfect for acid mine drainage, which accounts for the production of an environment with a pH <3. Even though Prussian and Turnbull's blue are CN_{SAD} and tend to be stable compounds, the pH of this model, unfortunately creates a higher probability to dissociate, releasing free cyanide. The scenario in an anoxic environment was different, with Turnbull's blue being the preferred cyanide compound, consuming 99 % of all cyanide in the system. Such an environment produces a pH > 8 according to the model, which increases the probability for the CN_{SAD} compounds to remain stable.

It can be concluded that the precipitation of iron-cyanide compounds is affected by the presence of oxygen, the pH and concentrations of cyanide and iron available in solution. The cyanide concentration did not affect the precipitation of the iron-cyanide compounds above the available concentration of iron.

In conclusion, this study shows that a reducing environment is a possible solution for cyanide remediation. Owing to the pH conditions (>8), the ~99 % consumption of available cyanide and the low probability of exposure to photolysis. Such an environment is a mine void.

Further studies will include the addition of other metal-cyanide compounds to the database and the effect that they may have on the production of Prussian and Turnbull's blue. Also including the analysis of blue samples from a tailings dam. Additionally, an investigation into photocatalytic degradation such as the method

mentioned in Sekar et al. (2022), Rabandi et al. (2021) and Bathula et al. (2021) or a sorption process (Faisal et al., 2022).

Acknowledgments

The authors would like to thank Liesl van der Westhuizen for editorial assistance.

Funding: Funding of this study was supplied by Ipakade – NRF, DST and the CMBG

6.7 References

Acheampong M.A., Meulepas R.J.W., Lens P.N.L., 2010. Removal of heavy-metals and cyanide from gold mine wastewater. J. Chem. Technol. Biotechnol. 85, 590–613. https://doi.org/10.1002/jctb.2358

Anning C., Wang J., Chen P., Batmunkh I., Lyu X., 2019. Determination and detoxification of cyanide in gold mine tailings: A review. Waste Manag. Res. 37, 11, 1117-1126. https://doi.org/10.1177/0734242X19876691

Bakatula E.N., Tutu H., 2016. Characterization and speciation modelling of cyanide in effluent from an active slime dam. S. Afr. J. Chem. 69, 140-147. http://dx.doi.org/10.17159/0379-4350/2016/v69a17

Bathula C., Rabani I., Sekar S., Youi H., Choy J., Kadam A., Shretha N.K., Seo Y., Kim H., 2021. Enhanced removal of organic dye by activated carbon decorated TiO_2 nanoparticles from Mentha Aquatica leaves via ultrasonic approach. Ceram. Int. 47, 6, 8732-8739. https://doi.org/10.1016/j.ceramint.2020.12.282

Faisal A.A.H., Khalid Ramadhan Z., Al-Ansari N., Sharma G., Naushad N., Bathula C., 2022. Precipitation of (Mg/Fe-CTAB) - Layered double hydroxide nanoparticles onto sewage sludge for producing novel sorbent to remove Congo red and methylene blue dyes from aqueous environment. Chemospher. 291, 1, 132693. https://doi.org/10.1016/j.chemosphere.2021.132693

Frimmel H.E., Groves D.I., Kirk J., Ruiz J., Chelsey J., Minter W.E.L., 2005. The Formation and Preservation of the Witwatersrand Goldfields, the World's Largest Gold Province. Econ. Geol. 100th Anniversary Volume. 769–797. https://doi.org/10.5382/AV100.23

Ghosh R.S., Dzombak D.A., Luthy R.G., 1999a. Equilibrium Precipitation and Dissolution Behavior of Iron Cyanide Solids. Environ. Eng. Sci. 16, 4, 293-313. https://doi.org/10.1089/ees.1999.16.293

Ghosh R.S., Dzombak D.A., Luthy R.G., Smith J.R., 1999. In situ treatment of cyanide-contaminated groundwater by iron cyanide precipitation. Water Environ. Res. 71, 6, 1272-1228. https://doi.org/10.2175/106143096X122456

Hansen R.N., 2018. Inter-comparison geochemical modelling approaches and implications for environmental risk assessments: A Witwatersrand gold tailings source term characterisation study. Appl. Geochem. 95, 71-84. https://doi.org/10.1016/j.apgeochem.2018.05.017

Jambor J.L., Martin A.J., Gerits J., 2009. The post-depositional accumulation of metal-rich cyanide phases in submerged tailings deposits. Appl. Geochem. 24, 2256-2265. https://doi.org/10.1016/j.apgeochem.2009.09.011

Jaszczak E., Polkowska Z., Narkowicz S., Namieśnik J., 2017. Cyanide in the environment – analysis – problems and challenges. Environ. Sci. Pollut. Res. 24, 15929-15948. https://doi.org/10.1007/s11356-017-9081-7

Kenan A.O., Chirenje E., 2016. Uranium in South Africa: Exploration and supply capacity. Nat. Resour. Conserv. 4, 2, 25-33. https://doi.org/10.13189/nrc.2016.040201

Kruger A., 2019. Gold mining is far from dead- in SA, Webmoney, https://www.moneyweb.co.za/news/south-africa/gold-mining-is-far-from-dead-in-sa/ - (accessed 28 November 2019)

Kyle J.H., 1997. Stability of metal-cyanide and hydroxide complexes. World Gold ’97 Conference, 163-169.

Mansfeldt T., Höhener P., 2016. Isotopic Fingerprints of Iron−Cyanide Complexes in the Environment. Environ. Sci. Technol. 50, 7382−7388. https://doi.org/10.1021/acs.est.6b01565

Naicker K., Cukrowska E., McCarthy T.S., 2003. Acid mine drainage arising from gold mining activity in Johannesburg, South Africa and enviros. Environ. Pollut. 122, 1, 29-40. https://doi.org/10.1016/S0269-7491(02)00281-6

Parkhurst D.L., Appelo C.A.J., 2013. Description of Input Examples for PHREEQC Version 3 – a Computer Program for Speciation, Batch-reaction, One-dimensional Transport, and Inverse Geochemical Calculations. book 6, chapter A43. US Geological Survey Techniques and Methods, 497. available only at. http://pubs.usgs.goc/tm/06/a43/.

Rabani I., Zafar R., Subalakshmi K., Kim H., Bathula C., Seo Y., 2021, A facile mechanochemical preparation of Co_3O_4@g-C_3N_4 for application in supercapacitors and degradation of pollutants in water. J. Hazard. Mater. 407, 124360. https://doi.org/10.1016/j.jhazmat.2020.124360

Rader W.S., Solujic L., Milosavijevic E.B., Hendrix J.L., 1993. Sunlight-induced photochemistry of aqueous solutions of hexacyanoferrate(II) and -(III) ions. Environ. Sci. Technol. 27, 9, 7382−7388. https://doi.org/10.1021/es00046a016

Roche C., Thygesen K., Baker E., 2017. Mine tailings storage: Safety is no accident. A UNEP Rapid Response Assessment. United Nations Environment Programme and GRID-Arendal, Nairobi and Arendal. New York, US: Springer.

Rösner T., van Schalkwyk A., 2000. The environmental impact of gold mine tailings footprint in the Johannesburg region, South Africa. Bull. Engin. Geol. Environ. 59, 2, 137-148. https://doi.org/10.1007/s100640000037

Sekar S., Bathula C., Rabanid I., WooLee J., Hyun Lee S., Seo Y., Lee S., 2022. Enhanced photocatalytic crystal-violet degradation performances of sonochemically-synthesized AC-CeO_2 nanocomposites. Ultrason. Sonochem., v. 90, 106177. https://doi.org/10.1016/j.ultsonch.2022.106177

Schonfeld S.J., Winde F., Albrecht C., Kielkowski D., Liefferink M., Patel M., Sewram V., Stoch L., Whitaker C., Schüz J., 2014. Health effects in populations living around the uraniferous gold mine tailings in South Africa: gaps and opportunities for research. Cancer. Epidemiol. 38, 5, 628-632. https://doi.org/10.1016/j.canep.2014.06.003

Sehmel G.A., 1989. Cyanide and Antimony Thermodynamic Database for the Aqueous Species and Solids for the EPA-MINTEQ Geochemical Code. Rep., PNL-6835, Pac. Northwest Lab., Richland, Wash. https://doi.org/10.2172/6236700

Tucker R.F., Viljoen R.P., Viljoen M.J., 2016. A review of the Witwatersrand basin. J. Inter. Geosci. 39, 2, 105–133. https://doi.org/10.18814/epiiugs/2016/v39i2/95771

Wei Y., Du L., Deng X., Liu X., Mei X., Shi D., 2018. Alkaline-assisted leaching of iron-cyanide complex from contaminated soils. Chem. Eng. J. 354, 53–61. https://doi.org/10.1016/j.cej.2018.07.152

Zagury G.J., Oudjehani K., Deschênes L., 2004. Characterization and availability of cyanide in solid mine tailings from gold extraction plants. Sci. Total. Environ. 320, 211-224. https://doi.org/10.1016/j.scitotenv.2003.08.012

Supplementary data

Table S6.1: Initial inputs for each of the models.

Parameter	Speciation model 1	Speciation model 2	Sensitivity analysis
Solution pH	7	7	7
Solution pE	4	4	4
Solution T (°C)	25	25	25
Cyanide in solution	0.5 $mg.L^{-1}$	0.5 $mg.L^{-1}$	Varying from 0.5 to 15 000 $mg.L^{-1}$
Gas phase	21 % O_2 and 79 % N_2	100 % N_2	Both a) 21 % O_2 and 79 % N_2 and b) 100 % N_2
Equilibrium phases/mineralogical phases	All phases from the QEMSCAN results	All phases from the QEMSCAN results	Average of phases from the QEMSCAN results. Pyrite, calcite and gypsum were increased.

Table S6.2: Mineralogical data from different tailing dams in the Free State goldfields (bdl – below detection limit)

	Tailings dams (wt%)															
Mineral	**FS01**	**FS02**	**FS03**	**FS04**	**FS05**	**FS06**	**FS07**	**FS08**	**FS09**	**FS10**	**W01**	**W02**	**W03**	**W04**	**W05**	**W06**
Quartz	78.61	75.31	73.56	69.36	78.37	81.07	82.84	74.80	77.47	78.19	76.43	69.26	73.33	75.94	64.61	78.16
Pyrophyllite	7.24	11.86	9.59	2.90	10.90	5.67	8.52	11.10	5.00	7.36	7.91	9.72	6.41	5.47	8.43	5.35
Mica	6.97	7.32	9.60	14.35	6.34	6.47	3.76	7.11	8.84	6.38	9.99	14.70	13.19	12.75	16.66	9.71
Chlorite	1.21	0.71	1.01	4.49	0.52	0.88	0.70	1.76	1.22	1.35	0.86	1.55	1.67	1.12	1.94	1.00
Plagioclase	0.84	0.48	0.72	1.36	0.29	0.23	0.42	0.69	0.38	0.70	0.59	0.64	0.60	0.55	0.99	0.52
Chloritoid	1.07	0.71	0.89	2.32	0.48	1.02	0.75	1.48	1.08	0.90	0.63	1.42	1.47	1.11	1.68	1.19
Amphibole	0.21	0.04	0.11	0.36	0.02	0.18	0.12	0.34	0.11	0.32	0.13	0.15	0.20	0.10	0.18	0.08
Pyroxene/Olivine	0.43	0.28	0.53	0.67	0.21	0.37	0.21	0.47	0.47	0.41	0.47	0.62	0.57	0.45	1.13	0.34
Zircon	0.10	0.01	0.07	0.03	0.05	0.02	0.11	0.07	0.02	0.02	0.11	0.06	0.07	0.10	0.05	0.13
Other silicates	0.19	0.03	0.05	0.87	0.34	0.10	0.17	0.24	0.14	0.30	0.07	0.19	0.12	0.07	0.24	0.12
Pyrite	2.18	2.02	2.28	2.41	1.75	2.58	1.79	0.96	4.40	2.67	0.88	0.25	0.61	1.05	1.21	1.59
Other sulphides	0.03	0.06	0.02	0.06	0.09	0.03	0.02	0.02	0.12	0.08	0.01	0.01	0.06	0.01	0.03	0.02
Fe-oxides	0.26	0.17	0.32	0.20	0.25	0.80	0.10	0.10	0.09	0.45	0.44	0.72	0.73	0.21	1.20	0.91
Rutile/Ilmenite	0.19	0.12	0.22	0.06	0.23	0.14	0.16	0.23	0.22	0.20	0.26	0.24	0.22	0.17	0.29	0.38
Other oxides	0.01	0.19	0.04	0.03	0.04	0.06	0.11	bdl	0.04	0.25	0.05	0.03	0.02	0.05	0.10	0.09
Dolomite	0.02	bdl	bdl	0.03	0.04	0.01	bdl	0.05	0.06	bdl	0.19	0.10	0.05	0.01	0.05	0.06
Calcite	0.25	0.01	0.08	0.41	0.03	0.06	0.07	0.36	0.11	0.16	0.01	0.01	0.01	bdl	0.10	0.08
Ankerite	bdl	bdl	0.01	bdl	Bdl	Bdl	0.01	0.04	0.01	0.01	bdl	0.03	0.01	bdl	0.01	0.02
Apatite	0.02	0.02	0.11	0.05	Bdl	0.01	0.02	0.03	bdl	0.03	0.01	0.01	0.01	0.01	0.01	0.02
Alunite	0.05	0.16	0.16	0.07	0.02	0.06	0.04	0.05	0.15	0.08	0.55	0.17	0.40	0.63	0.38	0.10
Gypsum	0.12	0.26	0.47	bdl	0.01	0.22	0.05	0.06	0.02	0.09	0.38	0.06	0.19	0.07	0.17	0.12
Other	0.02	0.23	0.16	0.02	0.04	0.02	0.05	0.02	0.04	0.03	0.03	0.05	0.05	0.13	0.24	0.03

Table S6.3: Speciation 1 modelling results displaying possible mineral precipitates produced for the minerals in Table 6.2 along with 0.5 mg.L^{-1} cyanide added to the solution and in an oxic environment. Initial conditions: pH 7, pE 4, temperature 25 °C. The grey blocks represent minerals that may precipitate

Minerals	Mineral composition	FS01	FS02	FS03	FS04	FS05	FS06	FS07	FS08	FS09	FS10	W01	W02	W03	W04	W05	W06
Anatase	TiO_2																
Berlinite	$AlPO_4$																
Boehmite	$AlO(OH)$																
CaZrO3	$CaZrO_3$																
CO_2(g)	CO_2 (g)																
Diaspore	$AlO(OH)$																
Gibbsite	$Al(OH)_3$																
Goethite	$Fe^{3+}O(OH)$																
Hematite	Fe_2O_3																
Jarosite	$KFe_3(SO_4)_2(OH)_6$																
Jarosite Na	$NaFe_3(SO_4)_2(OH)_6$																
Kaolinite	$Al_2Si_2O_5(OH)_4$																
Nontronite Ca	$Ca_{0.165}Fe2Al_{0.33}Si_{3.67}H_2O_{12}$																
Nontronite H	$H_{0.33}Fe_2Al_{0.33}Si_{3.67}H_2O_{12}$																
Nontronite K	$K_{0.33}Fe_2Al_{0.33}Si_{3.67}H_2O_{12}$																
Nontronite Mg	$Mg_{0.165}Fe_2Al_{0.33}Si_{3.67}H_2O_{12}$																
Nontronite Na	$Na_{0.33}Fe_2Al_{0.33}Si_{3.67}H_2O_{12}$																
Prussian blue	$Fe_4[Fe(CN)_6]_3$																
Rutile	TiO_2																
Strengite	$FePO_4{:}2H_2O$																
Turnbull's blue	$Fe_3[Fe(CN)_6]_2$																

Table S6.4: Possible precipitates in an anoxic environment produced from Speciation model 2 of the minerals in Table 6.2 when exposed to 0.5 mg.L^{-1} CN^{-} in solution. Initial conditions: pH 7, pE 4, temperature 25 °C. The grey blocks are representative of the minerals that may precipitate

Minerals	Mineral composition	FS01	FS02	FS03	FS04	FS05	FS06	FS07	FS08	FS09	FS10	W01	W02	W03	W04	W05	W06
Amesite 14A	$Mg_4Al_4Si_2O_{10}(OH)_8$																
Anatase	TiO_2																
Antigorite	$Mg_{48}Si_{34}O_{85}(OH)_{62}$																
Beidellite Ca	$Ca_{0.165}Al_{2.33}Si_{3.67}O_{10}(OH)_2$																
Beidellite Mg	$Mg_{0.165}Al_{2.33}Si_{3.67}O_{10}(OH)_2$																
Beidellite Na	$Na_{0.165}Al_{2.33}Si_{3.67}O_{10}(OH)_2$																
Boehmite	AlO_2H																
$CaZrO_3$	$CaZrO_3$																
Chrysotile	$Mg_3Si_2O_5(OH)_4$																
Clinochlore 14A	$Mg_5Al_2Si_3O_{10}(OH)_8$																
Clinoptilolite Ca	$Ca_{1.7335}Al_{3.45}Fe_{0.017}Si_{14.533}O_{36}{\cdot}10.922H_2O$																
Clinoptilolite hy Ca	$Ca_{1.7335}Al_{3.45}Fe_{0.017}Si_{14.533}O_{36}{\cdot}11.645H_2O$																
Clinoptilolite hy Na	$Na_{3.467}Al_{3.45}Fe_{0.017}Si_{14.533}O_{36}{\cdot}10.877H_2O$																
Clinoptilolite Na	$Na_{3.467}Al_{3.45}Fe_{0.017}Si_{14.533}O_{36}{\cdot}10.922H_2O$																
Diaspore	$AlHO_2$																
Dolomite	$CaMg(CO_3)_2$																
Dolomite ord	$CaMg(CO_3)_2$																
Gibbsite	$Al(OH)_3$																
Gismondine	$Ca_2Al_4Si_4O_{16}{\cdot}9H_2O$																
Kaolinite	$Al_2Si_2O_5(OH)_4$																
Laumontite	$CaAl_2Si_4O_{12}{\cdot}4H_2O$																
Mesolite	$Na_{0.676}Ca_{0.657}Al_{1.99}Si_{3.01}O_{10}{\cdot}2.647H_2O$																
Montmorillonite Ca	$Ca_{0.165}Mg_{0.33}Al_{1.67}Si_4O_{10}(OH)_2$																
Montmorillonite K	$K_{0.33}Mg_{0.33}Al_{1.67}Si_4O_{10}(OH)_2$																
Montmorillonite Mg	$Mg_{0.495}Al_{1.67}Si_4O_{10}(OH)_2$																
Montmorillonite Na	$Na_{0.33}Mg_{0.33}Al_{1.67}Si_4O_{10}(OH)_2$																
Nontronite Ca	$Ca_{0.165}Fe_2Al_{0.33}Si_{3.67}H_2O_{12}$																
Nontronite Mg	$Mg_{0.165}Fe_2Al_{0.33}Si_{3.67}H_2O_{12}$																
Nontronite Na	$Na_{0.33}Fe_2Al_{0.33}Si_{3.67}H_2O_{12}$																
Paragonite	$NaAl_3Si_2O_{10}(OH)_2$																
Ripidolite 14A	$Mg_3Fe_2Al_2Si_3O_{10}(OH)_8$																
Rutile	TiO_2																
Saponite Ca	$Ca_{0.165}Mg_3Al_{0.33}Si_{3.67}O_{10}(OH)_2$																
Saponite H	$H_{0.33}Mg_3Al_{0.33}Si_{3.67}O_{10}(OH)_2$																
Saponite K	$K_{0.33}Mg_3Al_{0.33}Si_{3.67}O_{10}(OH)_2$																
Saponite Mg	$Mg_{3.165}Al_{0.33}Si_{3.67}O_{10}(OH)_2$																
Saponite Na	$Na_{0.33}Mg_3Al_{0.33}Si_{3.67}O_{10}(OH)_2$																
Scolecite	$CaAl_2Si_3O_{10}{\cdot}3H_2O$																
Stilbite	$Ca_{1.019}Na_{0.136}K_{0.006}Al_{2.18}Si_{6.82}O_{18}{\cdot}7.33H_2O$																
Talc	$Mg_3Si_4O_{10}(OH)_2$																
Turnbull's blue	$Fe_3[Fe(CN)_6]_2$																

Table S6.5: Results produced from the Speciation models 1 and 2 according to the mineralogical data summarised in Table 6.2.

	Speciation model 1					Speciation model 2				
	pH	**pE**	**CN^- concentration ($mg.L^{-1}$)**	**Fe^{2+} concentration ($mg.L^{-1}$)**	**Fe^{3+} concentration ($mg.L^{-1}$)**	**pH**	**pE**	**CN^- concentration ($mg.L^{-1}$)**	**Fe^{2+} concentration ($mg.L^{-1}$)**	**Fe^{3+} concentration ($mg.L^{-1}$)**
FS01	2.76	17.81	0.50	0.17	10878.61	8.43	-4.77	0.50	0.26	0.18
FS02	2.85	17.71	0.50	0.17	9867.81	8.04	-4.24	0.50	0.26	0.18
FS03	2.93	17.63	0.50	0.17	11498.49	8.00	-4.06	0.50	0.27	0.18
FS04	3.16	17.38	0.50	0.17	11498.49	8.78	-5.26	0.50	0.26	0.17
FS05	2.77	17.81	0.50	0.17	9013.38	8.99	-5.55	0.50	0.26	0.17
FS06	2.56	18.01	0.50	0.16	12565.13	8.05	-4.27	0.50	0.26	0.18
FS07	2.60	17.98	0.50	0.16	8946.37	8.48	-4.68	0.50	0.27	0.18
FS08	3.08	17.47	0.50	0.17	5428.69	8.58	-4.81	0.50	0.27	0.18
FS09	2.61	17.95	0.50	0.17	21483.57	8.47	-4.65	0.50	0.27	0.18
FS10	2.72	17.85	0.50	0.17	13212.93	8.44	-4.78	0.50	0.26	0.18
W01	3.00	17.57	0.50	0.17	5051.74	7.99	-4.16	0.50	0.26	0.18
W02	3.08	17.48	0.50	0.17	2120.43	8.37	-4.51	0.50	0.27	0.18
W03	3.08	17.48	0.50	0.17	3676.28	8.00	-4.00	0.50	0.27	0.18
W04	3.07	17.49	0.50	0.17	5527.54	7.98	-4.15	0.50	0.26	0.18
W05	3.12	17.43	0.50	0.17	6746.08	8.13	-4.16	0.50	0.27	0.18
W06	2.89	17.68	0.50	0.17	8868.19	8.37	-4.50	0.50	0.27	0.18
Mean	2.89	17.67	0.50	0.17	9148.98	8.32	-4.53	0.50	0.27	0.18

Chapter 7

Re-evaluation of the stability of Prussian blue and Turnbull's blue – implications for the Witwatersrand gold-tailings environment

Megan D. Welman-Purchase[a,*], Robert N. Hansen[b]

[a] University of the Free State, Department of Geology, Bloemfontein, South Africa

[b] University of the Free State, Centre for Mineral Biogeochemistry, Bloemfontein, South Africa

*Corresponding author.

Email address: purchasemd@ufs.ac.za (MD Welman-Purchase).

Abstract

Cyanide, which has a high affinity for gold, has been used since 1889 in the gold extraction process. This creates the possibility for contamination of cyanide into the gold-tailings dam environment. Cyanide also has a high affinity for iron, which is available in the tailings dams. The aim of this study was to experimentally determine if a blue substance will form in different samples, followed by analysing them and finally to re-examine pH vs pE diagrams of an iron and cyanide environment. Methodologically XRD, FT-IR and XPS were used to analyse all blue products forms and PHREEPLOT was used for the modelling of the pH vs pE diagrams. FT-IR works well to determine the presence of an iron-cyanide bond and XPS can be used to obtain a general Fe^{2+}:Fe^{3+} ratio. The modelling showed that an increase in iron concentration increases the stability fields of iron-hydroxide compounds/complexes and an increase in cyanide concentration increases the stability fields of Prussian/Turnbull's blue. Yet iron that is available to react is still important for the precipitation of Prussian/Turnbull's blue, where the oxidation of pyrite produces this requirement. Prussian blue forms in an oxic environment and Turnbull's blue in both an oxic and anoxic environment, but a combination of these two compounds may form. The implications that this has for a gold-mine tailings environment, is due to the presence of pyrite in the ores, there is a higher probability for Prussian/Turnbull's blue to form.

Keywords: Prussian blue, Turnbull's blue, geochemical modelling, XRD, FT-IR, XPS

7.1 Introduction

South Africa produces a large quantity of gold yearly (Rademan and Groot, 2012), which generates large revenues. The four top companies in South Africa extract approximately 100 tons annually (Kruger, 2019) at a gold price of over ZAR 900 per gram. At an average grade of 5 g/ton of gold, these four mining companies are producing an estimated 20 million tons of waste rock annually. To accompany this waste rock, the majority of the gold mines in South Africa use the Carbon in Leach (CIL) method for extraction, which utilizes cyanide. Post extraction, waste material is deposited on tailing dams facilities, where cyanide has been found on South African dumps at concentrations <200 $mg.kg^{-1}$ (Bakatula and Tutu, 2016).

The use of cyanide to extract gold began around 1889 (Dorr, 1936), which has since become the most popular extraction option worldwide, amounting to its use in ~90% of mining processes (Johnson, 2015). Gold leaching cyanide solutions are prepared using the salts, NaCN, $Ca(CN)_2$ or KCN dissolved in H_2O (Johnson, 2015). Cyanide has a high affinity for gold and a strong complex is formed between the CN^- and Au^+ ions, described by the Elsner equation (Kyle, 1997):

$$4Au + 8NaCN + O_2 + 2H_2O \rightarrow 4NaAu(CN)_2 + 4NaOH \quad (1)$$

$$4Au + 8KCN + O_2 + 2H_2O \rightarrow 4KAu(CN)_2 + 4KOH \quad (2)$$

The gold is then released from the $NaAu(CN)_2/KAu(CN)_2$ compound using zinc cementation (lead can also be used), seen in equation 3 (Kyle, 1997). The zinc or lead replaces the gold, resulting in the production of the cyanide compounds $NaZn(CN)_2/KZn(CN)_2$ and $NaCN$:

$$Zn + 3NaCN + NaAu(CN)_2 \rightarrow Au + Na_2Zn(CN)_4 + 2NaCN \quad (3)$$

$NaCN$ is a readily soluble cyanide compound and thus easily releases cyanide into solution. $NaZn(CN)_2$ and $KZn(CN)_2$ are weak acid dissociable cyanide (CN_{WAD}) compounds, which release cyanide when exposed to neutral or acidic conditions (Zagury et al., 2004). Readily soluble cyanide compounds and CN_{WAD} compounds are able to dissolve releasing cyanide into the environment surrounding these tailings dams and possibly the groundwater. Other cyanide containing complexes include free

cyanide, and strong acid dissociable cyanide (CN_{SAD}) compounds (Zagury et al., 2004).

CN_{SAD} compounds are the most stable of the different cyanide compounds (Johnson, 2015), suggesting that they are the most intriguing when considering the immobilize the cyanide. Examples of CN_{SAD} are iron-cyanide compounds. Cyanide also has a high affinity for iron, which is generally found in most sediments, ores and soils. The presence of cyanide and iron increases the probability for Prussian blue $Fe_4^{3+}[Fe^{2+}(CN)_6]_3$ to precipitate (Johnson, 2015). Turnbull's blue $Fe_3^{2+}[Fe^{3+}(CN)_6]_2$ is also a likely precipitate, which is isostructurally related to Prussian blue (Johnson, 2015). Depending on the environment, other iron-cyanide solids may form, including Prussian brown/green ($Fe^{3+}[Fe^{3+}(CN)_6](s)$) and Berlin white ($Fe_2^{2+}[Fe^{2+}(CN)_6](s)$), where Berlin white converts to Prussian blue in aerobic environments (Ghosh et al., 1999a). Jambor et al. (2009) and Bakatula and Tutu (2016) mention the presence of a blue substance, probably Prussian blue (or a similar compound) in their samples from Western Ontario and the Central Rand goldfields, respectively.

According to Ghosh et al. (1999b), Prussian blue forms due to equations 4 and 5:

$$4Fe^{3+} + 3Fe^{2+}(CN)_6^{4-} \leftrightarrow Fe_4^{3+}[Fe^{2+}(CN)_6]_3 \quad (4)$$

$$3Fe^{2+} + Fe^{3+} + 3Fe^{3+}(CN)_6^{3-} \leftrightarrow Fe_4^{3+}[Fe^{2+}(CN)_6]_3 \quad (5)$$

Turnbull's blue forms according to equation 6 (Ghosh et al., 1999a):

$$3Fe^{2+} + 2Fe^{3+}(CN)_6^{3-} \leftrightarrow Fe_3^{2+}[Fe^{3+}(CN)_6]_2 \quad (6)$$

Kyle (1997) proposed that the production of iron-cyanide compounds could be an option to prevent the contamination of cyanide (dissolved) into groundwater in a tailings environment, and proposed two means of production. Firstly, by the addition of ferrous sulphate to the slurry to encourage the formation of iron-cyanide compounds. Secondly, to promote the dissolution of weak and moderately strong cyanide compounds, followed by the production of iron-cyanide compounds (Kyle, 1997). These suggestions originate from the insolubility of iron-cyanide compounds, which only dissolve in extreme acidic conditions (Zagury et al., 2004). Meeussen et al. (1994) and Ghosh et al. (1999a) suggest that the insolubility increases as the pH increases.

Another variable that affects the solubility of iron-cyanide compounds is its exposure to UV-radiation, resulting in the formation of toxic components, such as free cyanide (Jaszczak et al., 2017). This decomposition can be seen in equations 7 and 8 (Jaszczak et al., 2017):

$$Fe(CN)_6^{4-} + UVrad \rightarrow Fe(CN)_6^{3-} + CN^- \quad (7)$$

$$Fe(CN)_6^{3-} + 3H_2O + 3H^+ \leftrightarrow Fe(OH)_3(s) + 6HCN(aq) \quad (8)$$

The aim of this study is to examine the probability for iron-cyanide compounds to form in different scenarios and the compounds that form. The scenarios include an empirical study, investigation of a blue sample from a gold mine tailings dam (from The Free State gold fields, South Africa) and adding cyanide to a milled pyrite and Witwatersrand gold tailings. Additionally, pH vs pE diagrams are modelled with varying iron and cyanide compositions, classifying the results of the empirical study.

7.2 Methodology

7.2.1 Sampling procedure

A sediment blue sample (2.1blue and without blue staining - 2.1) was obtained from a tailings dam close to Welkom, which forms a part of the Free State goldfields. The sample was stored in a sterile sample bag (from Lasec) at stored for further analysis.

7.2.2 Experimental procedures

Chemicals and materials

Iron sources used in the experiments include a natural pyrite sample, laboratory grade (CP – gold line from ACE chemicals) $FeSO_4$ and $Fe_2(SO_4)_3$; and AMIS0515 (a gold ore powdered reference material from African Minerals Standards). The cyanide sources were laboratory grade, NaCN and $K_3[Fe(CN)_6]$, supplied by Merck and $K_4[Fe(CN)_6]$ by ACE chemicals. The solute used was deionized water - 18.25MΩ. The volumetric flasks and beakers were of Lasec grade (A) type.

General experimental procedure

The empirical investigation involved the addition of cyanide to different iron sources. The first phase involved the production of Prussian and Turnbull's blue with as little other elements in the system as possible, as shown in equations 9 (Prussian blue)

and 10 (Turnbull's blue). Quantities of chemicals were calculated in order to produce approximately 15 g of product. The two reactants were dissolved separately in ~100 ml of deionized water. The two solutions were then added to each other and the solutions were filtered. Experiments were completed in triplicate, labelled PBS 1-3 for the Prussian blue samples and TBS 1-3 for the Turnbull's blue samples. The pH and pE readings were taken after the two solutions were added to each other. The reaction is spontaneous and the precipitates were immediately filtered, left to dry in fume cabinet.

$$3K_4[Fe(CN)_6] + 2Fe_2(SO_4)_3 \rightarrow Fe_4[Fe(CN)_6]_3 + 6K_2SO_4 \quad (9)$$

$$2K_3[Fe(CN)_6] + 3FeSO_4 \rightarrow Fe_3[Fe(CN)_6]_2 + 3K_2SO_4 \quad (10)$$

The next phase of the empirical investigation examined the viability of Prussian/Turnbull's blue to form in natural samples. This was completed by adding a solution of 0.4 g.L^{-1} NaCN (4.33 mmol.L^{-1} cyanide dissolved in deionized H_2O) to 5 wt% of iron in pyrite, AMIS0515 (Fe_2O_3 – 3.09 wt%) and tailings dam samples (sample 2.1 without blue material, and sample 2.1-blue with blue material). The pyrite was a commercial sample. Sample 2.1 and sample 2.1-blue were taken from a tailings dam in the Free State goldfields (2.1 denoted the sample without blue material and 2.1-blue contained blue material). The concentration of cyanide and iron were sourced from Rademan and Groot (2012), which is based on the iron content of the Witwatersrand reef composition and the concentration of the cyanide is based on solution used in gold extraction. The pH and pE readings were taken using a Mettler Toledo FiveGo pH meter F2 after the addition of the NaCN solution to the iron-source.

7.2.3 Analytical procedures

X-ray diffractometer (XRD) analysis

The samples PBS 1-3, TBS 1-3, 2.1, 2.1-blue, pyrite (pre and post cyanide addition) and AMIS515 were milled using an agate mortar and pestle then analysed using a Malvern-PANalytical Empyrean XRD with Cu-Kα radiation and an X-Celerator detector. Analyses occurred from 3.5° to 70° 2θ at 40 mA and 45 kV on a silicon-zero background sample holder. The program used to collect the diffractograms was Data Collector and the interpretation completed using Highscore with the data base ICDD-PDF2-2021.

Fourier transform infrared (FT-IR) analysis

A Thermo Scientific Nicolet 6700 FT-IR was used to observe the bonds produced in the experiments. The samples PBS1, TBS1, pyrite with cyanide contamination and 2.1-blue were analysed. A pressed pellet was produced using 0.2 g of KBr and 0.001 g of sample. The powder was milled and then pressed to 10 tons of pressure to produce the pellet. A KBr pellet was also produced to determine the background of the analysis. Analysis was completed using a DTGS TEC detector, producing results in Transmittance format. Sixty-four scans were taken for each analysis with a resolution of four between the range 4000 – 400 wavenumber^{-1}.

X-ray photoelectron spectrum (XPS) analysis

XPS analyses was carried out on the samples PBS1, TBS1, pyrite with cyanide contamination, 2.1-blue and 2.1 using a PHI 5000 Scanning ESCA Microprobe. The X-ray source had an aluminium anode for X-ray generation and a quartz crystal monochromator. Calibration of the binding energy was completed on the high energy peak of Cu2p3 at 932.62 eV and the low energy peak of Au4f7 at 83.96 eV. Each sample surface was cleaned before analysis. A full survey was completed for each sample as well high-resolution survey of the C1s, N1s and Fe2p regions. The parameters of the analysis are displayed in Table 7.1.

Table 7.1: Parameters of the XPS PHI 5000 Scanning ESCA Microprobe used for analysis of this study

Analysis type	Al X-ray beam	Ar ion beam	Details
Survey	100 µm, 25 W, 15 kV		187 eV pass energy, 100 ms.step^{-1}, 3 cycles, 9.3x10^{-10} Torr UHV base pressure
High resolution	100 µm, 25 W, 15 kV		0.5 eV energy resolution
Sputter		2 kV, 2 µA	1x1 mm raster sputter rate of ~ 15 nm.min^{-1}

Total cyanide analysis

Sample 2.1 (19.7 g) and sample 2.1-blue (17.1 g) were sent to XLab Earth, 259 Kent avenue, Ferndale, South Africa for total cyanide soil analysis.

7.2.4 Modelling procedures

The modelling was completed using PHREEPLOT and PHREEQC, which is a United States Geological Survey project developed by Parkhurst and Appelo (2013). All necessary species involving cyanide were added to the database with the thermodynamic data and references displayed in Table 7.2. The following scenarios were investigated:

- Scenario 1 – Cyanide and iron parameters used in Ghosh et al. (1999a): iron in excess (cyanide - 0.6 mmol.L^{-1} and iron - 0.5 mmol.L^{-1}) and not in excess (cyanide - 0.6 mmol.L^{-1} and iron - 0.2327 mmol.L^{-1}) in order to compare the modelling in this study to previous studies.
- Scenario 2 – Cyanide and iron parameters taken from Rademan and Groot (2012) (in order to produce models for a wholistic, realistic view) with the addition of 8.16 mmol NaCN (4.33 mmol of cyanide) and 1 kg sample (containing ~5 % Fe_2O_3) per 1 L solvent:
  a) Varying the amount of total dissolved iron, while cyanide remains constant at maximum cyanide content
  b) Varying the amount of total dissolved iron, while cyanide remains constant at 4.33 mmol content

  b) Varying the amount of total dissolved cyanide, while iron remains constant

All experiments (see Section 7.2.2 below) pH and pE results were plotted in the modelled diagrams.

Table 7.2: The logK_{eq} values used in the database of PHREEPLOT for the modelling of this study.

Reaction	logK_{eq}	Reference
$Fe^{2+}(CN)_6^{4-} = Fe^{2+} + 6CN^-$	-45.61	Sehmel (1989)
$Fe^{3+}(CN)_6^{3-} = Fe^{3+} + 6CN^-$	-52.63	Sehmel (1989)
$Fe_3^{2+}[Fe^{3+}(CN)_6]_2 = 3Fe^{2+} + 2Fe^{3+} + 12CN^-$	-181.45	Welman-Purchase (2023)
	-173.00	Ghosh et al. (1999a)
$Fe_4^{3+}[Fe^{2+}(CN)_6]_3 = 4Fe^{3+} + 3Fe^{2+} + 18CN^-$	-263.01	Welman-Purchase (2023)
	-257.00	Ghosh et al. (1999a)
$K_4[Fe(CN)_6] = 4K^+ + Fe^{2+} + 6CN^-$	-48.82	Sehmel (1989)
$K_3[Fe(CN)_6] = 3K^+ + Fe^{3+} + 6CN^-$	-54.68	Sehmel (1989)

7.3 Results

7.3.1 Experimental results

The pH and pE results from the production of Prussian and Turnbull's blue precipitates in the empirical study are summarized in Table 7.3 (Table S7.1 is a display of all of the results). The pH and pE results from the NaCN solution were 10.49 and -3.31, respectively. After the addition of the two solutions together, solutions revealed that Prussian blue had lower pH and slightly higher pE values compared to Turnbull's blue. These precipitates will be used as references for the production The pH of the pyrite sample, after adding the NaCN solution to milled pyrite, was similar to that of the Prussian blue sample. The addition of the NaCN solution to AMIS0515 produced thin layers of blue material. The sample 2.1 did not produce a blue material.

Table 7.3: Average pH, pE and temperature results of the empirical study results for Prussian blue (PBS), Turnbull's blue (TBS), pyrite, AMIS0515 and sample 2.1.

	Experimental results		
	pH	**pE**	**T (°C)**
PBS	2,5±0,25	4,8±0,24	24,8±0,40
TBS	4,2±0,12	3,2±0,11	28,2±0,45
Pyrite	2,84	4,01	23,6
AMIS0515	4,94	2	23,5
2.1	4,57	5,28	23,8

XRD results

The Prussian and Turnbull's blue samples analysed with XRD, are displayed in Figure 7.1 with a reference pattern taken from Ghosh et al. (1999b). The Prussian blue samples could not be distinguished from the Turnbull's blue samples as they are isostructural (Ghosh et al., 1999a). The sharp peaks that do not appear in the reference diffractogram are attributed to salts that formed during the drying of the sample and the additional K^+ and SO_4^{2-} ions in the system. The main peak for Prussian blue is located between 16° and 18° (I = 100%) and the second peak (I = 48%) is between 34° and 36° (Ghosh et al., 1999b).

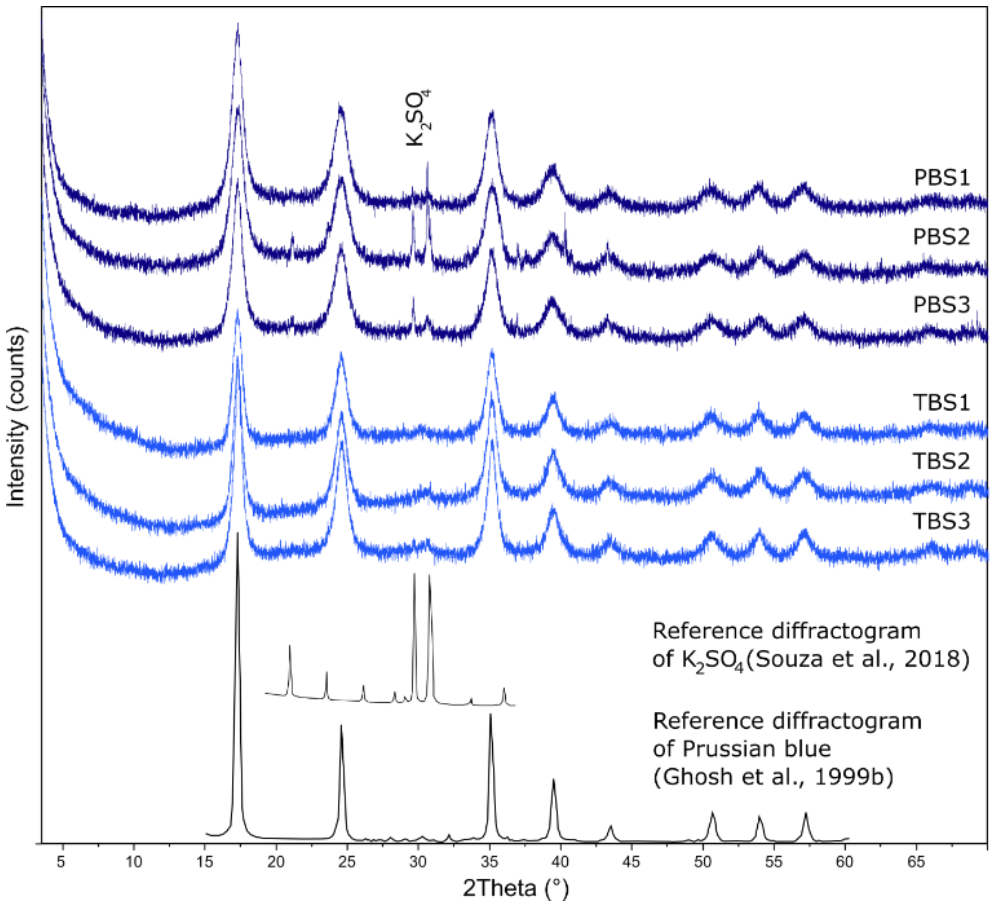

Figure 7.1: Diffractograms of the Prussian blue samples (PBS) and Turnbull's blue samples (TBS). The diffractograms are similar except for the presence of salts in the PBS samples. A reference diffractogram for reagent grade (Aldrich Chemical Company) Prussian blue modified after Ghosh et al. (1999b) was included and a reference diffractogram of K_2SO_4.

The XRD analysis showed that the pyrite sample prior to the addition of cyanide, semi-quantitatively contained pyrite (59 wt%), mica (30 wt%), quartz (7 wt%) and k-feldspar/rutile (4 wt%). K-feldspar and rutile have the same position for their main peak (Figure 7.2, diffractogram above). The second diffractogram in Figure 7.2 shows the same sample, after 0.4 $g.L^{-1}$ NaCN solution was added. In the diffractogram, the peaks of pyrite were still prominent, yet it appeared that there were peaks in the areas of the two main peaks of Prussian blue/Turnbull's blue.

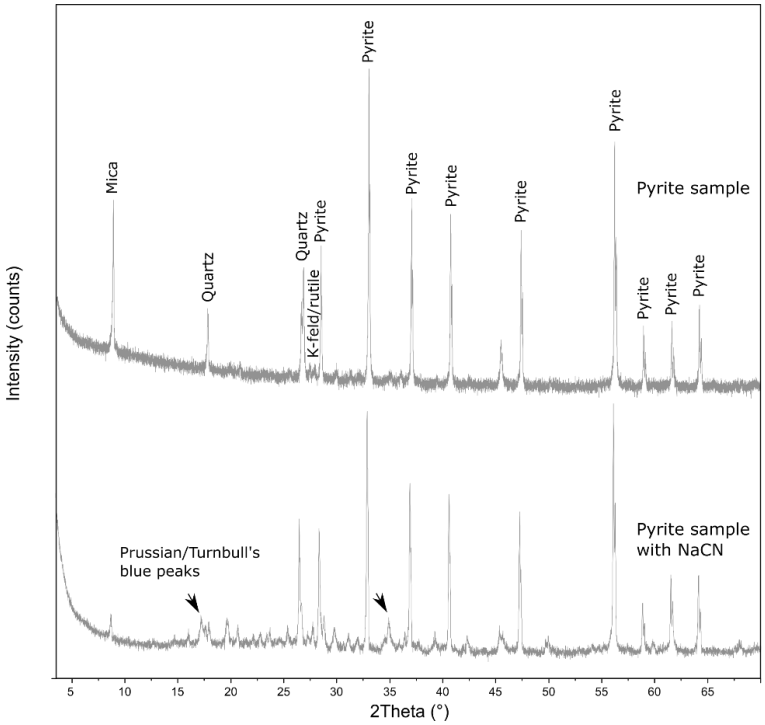

Figure 7.2: Diffractograms of the pyrite sample, before and after the addition of an NaCN solution.

The XRD analysis in Figure 7.3 showed that sample AMIS0515 semi-quantitatively consisted of quartz (56 wt%), talc (12 wt%), gypsum (9 wt%), jarosite (8 wt%), mica (8 wt%), pyrite (3 wt%), hematite (2 wt%) and plagioclase (2 wt%). There is a peak at the position of the main peak for Prussian blue. An image of the blue substance that formed is also shown.

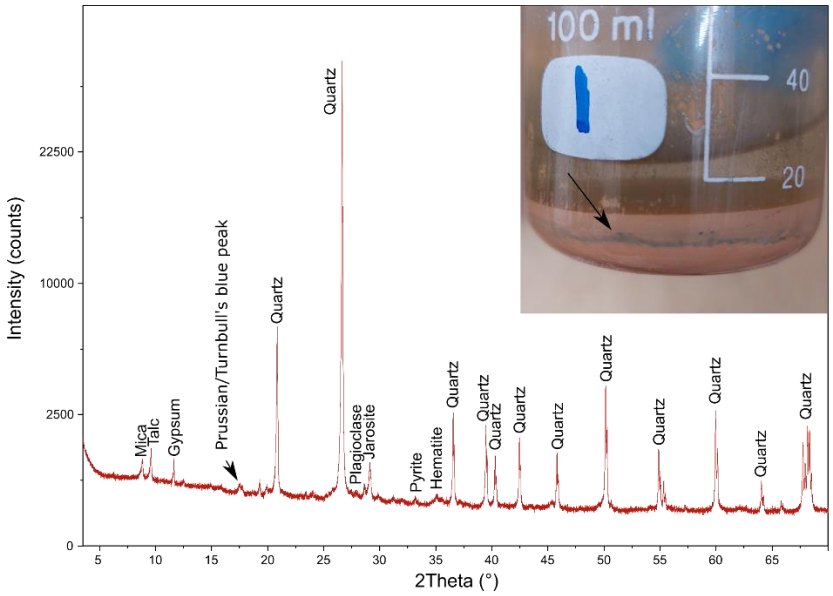

Figure 7.3: Diffractograms of sample AMIS0515, and an image of the blue substance that formed during the addition of the NaCN solution.

The diffractogram and image of sample 2.1-blue can be seen in Figure 7.4. During XRD sample preparation, an attempt was made to only analyse the blue material. The semi-quantitative results are quartz (54 wt%), calcite (12 wt%), talc (11 wt%), clinochlore (8 wt%), mica (8wt%), k-feldspar/rutile (4 wt%) and plagioclase (3 wt%). Unfortunately, the presence of Prussian or Turnbull's blue was too little to be observed in the diffractogram.

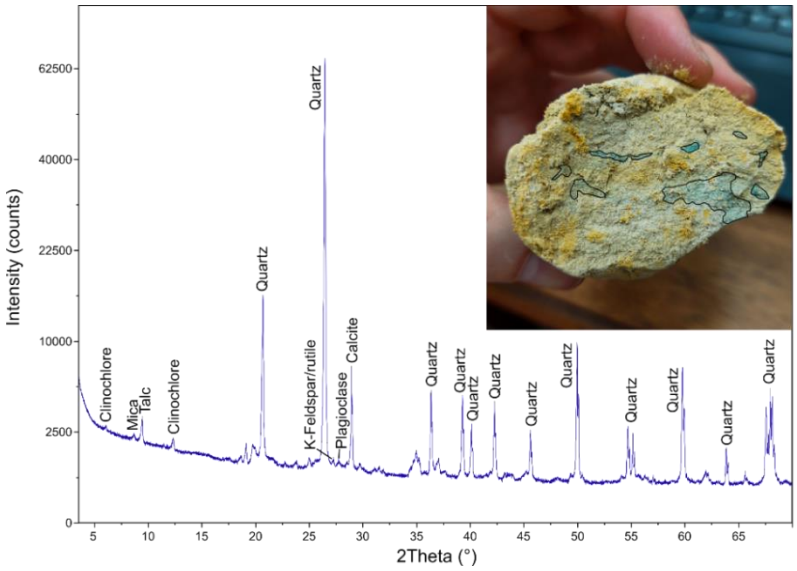

Figure 7.4: Diffractogram of a small portion of the blue material of Sample 2.1-blue found on a goldmine tailings dam in the Free State goldfields. No NaCN was added to this sample. The image of the sample is also displayed, where borders were drawn to highlight the blue material.

FT-IR results

The samples created in the experiments along with sample 2.1-blue were analysed with FT-IR. The results are displayed in Figure 7.5, along with a reference graph of Prussian blue (Institute of Chemistry University of Tartu, Estonia, 2021). The peaks at 3300 cm^{-1} are the H-O bonds, usually the hydration of the pellet as KBr readily absorbs moisture. The main peak of Prussian blue was at 2072 cm^{-1}, which according to Farah et al. (2012), denotes the iron-cyanide bond. This main peak for Prussian blue for PBS1, PBS2 and PBS3 is observed at 2085.10, 2083.85 and 2084.83 cm^{-1}, respectively, for TBS1, TBS2 and TBS3 found at 2103.16, 2082.77 and 2084.88 cm^{-1}, respectively. The cyanide doped pyrite sample (2081.56 cm^{-1}) and sample 2.1-blue (2084.16 cm^{-1}) also revealed such peaks. The peak at 1069.88 cm^{-1} of sample 2.1-

blue might have indicated the presence of quartz, which was expected as the sample consisted mostly of quartz.

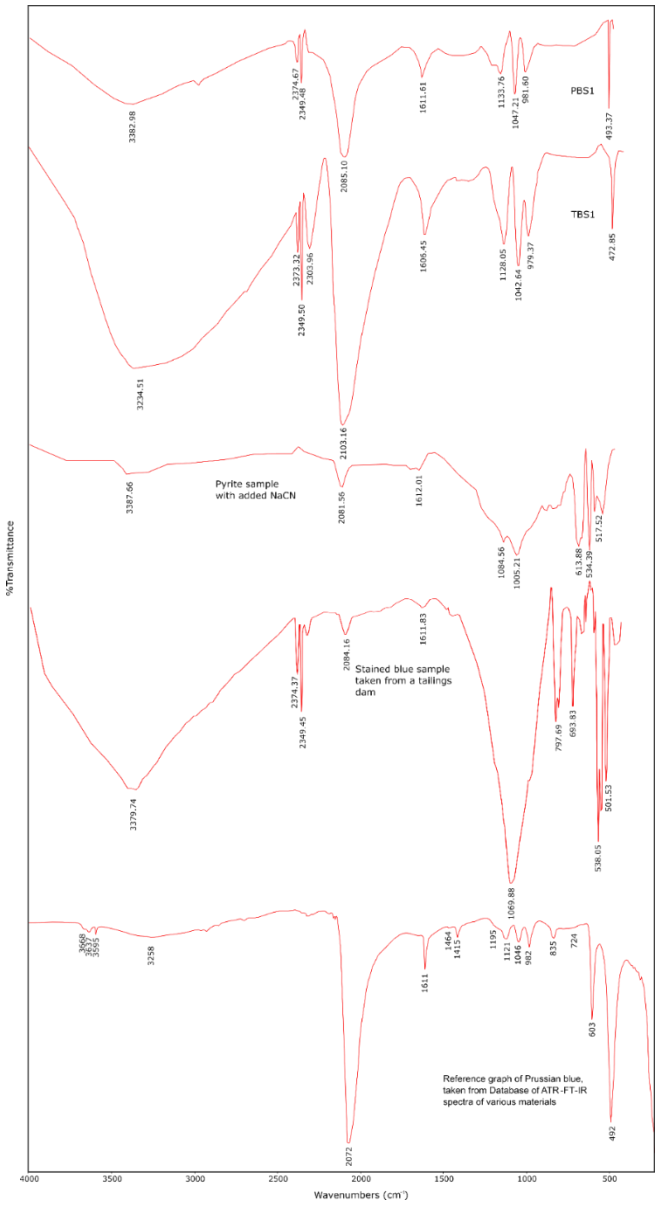

Figure 7.5: Fourier transform-infrared (FT-IR) graphs in order of PBS1, TBS1, pyrite samples doped with an NaCN solution, sample 2.1-blue (blue sample from a gold-mine tailings dam) and reference graph of Prussian blue (Institute of Chemistry University of Tartu, Estonia, 2021).

XPS results

One Prussian blue sample (PBS1), one Turnbull's blue sample (PBS2), pyrite sample doped with NaCN, sample 2.1 and sample 2.1-blue were submitted for XPS analysis. The 2.1 and 2.1-bue samples are the original samples collected, no cyanide was added to them. The full survey scan can be observed in Figure 7.6, where the red scan

was prior to cleaning (sputtered) of the surface and the blue scan after cleaning. Iron, carbon and nitrogen (Prussian and Turnbull's blue), with additional potassium, sulfur and oxygen (from chemical reagents used in the experiments) were found in PBS1 and TBS1. The pyrite sample consisted of iron and sulfur (pyrite), with additional potassium, silica, aluminium and oxygen (quartz, K-feldspar, mica). The presence of carbon and nitrogen indicated an iron-cyanide compound. Sample 2.1-blue contained magnesium, sodium, iron, silica, aluminium, sulfur and oxygen. Carbon was present but a very low concentration of nitrogen was found. Sample 2.1 consisted of the same chemicals as sample 2.1-blue, without sulfur. The KLL and LMM peaks are Auger lines and pertain to vacancies in the different electron-shells (Moulder et al., 1992).

The XPS measured atomic percentages from the full scan. Only the results for PBS1 and TBS1 are discussed here, as they are monomineralic (Table 7.4). The theoretical ratio of Fe:C/Fe:N (carbon to nitrogen ratio is the same) for Prussian blue is 1:2.6 and for Turnbull's blue is 1:2.4. The ratios from the results of the XPS are 1:5.6 and 1:2.4 (Fe:C) for Prussian and Turnbull's blue, respectively and 1:2.7 and 1:1.1 (Fe:N) for Prussian and Turnbull's blue, respectively.

Table 7.4: Atomic percentage results obtained from X-ray photoelectron spectrum (XPS) analyses. The calculated atomic ratios for Prussian and Turnbull's blue were also added for comparison purposes.

Sample	Compound	XPS result (at%)	Calculated results (at%)	Fe:C ratio	Fe:N ratio
PBS1 (Prussian blue)	C1s	56	42	1:5.6 (calculated - 1:2.6)	1:2.7 (calculated - 1:2.6)
	N1s	27	42		
	O1s	6			
	Fe2p3	10	16		
	K2p	2			
TBS1 (Turnbull's blue)	C1s	50	41	1:2.4 (calculated - 1:2.4)	1:1.1 (calculated – 1:2.4)
	N1s	23	41		
	O1s	4			
	Fe2p3	21	17		
	K2p	1			

The high-resolution surveys were taken of the areas C1s (Figure 7.7), N1s (Figure 7.8) and Fe2p (Figure 7.9). There is a difference between PBS1 and TBS1, whereas 2.1-blue and the Pyrite sample seem to mimic that of TBS1 with different peak heights.

According to Wu et al. (2015), who completed XPS analysis on Prussian blue microcubes, the main C1s peak is at 284.18 eV. The cyanide peak, according to Delpeux et al. (1998), is at 285.7 eV. The main peak for PBS1, TBS1, pyrite and sample 2.1-blue were found at 284.9, 285.1, 285.8 and 285.3 eV, respectively. These are believed to be the triple-bond of cyanide.

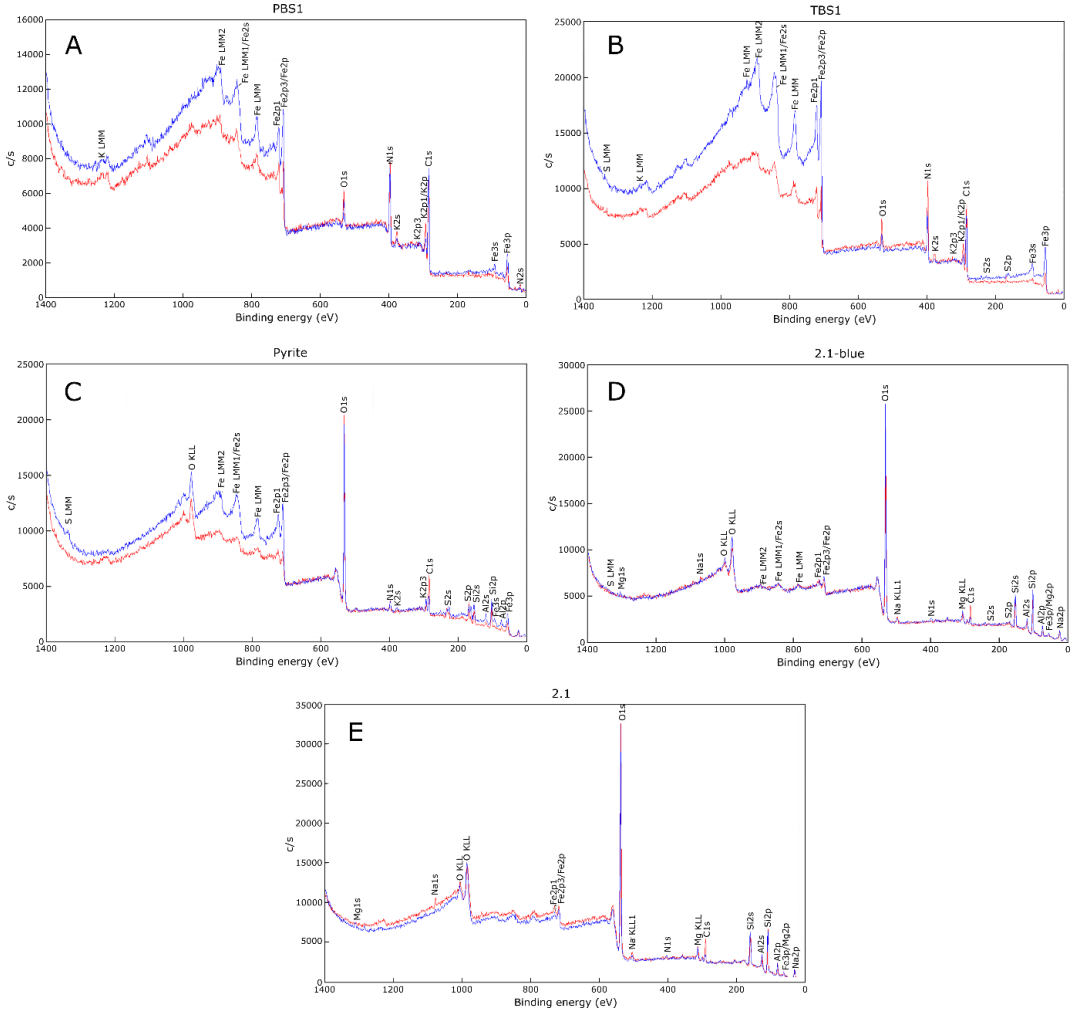

Figure 7.6: Full survey of the samples A) Prussian blue (PBS1), B) Turnbull's blue (TBS1), C) pyrite, D) sample 2.1-blue, and E) sample 2.1. The pyrite sample is a natural sample exposed to a NaCN solution to produce an iron-cyanide compound. Sample 2.1 and sample 2.1-blue (blue stained sample) were found on a gold-mine tailings dam of the Free State goldfields. Red scans are produced prior to cleaning (sputtered) of the surface and the blue scan after cleaning. KLL and LMM are Auger lines, displaying positions of different electrons in electron shells (e.g., KLL implies a vacancy in the K-shell and 2 in the L-shell).

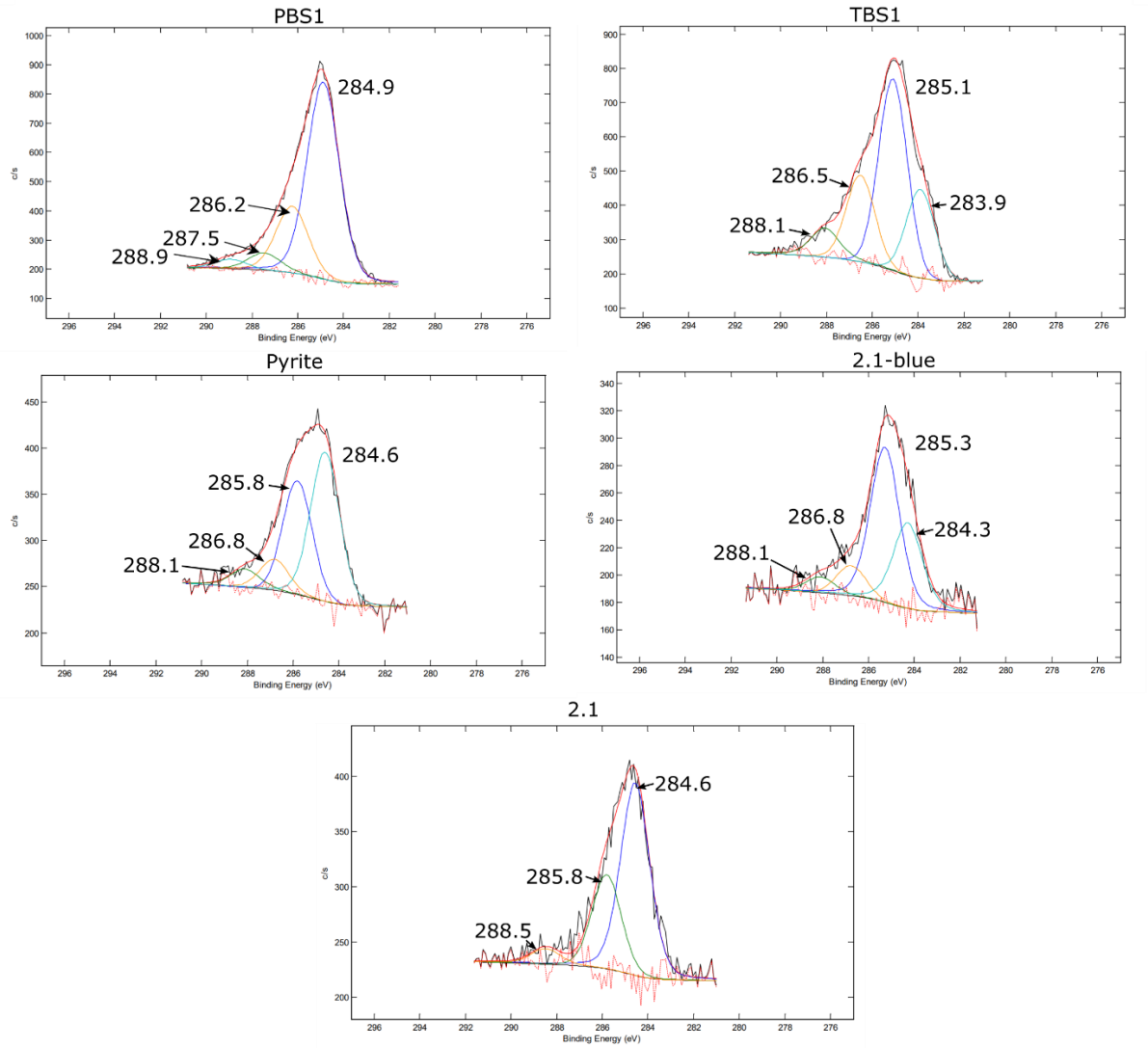

Figure 7.7: High resolution survey of the C1s area of Prussian blue (PBS1), Turnbull's blue (TBS2), pyrite, sample 2.1-blue and sample 2.1.

The N1s peaks of PBS1 and TBS1 were similar, yet the heights of peaks in the pyrite sample were different with an additional peak at 401.5 eV. The N1s concentration in sample 2.1-blue was too low for detection and the results of sample 2.1 are similar to that of the pyrite sample. Wu et al. (2015) states that the N1s spectra of Prussian blue has three components, namely 402.38, 399.28 and 397.28 eV, which were observed here. The additional peak in the pyrite may have equated to the NaCN bond found at 400.2 eV (U.S. Department of Commerce, 2012), also present in sample 2.1.

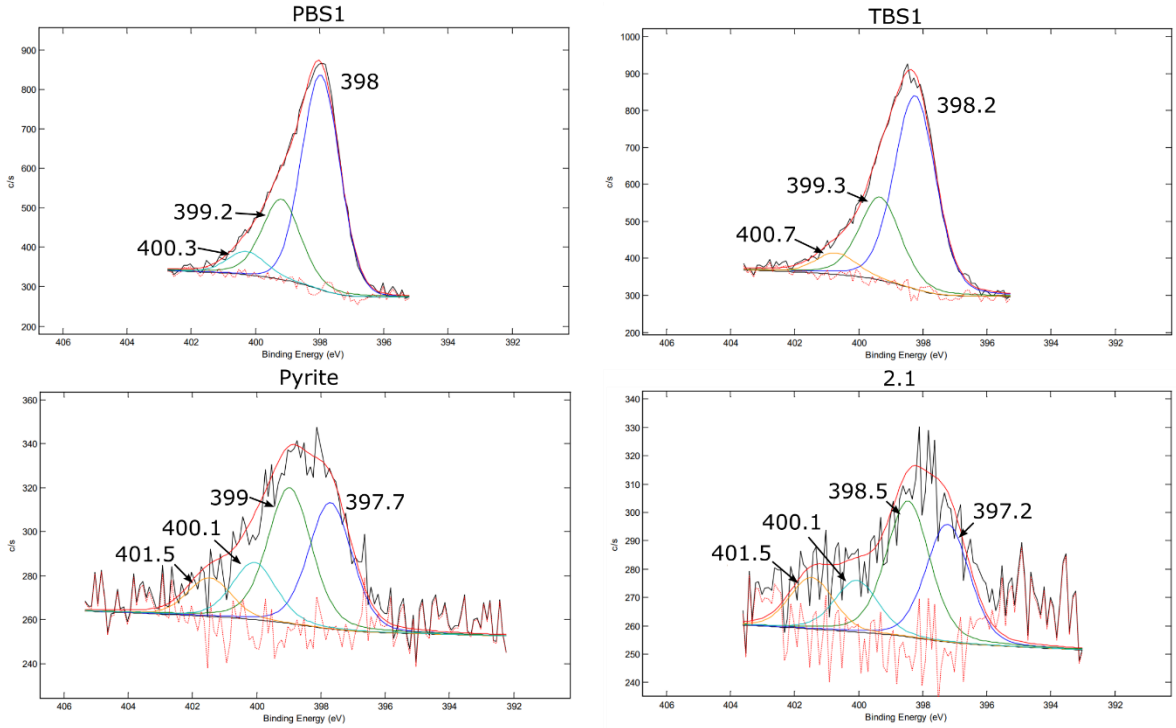

Figure 7.8: High resolution survey of the N1s area of Prussian blue (PBS1), Turnbull's blue (TBS2), pyrite and sample 2.1. The concentration of N in sample 2.1 was too low to detect with XPS.

Each iron peak formed part of a pair that were approximately 13.1 eV from each other. The main peak for PBS1 was at 708.9 eV, with additional peaks at 711.7, 710.3 and 707.4 eV and according to Wu et al. (2015), believed to be Fe^{2+}, Fe^{3+} in Prussian blue, Fe^{3+} and Fe^{2+} in $Fe(CN)_6^{4-}$, respectively. The TBS1 had a main peak at 707.4 eV, with additional peaks at 711.8, 710.4 and 709.0 eV, and according to Wu et al. (2015), believed to be Fe^{2+} in $Fe(CN)_6^{4-}$, Fe^{3+} in Prussian blue, Fe^{3+} and Fe^{2+}, respectively. The positionings of the peaks for PBS1 and TBS1 were similar, with different peak heights. The iron of pyrite in the Pyrite sample was at 708.7 eV (U.S. Department of Commerce, 2012). The peaks of samples 2.1-blue and sample 2.1 mimicked that in the pyrite sample. There was a possibility that jarosite was present in these samples, and Wang et al. (2014) mentioned that Fe^{3+} peak was found at 712.5 eV.

Comparing the peak heights of Fe^{2+} and Fe^{3+}, as stoichiometrically Prussian blue has an Fe^{2+}:Fe^{3+} ratio of 1:1.33 and Turnbull's blue 1:0.7. According to the XPS results The PBS1 samples has a ratio of 1:0.6 and for TBS1 1:0.9. The ratios for the pyrite and 2.1-blue are 1:1.2.

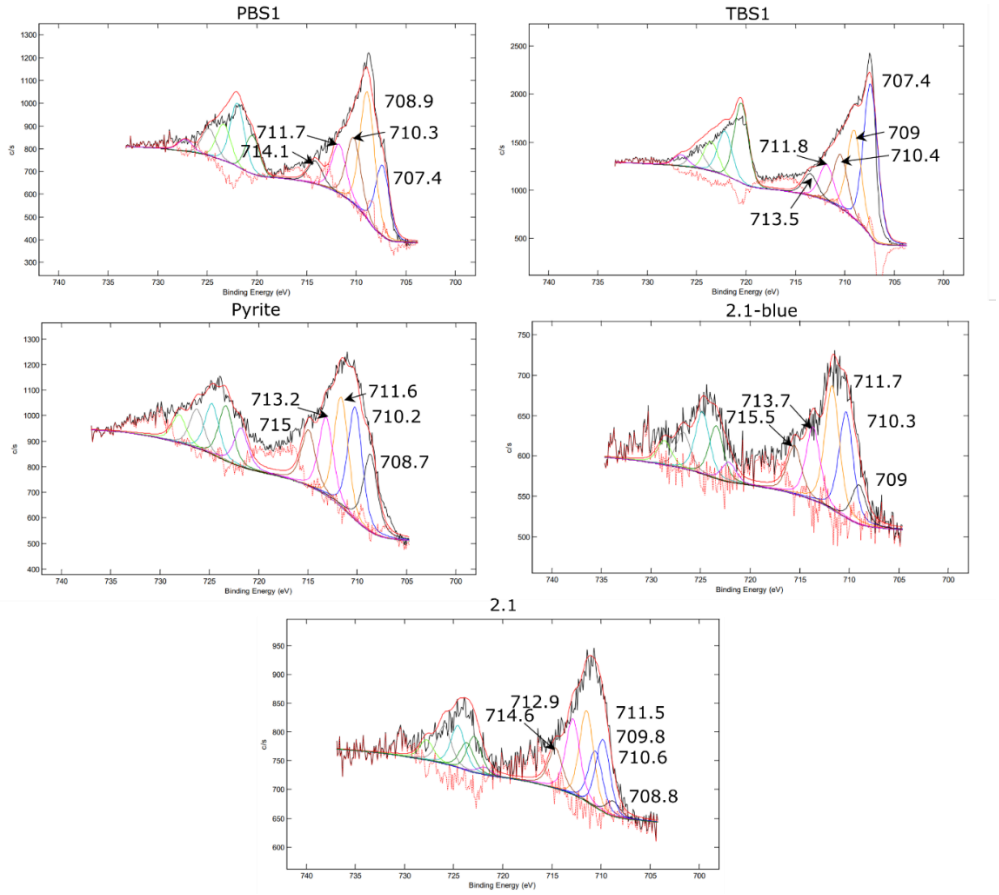

Figure 7.9: High resolution survey of the Fe2p area for Prussian blue (PBS1), Turnbull's blue (TBS2), pyrite and sample 2.1-blue and sample 2.1.

Due to the variation in the results regarding the presence of cyanide in sample 2.1-blue, an additional analysis of CN_{total} in soil samples was performed. A portion of sample 2.1 was also analysed to determine base value. The result revealed that sample 2.1-blue contained 4.6 mmol/kg CN_{total} in 17.1 g of sample and 2.1 contained 0.2 mmol/kg in 19.7 g of sample.

7.3.2 Modelling results

Scenario 1

The first scenario of modelling mimicked the inputs of Ghosh et al. (1999a) along with the $logK_{eq}$ values from Welman-Purchase and Hansen (2023) (Table 7.2). The results of iron in excess (0.5 $mmol.L^{-1}$) and iron not in excess (0.23 $mmol.L^{-1}$) are displayed in Figures 7.10A and B, respectively. The stability of Prussian blue with these input parameters favoured higher pE conditions compared to Turnbull's blue with lower pE/negative pE values. The stability field of Turnbull's blue extended over a wider area

of conditions than Prussian blue. With an increase in pH, both Prussian or Turnbull's blue were no longer the preferred cyanide compounds that formed, but rather other iron-cyanide complexes, such as $Fe(CN)_6^{3-}$ and $Fe(CN)_6^{4-}$ along with hydroxide compounds. Differences between the diagrams when comparing Figure 7.10A to 10B, is the decrease in the Fe^{2+} field and the presence of Fe^{3+}-hydroxide complexes in Figure 7.10A.

These models were duplicated using the $logK_{eq}$ values of Prussian and Turnbull's blue from Ghosh et al. (1999a) (Table 7.2). The pH vs pE/Eh diagrams produced were replicates of the diagrams in Figure 7.10. The only difference was a slight increase in the size of the stability field of $Fe(OH)^{2+}$ in Figure 7.10A.

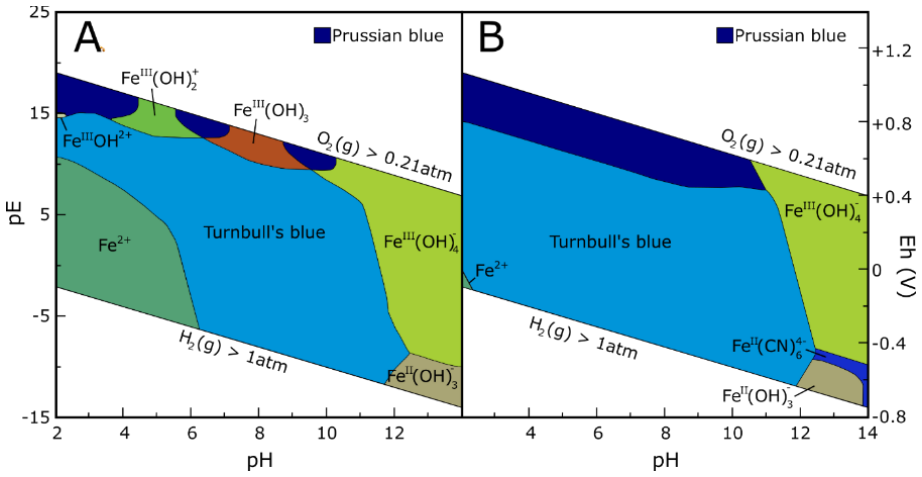

Figure 7.10: pH vs pE/Eh diagrams created using the same cyanide and iron parameters mentioned in Ghosh et al. (1999a), which are as follow - A) Excess iron (0.5 mmol.L^{-1}) and B) No excess iron (0.23 mmol.L^{-1}), other parameters for the diagrams are 0.6 mmol.L^{-1} CN, 0.4 mmol.L^{-1} K and 0.06 mmol.L^{-1} NaCl.

Scenario 2

The second scenario explored the parameters mentioned by Rademan and Groot (2012), a 5 % Fe_2O_3 source (630 mmol iron) added to 1 kg (1 L) of water. Modelling results, seen in Figure 7.11A-D, are of the iron concentrations increasing from 0 to 4 to 10 to 16 mmol.L^{-1}, respectively, with a cyanide concentration of 4.33 mmol.L^{-1}. The pH vs pE/Eh diagram using a concentration 630 mmol.L^{-1} of iron is identical to Figure 7.11D. Figure 7.11E-H also shows the variation in iron concentration, increasing from 0 to 7 to 14 to 16 mmol.L^{-1}, respectively, with a cyanide concentration of 36 mmol.L^{-1}. Figure 7.11I-L shows the variation in cyanide concentration, increasing from 0 to 12 to

24 to 36 mmol.L^{-1}, respectively, with an iron concentration of 16 mmol.L^{-1}. An increase in iron content resulted in an increase in iron-hydroxide complexes and an increase in cyanide results in an increase in iron-cyanide compounds. Diagrams do not change when adding higher concentrations than those displayed in Figure 7.11D, H and L. Again, this was duplicated with the logK_{eq} from Ghosh et al. (1999a) (Table 7.2). The results remained similar, except for the stability field of $Fe(OH)^{2+}$, which decreased in this case with an increase in iron.

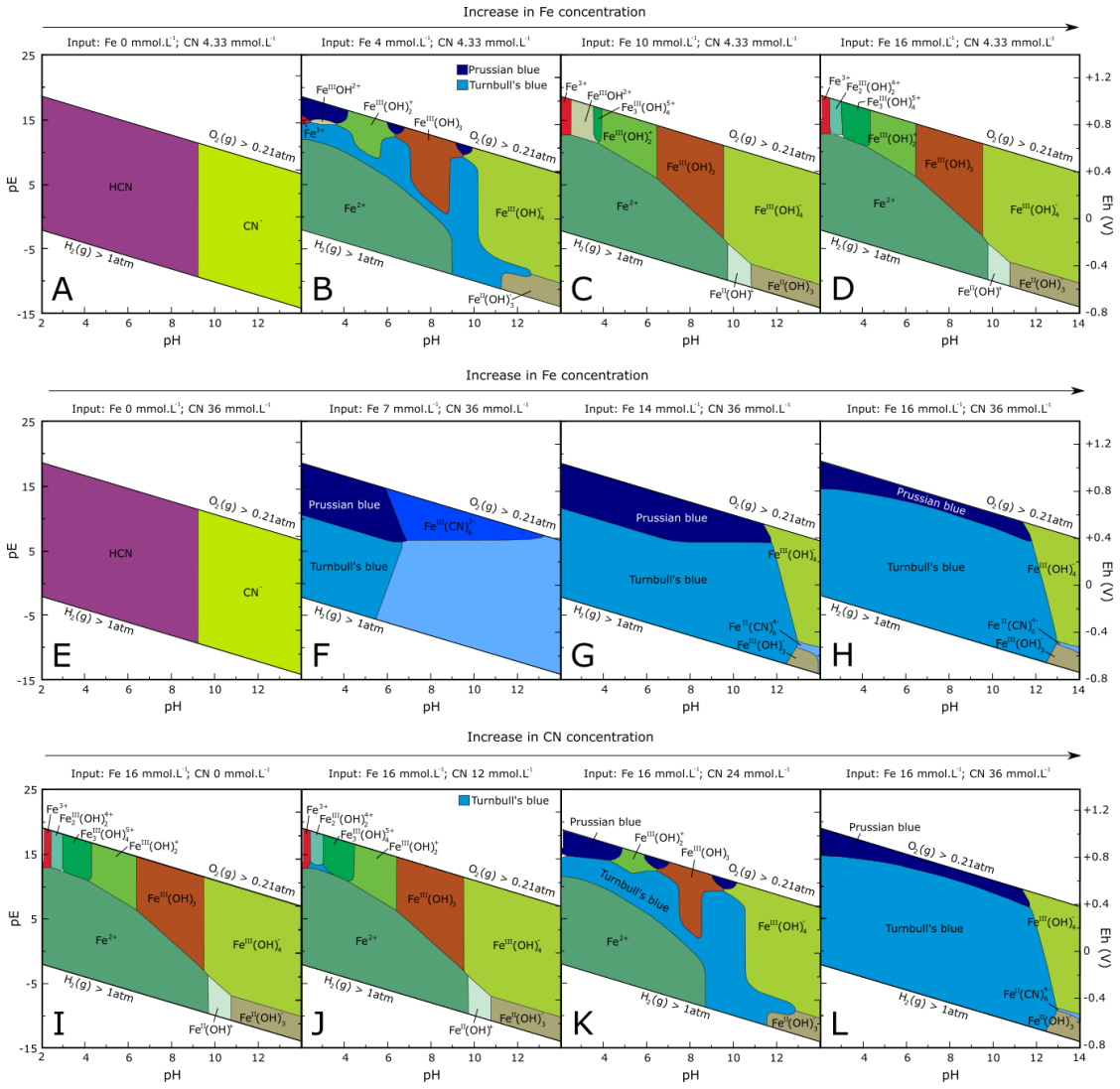

Figure 7.11: pH vs pE/Eh diagrams produced by adding 4.33 mmol cyanide in a 1 L solution (A-D). A) Iron content of 0 mmol.L^{-1}. The iron content increase from B) 4 to C) 10 to D) 16 mmol.L^{-1}. Higher concentrations of iron, did not alter the pH vs pE/Eh diagram from what is presented in D. Diagrams E-H are the same as those produced in A-D, yet an increase in cyanide concentration to 36 mmol.L^{-1} was made. I-L are diagrams produced with 16 mmol.L^{-1} iron. Cyanide content increases from I) 0 to J) 12 to K) 24 to L) 36 mmol.L^{-1}.

The comparison between the pH vs pE/Eh diagrams in this study and the previous study by Ghosh et al. (1999a) are presented in Figure 7.12A and B. The red lines are the outline of the stability fields of the results from Ghosh et al. (1999a) which was computed using the modelling software, MINEQL+. Included in the comparison, displayed in Figure 7.12C, is the inclusion of the cyanide stability fields of cyanide compounds and the oxidizing/reducing division.

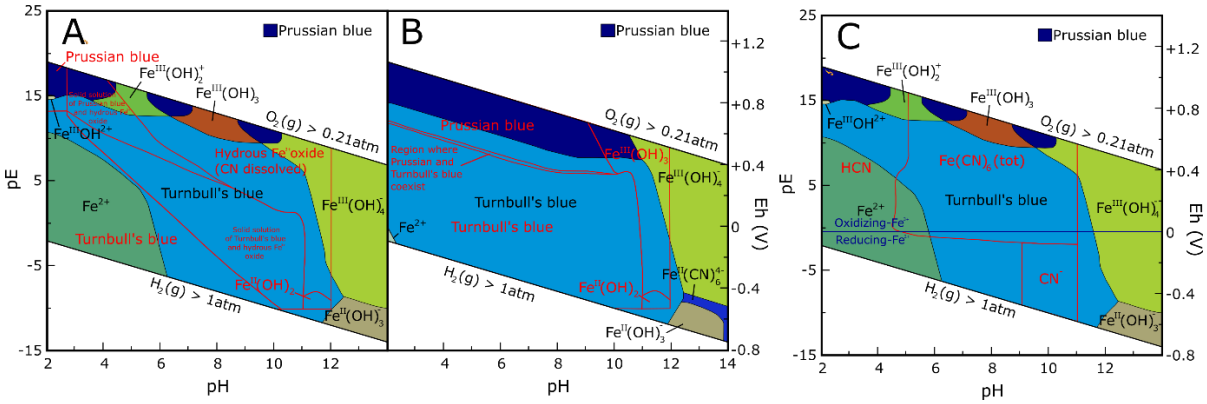

Figure 7.12: A comparison between this study using modelling software, PHREEPLOT and Ghosh et al. (1999a) using MINEQL+ (represented in red). A) The excess of dissolved iron (0.5 mmol); B) No excess iron (0.23 mmol). C) pH vs pE diagram with excess dissolved iron overlaid with the stability fields of the different cyanide compounds. The blue line separated the oxidizing and reducing conditions in the system. Other parameters for all diagrams were 0.6 mmol.L^{-1} cyanide, 0.4 mmol.L^{-1} potassium and 0.06 mmol.L^{-1} NaCl.

The pH and pE results from the PBS, TBS, AMIS0515, pyrite, 2.1-blue samples were plotted in the modelling results of Figure 7.10, revealing that they plot in the Turnbull's blue stability field (Figure 7.13).

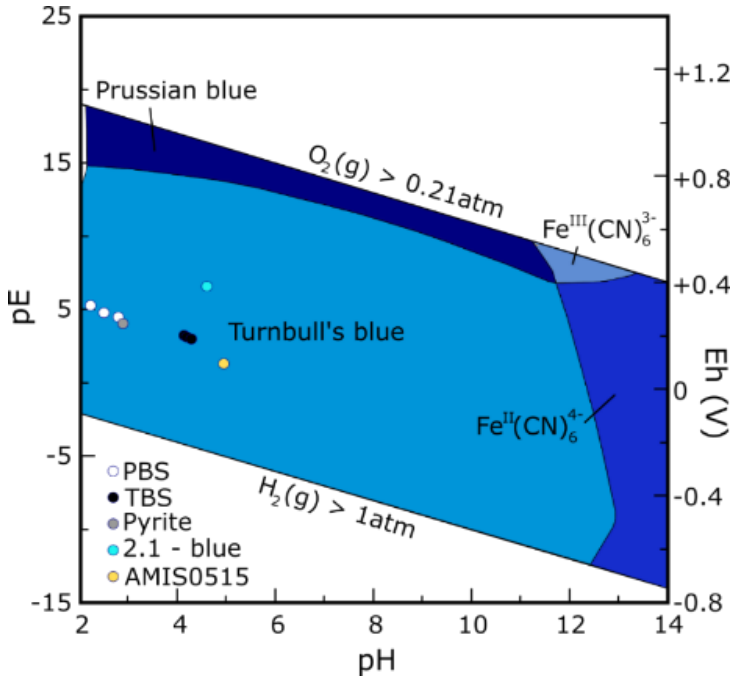

Figure 7.13: pH vs pE diagram produced in the modelling of this study with the pH and pE results from the experiments. All the results plotted in the Turnbull's blue stability field. Parameters: 4.33 mmol.L^{-1} and 16 mmol.L^{-1} iron, yet cyanide was chosen as the main element in the model.

7.4 Discussion

This study investigated iron-cyanide compounds, specifically blue compounds Prussian and Turnbull's blue, forming in different sample. The samples included a Pyrite sample, a certified reference material of a Witwatersrand gold and uranium ore (AMIS0515) and a tailings sample (2.1). Adding a NaCN solution to each of the samples, produced a blue sample in the Pyrite sample and the AMIS0515 sample. These samples both contained pyrite. The oxidation of pyrite by oxygen in water occurs according to equation 11 (Hansen, 2018, Lindsay et al., 2015, Nordstrom and Alpers, 1999, Singer and Stumm,1970):

$$FeS_2(s) + \frac{7}{2}O_2 + H_2O \rightarrow Fe^{2+} + 2SO_4^{2-} + 2H^+ \qquad (11)$$

This oxidation of pyrite process produces Fe^{2+} ions, that are available to produce iron-cyanide compounds. According to the pH vs pE diagrams, the blue substance that formed in the pyrite and AMIS0515 samples is Turnbull's blue. The tailings sample – 2.1 did not form a blue substance due to a lack of available iron for the cyanide to react with.

This study also included laboratory made iron-cyanide compounds (PBS and TBS samples) that were used as reference materials for further analysis. A tailings sample that has blue staining (2.1-blue) was also included in the analysis of this study. XRD and FT-IR analysis proved to be successful in determining the presence of iron-cyanide compounds. Prussian/Turnbull's blue has a main peak at ~17 °2θ in XRD results and the iron-cyanide bond produces a peak at 2072 cm^{-1} when analysed by the FT-IR.

Wu et al. (2015) conducted XPS analysis on Prussian blue microcubes, the results revealed a C1s peak in a cyanide bond is present between 285 – 286 eV. The N1s survey displayed three components, namely ~402.38, ~399.28 and ~397.28 eV. The Fe2p survey revealed the following peaks, Fe^{3+} (~711.2 and ~724.3 eV), Fe^{2+} (~709.8 and ~722.8 eV), Fe^{2+} in $[Fe(CN)_6]^{4-}$ (~708.18 and ~720.88 eV) in Prussian Blue (~713.18 eV) (Wu et al., 2015). Cano et al. (2019) searched for XPS peak shifts of the N1s scan when cyanide was bonded to different metals. They expressed that the peak for the triple bond of nitrogen in cyanide was at 398 eV, which was similar to this study. XPS results are available on Prussian blue samples, although there are no publications on XPS of Turnbull's blue.

This study showed that the XPS data of the PBS1 and TBS1 samples were similar, yet samples 2.1-blue and Pyrite were different to PBS1 and TBS 1 but similar to each other. It was concluded from the Fe^{2+}:Fe^{3+} ratio that PBS1 and TBS1 have ratios very close to the Turnbull's blue and samples 2.1-blue and Pyrite to Prussian blue. It was also noted that the ratios were not completely the same, thus reiterating the results of the other methods, that there is probably a solid solution between Prussian and Turnbull's blue.

pH and pE results taken after the addition of NaCN or after mixing the different solutions were plotted on the models produced in this study. Results showed that the conditions of formation plot in the Turnbull's blue stability field.

The authors have determined and suggest that the best method for detecting the presence of an iron-cyanide compound is FT-IR and in determining which iron-cyanide compound, XPS is a great solution.

The second section of this study involved re-examining pH vs pE diagrams of Prussian and Turnbull's blue. Included in this was the production of pH vs pE diagrams based on cyanide (4.33 mmol.L^{-1}) and iron (<633 mmol.L^{-1}) concentrations from tailings samples. The stability fields determined in this study are larger than those in Ghosh et al. (1999a), which may be due to the concept that this study did not include the possibility for solid solution fields. It was also observed that iron is required in the model for iron-cyanide compounds/complexes to form, yet increasing the iron concentration increases the amount of iron-hydroxide compound/complex fields and their sizes. The cyanide concentration affects the iron-cyanide stability fields. The size of the Turnbull's blue stability field is also a lot larger than that of the Prussian blue stability field and Turnbull's blue can form in both an oxidizing and reducing environment. Turnbull's blue thus has a higher probability of forming compared to Prussian blue.

The implications, that this has on a Witwatersrand sulfidic gold-tailings environment, is that, if there is available iron source without the presence of iron-hydroxide minerals present, the cyanide will form an iron-cyanide mineral. In an environment where pyrite, such as the tailings considered here, the oxidation of pyrite will allow for the presence of available iron cations, if there is available cyanide then Prussian/Turnbull's blue will be the main iron-cyanide compound forming.

7.5 Conclusion

This study delved into the investigation for Prussian/Turnbull's blue to form in different samples and what governs the formation of these compounds. Adding a NaCN solution to samples that contain pyrite, produced blue substances as iron cations are easily produces and are available for reacting with the cyanide. From this study it can be suggested that FT-IR be used to determine the presence of an iron-cyanide compound and XPS be used to determine the Fe^{2+}:Fe^{3+} ratio, to determine the main compound present.

We re-examined iron-cyanide stability diagrams with specific reference to the conditions in a goldmine tailing environment, including the investigation of a blue substance found at a goldmine tailings facility in the Free State goldfields. According to the modelling, Prussian blue forms in an oxic environment and Turnbull's blue in

both an oxic and anoxic environment. The stability fields in said models, are larger than initially thought and a combination of iron-cyanide compounds is believed to form.

7.6 References

Bakatula EN and Tutu H, 2016, Characterization and speciation modelling of cyanide in effluent from an active slime dam, South African Journal of Chemistry, v. 69, p. 140-147.

Brown JB, 1971, Jarosite-Goethite Stabilities at 25 °C, 1 ATM, Mineralogical Deposita, v. 6, p. 245-252.

Cano A, Avila Y, Avila M and Reguera E, 2019, Structural information contained in the XPS spectra of nd^{10} metal cyanides, Journal of Solid State Chemistry, v. 276, p. 339-344.

Delpeux S, Beguin F, Benoit R, Erre R, Manolova N and Rashkov I,1998, Fullerene core star-like polymers-1: Preparation from fullerenes and monoazidopolyehers, European Polymer Journal, v. 34, n.7, p. 905-915.

Dorr JVN, 1936, Cyanidation and concentration of gold and silver ores, McGraw-Hill, New York, 485 pp.

Farah AM, Shooto ND, Thema FT, Modise JS and Dikio ED, 2012, Fabrication of Prussian Blue/Multi-Walled Carbon Nanotubes Modified Glassy Carbon Electrode for Electrochemical Detection of Hydrogen Peroxide, International Journal Electrochemical Science, v. 7, p. 4302-4313.

Ghosh RS, Dzombak DA and Luthy RG, 1999a, Equilibrium precipitation and dissolution of iron cyanide solids in water, Environmental Engineering Science, v.16, n. 4, p. 293-313.

Ghosh RS, Dzombak DA, Luthy RG and Smith JR, 1999b, In situ treatment of cyanide-contaminated groundwater by iron cyanide precipitation, Water Environment Research, v. 71, n. 6, p. 1272-1228.

Hansen RN, 2018, Inter-comparison geochemical modelling approaches and implications for environmental risk assessments: A Witwatersrand gold tailings source term characterisation study, Applied Geochemistry, v. 95, p. 71-84.

Hansen RN, 2020, Process network modelling of the geochemical reactions responsible for acid mine drainage emanating from the Witwatersrand tailings facilities, South African Journal of Geology, v. 123, n. 3, p. 357–368.

Institute of Chemistry University of Tartu, Estonia, 2021, Database of ATR-FT-IR spectra of various materials - accessed 29 Aug 2021 https://spectra.chem.ut.ee/paint/pigments/prussian-blue/.

Ito A, Suenaga M and Ôno K, 1968, Mössbauer study of soluble Prussian Blue, insoluble Prussian Blue, and Turnbull's Blue, Journal of Chemical Physics, v. 48, n. 8, p. 3597-3599.

Jambor JL, Martin AJ and Gerits J, 2009, The post-depositional accumulation of metal-rich cyanide phases in submerged tailings deposits, Applied Geochemistry, v. 24, p. 2256-2265.

Jaszczak E, Polkowska Z, Narkowicz S and Namieśnik J, 2017, Cyanide in the environment – analysis – problems and challenges, Environmental Science and Pollution Research, v. 24, p. 15929-15948.

Johnson CA, 2015, The fate of cyanide in leach wastes at gold mines: An environmental perspective, Applied Geochemistry, v. 57, p. 194-205.

Kruger A, 2019, Gold mining is far from dead in SA, Webmoney, accessed 28 November 2019 - https://www.moneyweb.co.za/news/south-africa/gold-mining-is-far-from-dead-in-sa/.

Kyle JH, 1997, Stability of metal-cyanide and hydroxide complexes, World Gold ’97 Conference, p. 163-169.

Lindsay MBJ, Moncur MC, Bain JG, Jambor JL, Ptacek CJ and Blowes DW, 2015, Geochemical and mineralogical aspects of sulfide mine tailings, Applied Geochemistry, v. 57, p. 157–177.

Maer K JR, Beasley ML, Collins RL and Milligan WO, 1968, The structure of the titanium-iron cyanide complexes, Journal of the American Chemical Society, v. 90, n. 12, p. 3201-3208.

Meeussen JCL, Keizer MG, van Riemsdijk WH and de Haan FAM, 1994, Solubility of cyanide in contaminated soils, Journal of Environmental Quality, v. 23, p. 73-85.

Moulder JF, Stickle WF, Sobol PE and Bomben KD, 1992, Handbook of X-Ray Photoelectron Spectroscopy: A Reference Book of Standard Spectra for Identification and Interpretation of XPS Data, Physical Electronics Division, Perkin-Elmer Corp, USA, 261 pp.

Nordstrom DK and Alpers CN, 1999, Geochemistry of acid mine waters, In: Plumlee GS and Logsdon MJ (Eds.), The environmental geochemistry of mineral deposits, Reviews Economic Geology, v. 6A, p. 133–160.

Parkhurst DL and Appelo CAJ, 2013, Description of Input Examples for PHREEQC Version 3 – a Computer Program for Speciation, Batch-reaction, One-dimensional Transport, and Inverse Geochemical Calculations. book 6, chapter A43, US Geological Survey Techniques and Methods, pp. 497, available only at http://pubs.usgs.goc/tm/06/a43/.

Rademan L and Groot DR, 2012, Cyanidation of reef and surface gold ores, Journal of the Southern African Institute of Mining and Metallurgy, v. 112, p. 295-300.

Reguera E, Fernandez-Bertran J, Dago A and Diaz C, 1992, Mössbauer spectroscopic study of Prussian Blue from different provenances, Hyperfine Interactions, v. 73, p. 295-308.

Sehmel GA, 1989, Cyanide and Antimony Thermodynamic Database for the Aqueous Species and Solids for the EPA-MINTEQ Geochemical Code, Rep., PNL-6835, Pac. Northwest Lab., Richland, Wash.

Singer PC and Stumm W, 1970, Acid mine drainage: the rate-determining step, Science167, p. 1121–1123.

Souza RFM, Navarro RCs, Grillo A and Brocchi E, 2018, Potassium alum thermal decomposition study under non-reductive and reductive conditions, Journal of Materials Research and Technology, v. 8, n. 1, p. 745–751.

U.S. Department of Commerce, 2012, National Institute of Standards and Technology (NIST) and Material Measurement Laboratory (MML) – accessed 01 November 2021 https://srdata.nist.gov/xps/selEnergyType.aspx.

Wang Z, Xiao D, Liu R, Guo Y, Lou X and Liu J, 2014, Fenton-like Degradation of Reactive Dyes Catalyzed by Biogenic Jarosite, Journal of Advanced Oxidation Technologies, v. 17, n. 1, p. 104-108.

Welman-Purchase MD and Hansen RN, 2023, Cyanide within gold mine waste of the free state goldfields: A geochemical modelling approach, Environmental Pollution, 120825. 10.1016/j.envpol.2022.120825

Wu Q, Wu G, Wang L, Hu W and Wu H, 2015, Facile synthesis and optical properties of Prussian Blue microcubes and hollow Fe_2O_3 microboxes, Material Science in Semiconductor Processing, v. 30, p. 476-481.

Zagury GJ, Oudjehani K and Deschênes L, 2004, Characterization and availability of cyanide in solid mine tailings from gold extraction plants, Science of the total environment, v. 320, p. 211-224.

Supplementary data

Table S7.1: pH, pE and temperature results of the empirical study and related modelling results for Prussian blue (PB), Turnbull's blue (TB), pyrite, and AMIS0515.

Sample name	Iron source	Cyanide source	Solvent	pH	pE	T (°C)
PBS1	$Fe_2(SO_4)_3$	$K_4[Fe(CN)_6]$	Deionized water	2.24	5.08	24.3
PBS2	$Fe_2(SO_4)_3$	$K_4[Fe(CN)_6]$	Deionized water	2.53	4.80	25.0
PBS3	$Fe_2(SO_4)_3$	$K_4[Fe(CN)_6]$	Deionized water	2.74	4.60	25.0
TBS1	$FeSO_4$	$K_3[Fe(CN)_6]$	Deionized water	4.23	3.17	27.7
TBS2	$FeSO_4$	$K_3[Fe(CN)_6]$	Deionized water	4.13	3.26	28.2
TBS3	$FeSO_4$	$K_3[Fe(CN)_6]$	Deionized water	4.36	3.04	28.6
Pyrite	Pyrite	NaCN	Deionized water	2.84	4.01	23.6
AMIS0515	Pyrite, hematite, jarosite	NaCN	Deionized water	4.94	2.00	23.5

Chapter 8

Modelling the behaviour of ferric and ferrous iron in a goldmine tailings environment, Free State – South Africa

Megan D. Welman-Purchase[a,*], Robert N. Hansen[b]

[a] University of the Free State, Department of Geology, Bloemfontein, South Africa

[b] University of the Free State, Centre for Mineral Biogeochemistry, Bloemfontein, South Africa

*Corresponding author.

Email address: purchasemd@ufs.ac.za (MD Welman-Purchase).

Abstract

Cyanide has a high affinity for gold and other metals (including iron) attributing to its usage in the goldmine extraction process. After the extraction process, waste material is disposed of onto tailings facilities, where cyanide has previously been found. This study delves into the modelling of the behaviour of iron in a tailings system and the effect that cyanide and iron-cyanide compounds/complexes have on this. Results of this study revealed that jarosite and goethite/ferrihydrite affect the formation of Prussian blue but requires Fe^{2+} in the system to form.

Keywords: Cyanide, ferric/ferrous iron, Prussian blue, goethite/ferrihydrite, jarosite

8.1 Introduction

Cyanide, that is still widely used worldwide in the gold extraction process, has a high affinity for metals (such as iron and gold) (Bakatula and Tutu, 2016; Wang and Forssberg, 1990; Zagury et al., 2004). A portion of this cyanide is believed to be expelled of onto tailings dams, where iron and aluminium are among the most copious metal cations existing in acid mine drainage (AMD) (Sánchez-España et al., 2005).

Iron in this environment, originates from the oxidation of pyrite, according to the equation 1 (Williamson and Rimstidt 1994). In environments where the pH is less than 3, the Fe^{2+} product from equation 1, is further oxidised to Fe^{3+} in equation 2 (Stumm and Lee 1961, Jones et al. 2014). Above pH 3, iron- hydroxide minerals form. As the concentration of Fe^{3+} increases, the oxidation of pyrite is further enhanced according to the equation 3 (Williamson and Rimstidt 1994). Contrarily, if the pH of the system is greater than 3, hydroxide minerals form (equation 4) (Jones et al. 2014):

$$FeS_2(s) + \frac{7}{2}O_2 + H_2O(l) \leftrightarrow Fe^{2+} + 2SO_4^{2-} + 2H^+ \quad (1)$$

$$Fe^{2+} + \frac{1}{4}O_2 + H^+ \leftrightarrow Fe^{3+} + \frac{1}{2}H_2O + e^- \quad (2)$$

$$FeS_2 + 14Fe^{3+} + 8H_2O = 15Fe^{2+} + 2SO_4^{2-} + 16H^+ \quad (3)$$

$$4Fe^{2+} + 10H_2O + O_2 = 4Fe(OH)_3(s) + 8H^+ \quad (4)$$

Ferrous iron (Fe^{2+}) is more soluble than ferric iron (Fe^{3+}), remaining in solution at a pH <8, whereas Fe^{3+}, seen in the reaction 4, precipitates as a variety of ocherous minerals (pH >3) (Sánchez-España 2007). The distribution of the precipitation of iron species is thus pH dependent. In the environment discussed in this study, not only iron is present but also SO_4^{2-} ions, which strongly affects the complexation of iron (Sánchez-España et al. 2005). Thus, the ocherous minerals include jarosite ($KFe_3(SO_4)_2(OH)_6$ - forms at a pH of ~ 2), schwertmannite ($Fe_8O_8(OH)_6.nH_2O$ - forms at a pH of ~ 2.5-4) and ferrihydrite ($Fe(OH)_3$ - forms at a pH of > 5). According to Villacís-Garcia et al. (2015), goethite forms from an increase in temperature and aging of ferrihydrite.

These matters have been studied, whereas this research focuses on iron and the mineralization of iron-cyanide compounds and the effect that ocherous mineral mineralization in the goldmine tailings dams has on the formation of iron-cyanide compounds. Specifically on Prussian blue – $Fe_4[Fe(CN)_6]_3$ and Turnbull's blue – $Fe_3[Fe(CN)_6]_2$ (Ghosh et al., 1999) and possible compounds associated with them.

8.2 Geological setting

A large percentage of South Africa's gold is extracted from the Witwatersrand supergroup, which has generated approximately a third of the world's gold to date (Tucker et al. 2016). This supergroup comprises successions of sedimentary deposits within the Witwatersrand basin which extends from the north of Johannesburg to south of Welkom (Tucker et al. 2016). The goldfields of the Witwatersrand supergroups are the Evander, East Rand, Central Rand, West Rand, South Deep, Western Areas, Carletonville, Far West Rand and Free State Rand goldfields (Frimmel et al. 2005). This study involves samples from a tailings dam outside of Welkom in the Free State goldfields.

Post gold extraction, the waste material is discarded of on tailings dams, consisting gangue minerals (such as quartz, mica, plagioclase), as well as possible contaminants

used in the extraction process (such as cyanide, metals). According to Hansen (2018), the tailings dams display the zones in figure 8.1, which are believed to be onion like, not horizontal. The outer zone is the oxidation zone, adjacent to the transition zone and the core is the reducing zone.

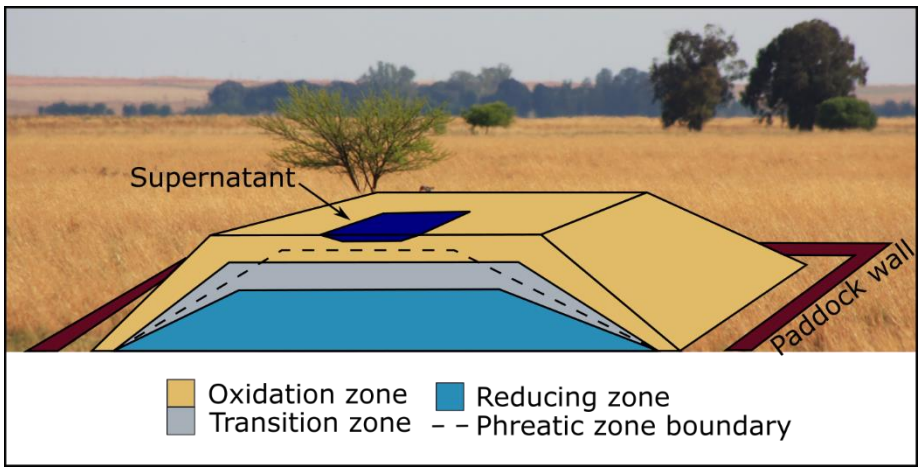

Figure 8.1: A simplified diagram displaying the geochemical structure of a tailings dam, modified after Hansen (2018).

8.3 Methods

9 samples were collected from a tailings dam close to Welkom in the Free State goldfields, South Africa. 3 samples were extracted at different depths from 3 different positions on the tailings dams. Samples 1.1 – 2.3 were collected from the top surface of the tailings dam and 3.1 – 3.3 from the side slope. The samples were milled in a carbon steel ring and puck mill, followed by the determination of the loss on ignition (LOI) by weighing sample loss after heating a portion of the sample to 950 °C. A fusion disc and pressed pellet (Na_2O only) were produced for each sample to analyse major elements using a Rigaku, Primus IV (4kW generator) X-ray Fluorescence (XRF). Total cyanide of sample 2.1 was determined by X-Lab earth laboratories in Johannesburg. Modelling was completed with PHREEQC, a United States Geological Survey project developed by Parkhurst and Appelo (2013). Parameters used for the modelling were taken from Sánchez-España (2007), where the solution contains 0.1 M of SO_4^{2-} and 0.02 M of Fe^{3+} as a function of pH. In addition to this, the concentration of cyanide found in the tailings sample 2.1 was also added to the solution to model the effects that it may have on the precipitation of other ocherous minerals. Sensitivity analysis was also completed, altering the Fe^{3+}, cyanide and oxygen concentrations.

8.4 Results

Samples from the tailings dam are fine grained and vary from pale to more orange in colour. This is an indication of the iron present in the samples. A blue staining was found in the sample 2.1, seen in figure 8.2, believed to be an iron-cyanide compound. This total sample contained 10 $mg.L^{-1}$ total cyanide.

Figure 8.2: Blue staining found on the tailings dam in Welkom, South Africa. This is believed to be an iron-cyanide *compound and is ~3 cm in length.*

The XRF results are displayed in Table 8.1, where the tailings consist mostly of SiO_2 (85.66 – 88.62 wt%) followed by Al_2O_3 (5.82 – 8.43 wt%). For this study the Fe_2O_3 composition is important, with an average of 2.25 wt%.

Table 8.1: XRF results of the 12 samples from a tailings dam in the Free State goldfields.

XRF major elements (wt%)	1.1	1.2	1.3	2.1	2.2	2.3	3.1	3.2	3.3
SiO_2	87.18	87.41	88.62	86.93	86.38	85.66	85.94	85.66	87.46
TiO_2	0.25	0.28	0.28	0.31	0.35	0.35	0.27	0.26	0.27
Al_2O_3	5.82	6.52	6.39	7.17	7.88	8.43	6.38	6.30	6.40
Fe_2O_3	2.69	1.69	2.27	2.09	2.48	2.54	2.21	2.14	2.15
MgO	1.26	0.40	0.49	0.56	0.41	0.44	0.46	0.44	0.45
MnO	0.02	0.02	0.02	0.04	0.03	0.03	0.02	0.02	0.02
CaO	0.68	0.41	0.41	0.31	0.69	0.43	0.52	0.50	0.51
Na_2O	0.28	0.43	0.34	0.54	0.49	0.45	0.31	0.31	0.37
K_2O	0.31	0.48	0.52	0.55	0.46	0.52	0.44	0.44	0.43
P_2O_5	0.03	0.02	0.03	0.03	0.03	0.03	0.03	0.02	0.03
LOI	2.01	2.28	2.42	2.53	2.73	2.91	2.44	2.35	2.43
Total	100.53	99.94	101.80	101.05	101.92	101.78	99.02	98.43	100.51

The results from the modelling are displayed in figure 8.3 and 8.4. Figure 8.3 is a display of the oxidation states of iron in the modelling in solution, revealing that a small

portion of the iron is in the state Fe^{2+} from a pH of 1. This Fe^{2+}, displayed in Figure 8.4, is consumed in the production of Prussian blue, which also forms from pH 1. The Prussian blue molality is affected between pH 2 and 3 when $FeSO_4$, $Fe_2OH_2^{4+}$ and $FeOH^{2+}$ forms.

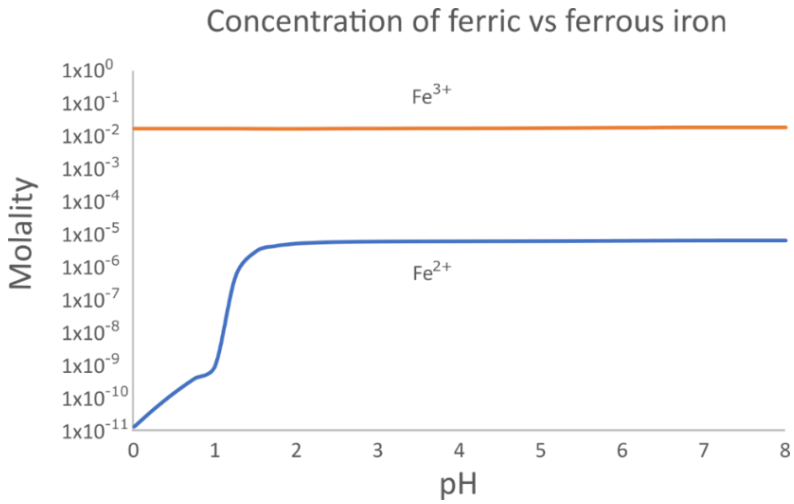

Figure 8.3: Modelling results of the oxidation states of iron in solution.

At pH values between 0 and 3, SO_4 compounds form, which correlates with the literature as the conditions where jarosite forms. Above a pH of 3, hydroxide complexes form, where above a pH of 6, ferrihydrite forms. Between a pH of 8 and 14 all compounds decrease to <0.01% and 99.99% of the Fe^{3+} in the modelling produces $Fe(OH)_4^-$. Included in Figure 8.4 is the concentrations of cyanide compounds. This graph reveals that initially HCN is produced, which is consumed as soon as Prussian blue precipitates. At a pH of >4, Turnbull's blue precipitates, consuming a small portion of the production of Prussian blue.

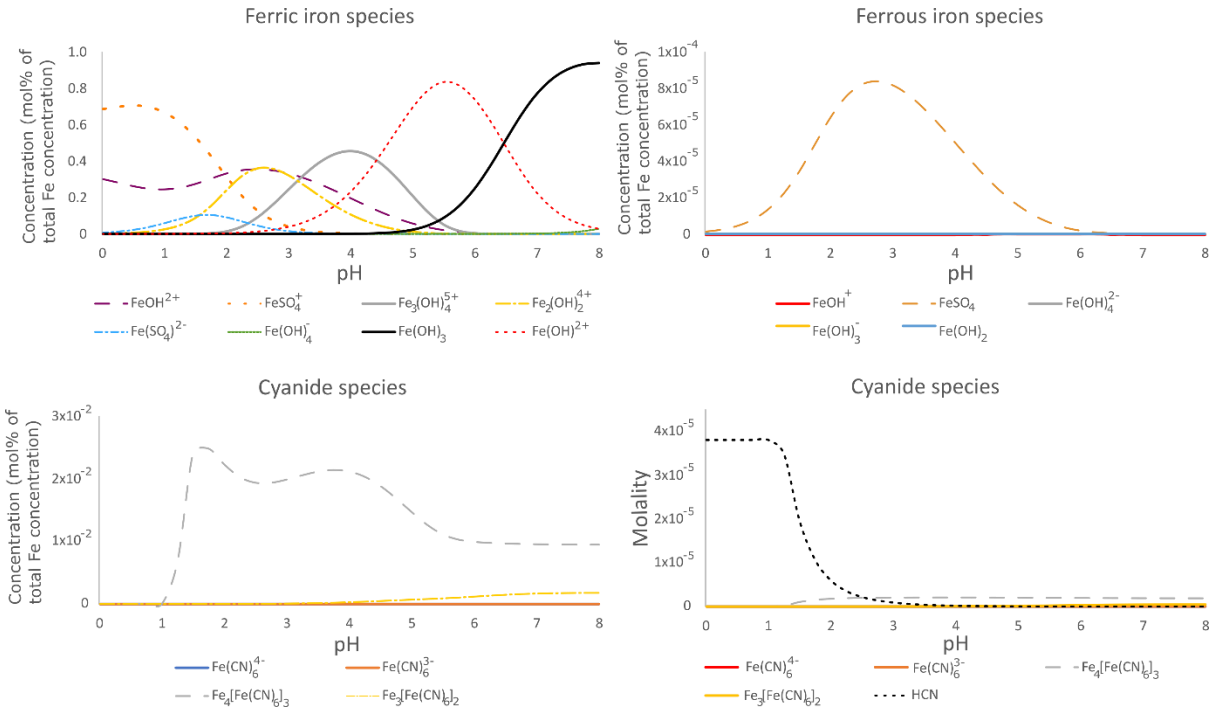

Figure 8.4: Speciation results of the PHREEQC modelling. 0.02 M ferrous iron, 0.1 M of SO_4^{2-} and 10 mg.L^{-1} cyanide *were added to the model in order to compare them to the results in Sánchez-España (2007). Owing to the large discrepancies in the concentration, the results were displayed in separate diagrams.*

Increasing the Fe^{3+} concentration results in the higher concentrations of the same compounds, exclusive of the concentration of the iron-cyanide compounds. Contrarily, increasing the cyanide concentration in solution, results in the majority of the formation of Prussian blue. In addition to this, a model was run in a reducing environment, in order to mimic the core of the tailings dam. The only compounds that formed are Turnbull's blue and Fe^{2+} ions. No ocherous minerals form. Increasing the cyanide concentration in solution

8.5 Discussion

The iron-cyanide compounds have previously been found by other authors in tailings samples, namely Bakatula and Tutu (2016) (South Africa – Central Rand goldfields) and Jambor et al. (2009) (Balmer lake in Canada - gold mining discharge). These compete for the iron in the system, with minerals such as ferrihydrite and jarosite. All of the above-mentioned minerals, including iron-cyanide compounds, require an Fe^{3+} source, additionally Prussian and Turnbull's blue require an Fe^{2+} source. Modelling revealed that the production of jarosite, ferrihydrite and other iron-hydroxide minerals

are dependent on the pH and only form in an oxidizing environment. Goethite forms with an increase in temperature or from aging. Comparing these results to the study by Sánchez-España (2007) is displayed in Figure 8.5, where the largest difference is a shift of all peaks. This may be due to the addition of cyanide or that an additional compound is present in the modelling. Yet further studies will need to be completed to confirm this.

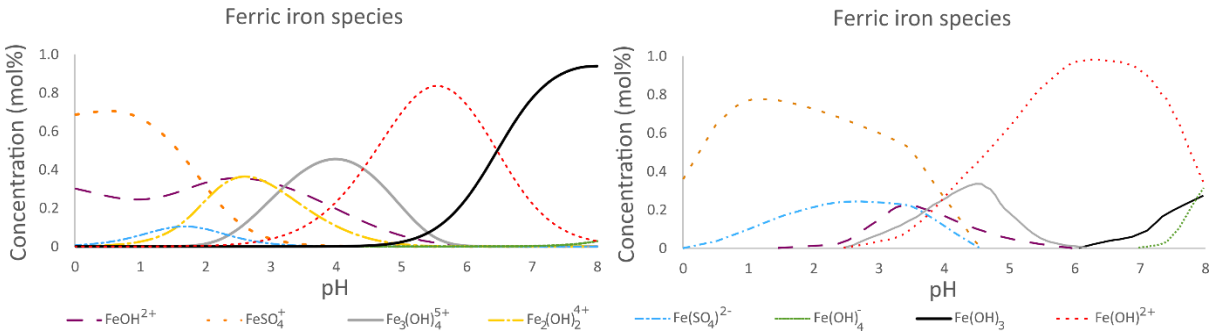

Figure 8.5: Comparison between the results of this study (left) and the results of Sánchez-España (2007) (right). The results of this study are shifted to the left.

Prussian blue precipitation is dependent on the presence of both Fe^{2+} and Fe^{3+} and on the redox conditions. The modelling revealed that Prussian blue is the dominant iron-cyanide compound that forms in an oxidizing environment but Turnbull's blue coprecipitates with Prussian blue above a pH of 4. As these compound precipitate, so the concentration of HCN diminishes to 0.04% of the cyanide compounds. In a reducing environment only Turnbull's blue precipitates. Kyle (1997) proposed that producing iron-cyanide compounds could assist in cyanide remediation. Iron-cyanide complexes are CN_{SAD} (strong acid dissociable cyanide compounds) (Zagury et al., 2004), and thus are stable. If these compounds are stable, precipitate spontaneously and prevent the production of HCN, then they may be a good candidate for remediation.

8.6 Conclusions

This study intended to understand the behaviour of the different oxidation states of iron, their precipitates and the effect that the addition of cyanide to the system may have using PHREEQC modelling. In order to mimic gold mine tailings environments. It was determined that the precipitation of jarosite, ferrihydrite and other hydroxide minerals, which has been studied previously, is dependent on pH in an oxidizing

environment. Fe^{3+} was added to the solution, yet a small portion converts to Fe^{2+}, this allows for Prussian blue to form, which decreases in concentration when $FeSO_4$, $Fe_2OH_2^{4+}$ and $FeOH^{2+}$ forms and at a pH higher than 4, Turnbull's blue and $Fe(OH)_3$ forms. Prussian blue also results in the consumption of the cyanide in the system and thus preventing the production of HCN (to less than 0.04%). This study revealed that the precipitation of Prussian blue is affected by the presence of jarosite and goethite/ferrihydrite but requires Fe^{2+} in the system to form.

Acknowledgements

The authors would like to thank Iphakade and the CMBG for financial support.

8.7 References

Bakatula EN and Tutu H, 2016, Characterization and speciation modelling of cyanide in effluent from an active slime dam, South African Journal of Chemistry, v.69, p.140-147.

Frimmel HE, Groves DI, Kirk J, Ruiz J, Chelsey J and Minter WEL, 2005, The Formation and Preservation of the Witwatersrand Goldfields, the World's Largest Gold Province, Economic Geology 100th Anniversary Volume, p. 769–797.

Ghosh RS, Dzombak DA, Luthy RG and Smith JR, 1999, In situ treatment of cyanide-contaminated groundwater by iron cyanide precipitation, Water Environ Research, p. 71, n. 6, p. 1272-1228.

Hansen RN, 2018, Inter-comparison geochemical modelling approaches and implications for environmental risk assessments: A Witwatersrand gold tailings source term characterisation study, Applied Geochemistry, Elsevier, v. 95, p. 71-84.

Jambor JL, Martin AJ and Gerits J, 2009, The post-depositional accumulation of metal-rich cyanide phases in submerged tailings deposits, Applied Geochemistry, v. 24, p. 2256-2265.

Jones AM, Griffin PJ, Collins RN and Waite TD, 2014, Ferrous iron oxidation under acidic conditions – the effect of ferric oxide surfaces, Geochimica Cosmochimica Acta, v. 145, p. 1–12.

Kyle JH, 1997, Stability of metal-cyanide and hydroxide complexes, World Gold '97 Conference, p. 163-169.

Parkhurst DL and Appelo CAJ, 2013, Description of Input Examples for PHREEQC Version 3 – a Computer Program for Speciation, Batch-reaction, One-dimensional Transport, and Inverse Geochemical Calculations. book 6, chapter A43. US Geological Survey Techniques and Methods, pp. 497, Available only at http://pubs.usgs.goc/tm/06/a43/.

Sánchez-España J, 2007, The Behavior of Iron and Aluminum in Acid Mine Drainage: Speciation, Mineralogy, and Environmental Significance. Thermodynamics, Solubility and Environmental Issues, Chapter 7.

Sánchez-España J, López Pamo E, Santofimia E, Aduvire O, Reyes J and Barettino D, 2005, Acid mine drainage in the Iberian Pyrite Belt (Odiel river watershed, Huelva, SW Spain): Geochemistry, mineralogy and environmental implications, Applied Geochemistry, v. 20, n. 7, p. 1320-1356.

Stumm W and Lee GF, 1961, Oxygenation of ferrous iron, Industrial and Engineering Chemistry, v. 53, p. 143–146.

Tucker RF, Viljoen RP and Viljoen MJ, 2016, A Review of the Witwatersrand Basin - The World's Greatest Goldfield. IUGS, Journal of International Geosciences, Episodes, v. 39, n. 2, p. 105-133.

Villacís-Garcia M, Ugalde-Arzate M, Vaca-Escobar K, Villalobos M, Zanella R and Martínez-Villegas, 2015, Laboratory synthesis of goethite and ferrihydrite of controlled particle sizes, Geológica Mexicana, p. 67, n. 3, p.433-446.

Wang X and Forssberg KSE, 1990, The chemistry of cyanide-metal complexes in relation to hydrometallurgical processes of precious metals. Mineral Processing and Extractive Metallurgy Review, v. 6, p. 81-125.

Williamson MA and Rimstidt JD, 1994, The kinetics and electrochemical rate-determining step of aqueous pyrite oxidation, Geochimica Cosmochimica Acta, v. 58, p. 5443–5454.

Zagury GJ, Oudjehani K and Deschênes L, 2004, Characterization and availability of cyanide in solid mine tailings from gold extraction plants, Science of the Total Environment, v. 320, p. 211-224.

Chapter 9

First insight into the natural biodegradation of cyanide in a gold tailings environment enriched in cyanide compounds

Megan D. Welman-Purchase[a,*], Julio Castillo[b], Andisiwe Matu[b], Alba Gomez-Arias[c], Robert N. Hansen[d]

[a] University of the Free State, Department of Geology, Bloemfontein, South Africa

[b] University of the Free State, Department of Microbiology and Biochemistry, Bloemfontein, South Africa

[c] University of the Free State, Department of Chemistry, Bloemfontein, South Africa

[d] University of the Free State, Centre for Mineral Biogeochemistry, Bloemfontein, South Africa

*Corresponding author.

Email address: purchasemd@ufs.ac.za (MD Welman-Purchase).

Abstract

Cyanide, which is still used in numerous countries in the gold extract processes, has been found in gold tailings dams. This study involved the investigation of 9 sediment tailings samples from a tailings dam in the Free State goldfields, South Africa. There are numerous studies reporting on cyanide degradation in bioreactors, yet the aim of this study was to determine the naturally occurring cyanide-degrading bacteria in the oligotrophic environment of goldmine tailings. The analysis employed obtained a geochemical, metagenomics, and bioinformatics snapshot of the bacteria, genes, and pathways to determine the natural cyanide biodegradation in gold tailings. All of the samples contained cyanide and the hydrolytic/assimilatory cyanide pathways are most prominent in the system, where most bacteria present can perform cyanide degradation and assimilation. Cyanide is an excellent source of carbon and energy in oligotrophic systems, whose biodegradation is key in the natural remediation of gold tailings.

Keywords: gold tailings, cyanide, metagenomes, natural biodegradation

9.1 Introduction

Cyanide remains the most popular chemical used worldwide in leaching techniques used for gold extraction (Luque-Almagro et al., 2016). Cyanidation extraction ensures financial viability when extracting gold from deposits with low concentrations (Mudder

et al., 2001). Gold mines in South Africa have used this method since 1890 (Fivaz, 1988), where the Witwatersrand Supergroup (in South Africa) has produced over 40000 metric tons of gold (Norman and Whitfield, 2006). 40000 metric tons of gold is extracted using about 21 million tons of a cyanide compound and produces approximately 7 million tons of waste rock as tailings (based on a 5 $g.ton^{-1}$ grade). The waste materials consists of gangue minerals, salts, metals, metalloids (e.g. Fe, Cu, Zn, As, Sb, Cd, Hg, Pb) (Haung et al., 2012) and cyanide (Bakatula and Tutu, 2016). The waste materials are then deposited as fine-grained material in the form of a slurry onto tailings dams that extend over areas of over 150 ha thus far (Eisler and Wiemeyer, 2004). Cyanide within these tailings, has the potential to affect plants, agricultural areas and groundwater, ultimately posing a risk for animal and human health (Khan et al., 2020). There have been incidences where cyanide has leaked into the environment resulting in the deaths of wildlife. The only case reported goldmine tailings fail in South Africa, is the collapse of the Merriespruit tailings dam in 1994 yet the concentrations and contamination of cyanide was not monitored (Moran, 1998).

Cyanide (in the form CN^-) found in tailings tend to form iron-cyanide complexes (Jaszczak et al., 2017). Iron-cyanide complexes (solids) form part of the strong acid-dissociable cyanides (CN_{SAD}), which are the most stable of the cyanide compounds (Zagury et al., 2004). CN_{SAD} complexes render cyanide immobile unless exposed to extreme acidic conditions or photolysis (Jaszczak et al., 2017). Microbial activity may also affect the stability of these cyanide compounds as they may cause the solubilisation of minerals. Free cyanide can be used as a carbon and nitrogen source for microorganisms. Indeed, members of the genera *Acinetobacter sp., Alcaligenes sp., Arthrobacter, Azotobacter sp., Azospirillum sp., Bacillus sp., Brevibacterium, Chromobacterium violoaceum, Corynebacterium, Desulfotomaculum nitrifican, Enterobacter sp., Escherichia coli, F. oxysporum, Ferrobacillus ferroxidans, Fusarium solani, Herbaspirillum seropedicae, Klebsiella sp., Nocardia sp., Pseudomonas sp., Rhodococcus rhodochrous, Rhodopseudomonas gelatinosa, Rhodospirillum rubrum, Streptomyces thermoautotrophicus and Thermobacillus denitrificans* have been reported to degraded cyanide (Alvillo-Rivera et al. 2021). These microorganisms use different degradation pathways (such as the hydrolytic, oxidative, reductive, substitution/transfer and hydrolytic degradation of nitrile reaction pathways) carried out by several enzymes such as *cyanide hydratase*, *cyanidase*, *nitrile hydratase*, *nitrilase*,

cyanide monooxygenase, *cyanase*, *cyanide dioxygenase*, *nitrogenase*, *cyanoalanine synthase* and *thiosulfate sulfurtransferase* (*rhodanase*) (Alvillo-Rivera et al. 2021). Thus, these microorganisms (especially bacteria) are able to act as natural barriers to prevent environmental contamination by dissociating cyanide.

However, the occurrence of bacterial diversity associated with the degradation of cyanide and the prevalent pathways that trigger the use of cyanide as an energy and carbon source in extreme and oligotrophic environments such as tailing is still unclear. Indeed, a literature search on the Web of Science using the keywords “metagenomics + gold tailings + cyanide” (last time checked 16/03/2023) indicated that no publications were found on this topic. Unlike this, there are various studies that have documented on cyanide degradation in bioreactors (Mirizadeh et al., 2014; Kantor et al., 2015; Aslıyüce and Denizli, 2017; Luque-Almagro et al., 2018; Shin et al., 2020; among others). Some of these studies have used metagenomics and bioinformatics tools to reveal microbial topology or identify novel metabolisms that drive the biodegradation of cyanide in these bioreactors. For instance, the study performed by Kantor et al. (2015) revealed the dominance of *Thiobacillus* spp. in a bioreactor system, whose genomes harbour a previously unreported operon for thiocyanate (SCN^-) degradation.

This study aims to reveal the genomic machinery that indigenous microorganisms of gold tailings possess to tolerate and potentially use cyanide as a nitrogen and carbon source. Even though the fungi kingdom may play an important role in the degradation of cyanide, this study attempts to discuss only the role of bacteria communities involved in the natural degradation and detoxification of cyanide in gold tailings. Geochemistry, metagenomics, and bioinformatics tools were used to obtain a snapshot of the bacteria, genes, and pathways that control the primary biogeochemical cycles (i.e., C, N, and S) and gather knowledge on the natural attenuation process involved in cyanide biodegradation in gold tailings containing significant concentrations of cyanide.

9.2 Methodology

9.2.1 Sample collection

Sediment tailings samples (9) were collected from a tailings dam located near Welkom in the Free State, which forms part of the Free State goldfields (Figure 9.1).

Wastewater from a nearby sewerage system has believed to have infiltrated the water used in the tailing dams. The samples were taken from 3 different locations on the tailings dam, namely Profile 1 – 3. The samples were taken in triplicate at depths of ~0.2 m (Profile 1.1, 2.1, 3.1), 0.5 m (Profile 1.2, 2.2, 3.2)and 0.9 m (Profile 1.3, 2.3, 3.3). Slabs of sample (~10-20 x 10 x 8 cm) were taken to preserve the microbial population within the sample. The slabs were collected in sterile sample bags (purchased from Lasec) to prevent contamination and stored at 4 °C for further chemical and metagenomic analysis.

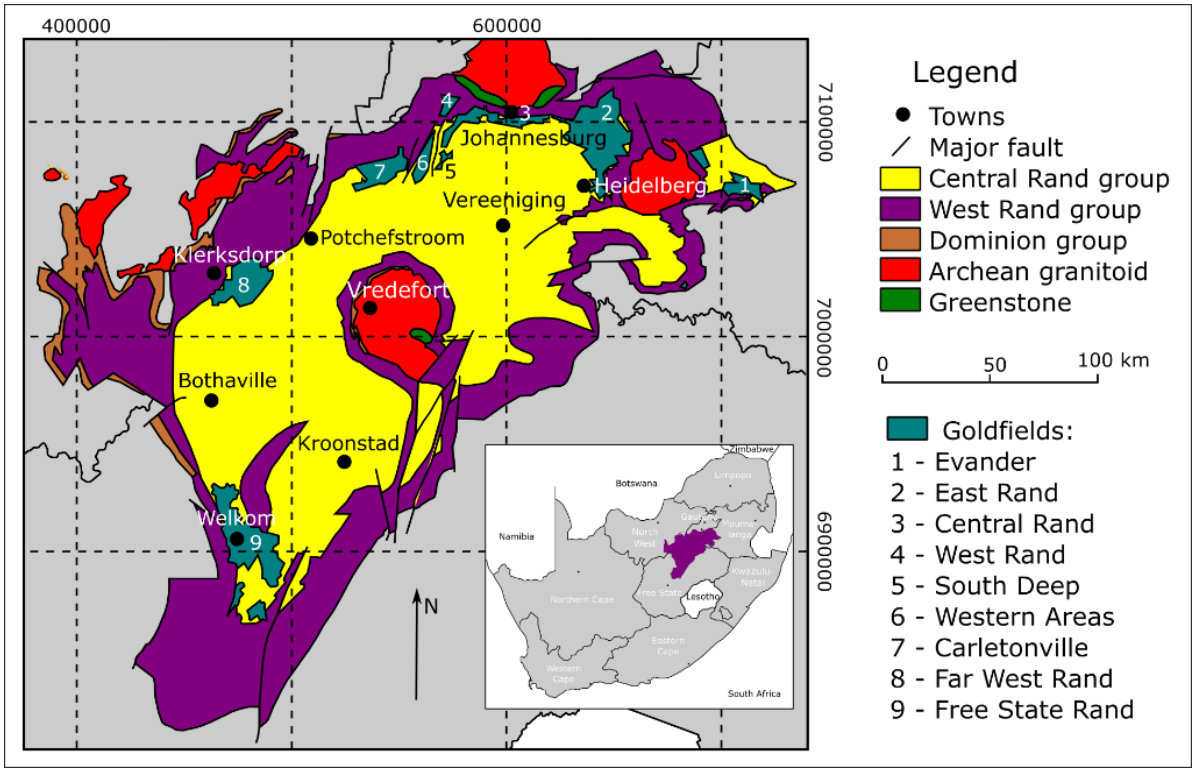

Figure 9.1: A map displaying the Witwatersrand basin that hosts one of South Africa's gold sources. Gold from this basin is mined at 9 different goldfields, where the Free State gold field is depicted at point 9. Samples were extracted from a tailings dam facility in this area, close to Welkom (Modified after Hansen, 2018 and Frimmel et al., 2005)

9.2.2 Chemical analysis

a. Paste pH measurement

The pH and ORP (Oxidation-Reduction Potential – corrected to standard hydrogen electrode) converted to Eh of the samples was determined using a ratio of 1:2

(sample:distilled water), in a laboratory. pH, ORP and temperature were measured using a portable multiprobe (Hach HQ40d).

b. Mineralogical characterization

The mineralogical composition of the samples was determined using a Panalytical Empyrean X-Ray Diffractometer (XRD), equipped with a side-window tube (anode consisting of copper and a tungsten cathode) with an X-Celerator detector. The X-ray tube produces a $CuK_{\alpha 1}$ beam with a Bragg-Brentano geometry focus position along with a Theta-Theta goniometer configuration. Samples are scanned between 3.5° and 70° 2θ at tube settings of 45 kV and 40 mA. Data Collector v3.0c is used for data collection and phase identification occurred using the X'Pert Highscore Plus software. Rietveld method was used to estimate the relative phase amounts.

c. Analysing the bioavailable fraction in the samples and $Fe_2O_{3(t)}$ and arsenic concentrations

The bioavailable fraction of the samples was analysed using Inductively Coupled Plasma - Optical Emission Spectrometry (ICP-OES, Prodigy7). The samples were digested using 0.5 g of sample and 40 ml of 0.11 M acetic acid. A blank of only 0.11 M acetic acid along with a control of sample (0.5 g) and deionized water (40 ml) were also prepared and analysed. These solutions were mixed for 16 hours and then centrifuged at 5000 rpm at 4 ºC for 20 min. The supernatant was then removed using a filter (0.45 µm disc filter - PALL corporations) and syringe. The supernatant was then acidified using 2 ml of 65 % Merck nitric acid.

d. SO_3, total nitrogen, total carbon and total cyanide analysis

SO_3 was analysed using the general scan function of a Rigaku Primus IV WDXRF on a pressed pellet, contain 8 g sample and 3 g of Hoechst wax. Total cyanide concentration was determined at XLab Earth, 259 Kent Avenue, Ferndale, South Africa. Total nitrogen and carbon were analysed using thermal conductivity detector in a CNS analyzer (LECO).

9.2.3 Biological analysis

a. DNA extraction

Sterile blades were used to remove the outer layer of the slabs in order to obtain an uncontaminated sample from within. 6g of the inner sample was used for extraction. QIAGEN DNeasy PowerLyzer Powersoil® DNA isolation kit was used to extract the DNA from the samples following the kit's instructions. The DNA was eluted with deionized H_2O and stored at -20 ºC. The quality and concentration of the samples' DNA was determined via a Thermo Scientific Nanodrop spectrophotometer. An agarose gel electrophoresis (0.8% agarose, SeaKem ®LE Agarose) was also prepared to confirm the presence of environmental DNA (eDNA). The DNA extracted was pooled into one sample per profile and were sent for metagenomic analysis at CosmosID.

b. Metagenome shotgun sequencing

The quantity and quality of the eDNA was analysed at CosmosID using a Qubit 4 fluorometer and Thermofischer Qubit™ dsDNA HS Assay kit. The DNA libraries (total DNA input – 1 ng) were created using the Nextera XT DNA Library Preparation Kit (Illumina) and IDT Unique Dual Indexes. A relational amount of Illumina Nextera XT fragmentation enzyme was used to fragment the genomic DNA. The construction of the libraries occurred by adding unique dual indexes to the samples and 12 cycles of PCR were completed. Purification of the libraries occurred using AMpure Beckman Coulter magnetic Beads and then eluted in a QIAGEN EB buffer. Quantification of the libraries occurred using Qubit 4 fluorometer and Qubit™ dsDNA HS Assay Kit. Sequencing of the libraries was then completed on an Illumina NextSeq 2000 platform 2x150bp.

9.2.4 Statistic and Bioinformatics Analysis

a. Taxonomy identification

CosmosID-HUB Microbiome Platform (CosmosID Inc., Germantown, MD) was used to directly analyse the unassembled sequencing reads (Ottesen et al., 2016; Ponnusamy et al., 2016; Hasan et al., 2014; and Lax et al., 2014) and achieve taxonomy identification at the species, subspecies, and/or strain level and quantification of relative abundance of the identified taxa.

Briefly, the system utilizes curated genome databases and a high-performance data-mining algorithm to rapidly disambiguate millions of metagenomic sequence reads into

discrete microbial taxa. The pipeline has two separable comparators. The first consists of a pre-computation phase and a per-sample computation. The input to the pre-computation phase is a curated reference microbial database and its output is a whole genome phylogeny tree, together with sets of fixed length n-mer fingerprints (biomarkers) that are uniquely identified to distinct nodes of the tree. The second per-sample, computational phase searches the millions of sequence reads against the fingerprint sets. The resulting statistics are analyzed to give fine-grain composition and relative abundance estimates at all nodes of the tree. Overall classification precision is maintained through aggregation statistics.

b. Quality Control, assembly and annotation

The unassembled sequencing reads have been assembled and analysed using the software DiTing (Xue et al., 2021) and metaSPAdes v3.11.0 (Bankevich et al., 2012) with default settings. Prior the assembling and analysis, the quality of the unassembled sequencing reads were assessed with FastQC version 0.11.6 and low-quality bases (per base sequence quality <28) were removed with Trimmomatic version 0.36 (Bolger et al., 2014). The filter reads were merged using PEAR with a minimum specified overlap of 10 bases, minimum assembled length of 50 bases, and a minimum alignment p-value of 0.01, resulting in an average assembly efficiency of 99%. The merged sequences were analysed using the software DiTing to infer and compare biogeochemical pathways. The input datasets were assembled by metaSPAdes v3.12.0 (Nurk et al., 2017). Genes are then predicted and translated from the assembled contigs by Prodigal v2.6.3 with the “-p meta” option (Hyatt et al., 2010). DiTing annotates protein sequences based on the KEGG database (Ogata et al., 1999) for most microbial-mediated biogeochemical cycles (e.g., carbon, nitrogen, sulphur, metals, among others). The relative abundance of each functional gene was calculated followed by the relative abundance of each pathway, which is calculated according to a customized formula (Xue et al., 2021). Heatmaps and sketch plots for easier visualization and comparison of the biogeochemical cycles were also generated with software DiTing. The assembly contigs generated by metaSPAdes v3.11.0 were also assessed using MetaQUAST (Mikheenko et al., 2016) and used for Binning.

c. Binning of the metagenomes and identification of proteins associated to cyanide degradation

Contigs were organised into genome bins or metagenome-assembled genomes (MAGs) based on tetra-nucleotide sequence composition with MetaBAT2 v2.11.3 (Kang et al., 2015). The completeness, coverage, contamination, and strain heterogeneity of the MAGs were estimated using CheckM v1.0.11 with the single-copy marker gene (Parks et al., 2015). Only MAGs of completeness between 70 to 99% and low contamination (< 1%) were selected for further analysis.

In order to identify proteins associated to cyanide degradation, the selected MAGs were deposited in RAST. Then, the genome bins were aligned to reference sequences of characterized proteins of interest using BLAST. The sequences of proteins of interest were obtained from Uniprot (https://www.uniprot.org/).

9.3 Results and discussion

9.3.1 Geochemistry of the study site

The tailings samples from all profiles display acidic and oxidizing conditions (Table 9.1). This corresponds with the tailings dam model reported by Hansen et al. (2018), where the outermost layer (~2 m) of tailings dams has oxidizing conditions and the system is acidified due to the dissociation of pyrite (Eq. 1) (Williamson and Rimstidt, 1994). The presence of jarosite and the high sulfur-content detected in the samples can be associated with the dissociation of pyrite. The presence of jarosite also suggests that the pH was buffered with carbonate minerals, as jarosite forms at a pH of ~2 (Sánchez-España, 2007).

Table 9.1: Average physiochemical results from the samples obtained in this study. The detection limit for total cyanide is 0.1 mg.L-1. SE – standard error. Standard deviation added. pH, Eh and T were determined in a laboratory. Detailed results are displayed in Table S9.1 of the supplementary material. (bdl – below detection limit)

	Physicochemical parameters						
Units	pH	Eh (mV)	T (ºC)	S (wt%)	Total carbon (wt%)	Total nitrogen (wt%)	Total cyanide ($mg.L^{-1}$)
	n = 3 Mean ± SE	*n* = 3 Mean ± SE	*n* = 3 Mean ± SE	*n* = 3 Mean ± SE	*n* = 3 Mean ± SE	*n=3* Mean ± SE	*n* = 3 Mean ± SE
Profile 1	4.92 ± 0.07	253.1 ± 40.91	24.0 ± 0.15	0.77 ± 0.1	0.17 ± 0.005	bdl	1.93 ± 0.57

Profile 2	4.61 ± 0.08	328.5 ± 59.53	23.9 ± 0.15	0.84 ± 0.26	0.17 ± 0.012	bdl	5.63 ± 4.74
Profile 3	4.58 ± 0.19	263.7 ± 59.75	24.2 ± 0.15	0.88 ± 0.06	0.17 ± 0.000	bdl	3.00 ± 0.26

The total carbon concentration is moderately high in all the tailing samples (Chung et al., 2019) (Table 9.1). The carbon content can be attributed mainly to the carbonate minerals detected in the samples such as siderite ($FeCO_3$), (others may include ankerite $Ca(Fe,Mg)(CO_3)_2$, calcite $CaCO_3$, dolomite $CaMg(CO_3)_2$) (Table 9.2). Cyanide compounds might represent the organic carbon content in the tailing samples, which are commonly described as oligotrophic environments.

Contrarily, the nitrogen concentrations (Table 9.1) were not detected in the sediment samples; thus, atmosphere nitrogen uptake might play a crucial role to sustain life in the tailing. Nitrogen also tends to remain in solution, concentrating in the return water dam (Revey, 1996). Other sources of nitrogen, such as cyanide, were detected in all the samples, which is especially higher in the profile 2, where the cyanide concentration closest to the surface was 10 $mg.L^{-1}$ decreasing to 0.6 $mg.L^{-1}$ 0.9 m below the first sample (Table 9.1).

Table 9.2: The mineralogical data obtained from XRD analysis, , full set of results can be found in Table S2. Results are quantitative from Rietveld refinement. Diffractograms are displayed in Figures S9.1 – S9.9.

	Mineralogical results (wt%)								
Units	Quartz	Pyrophyllite	Chlorite	Jarosite	Muscovite	Plagioclase	Microcline	Diopside	Siderite
	n = 3 Mean ± SE	n = 3 Mean ± SE	n = 3 Mean ± SE	n = 3 Mean ± SE	n = 3 Mean ± SE	n = 3 Mean ± SE	n = 3 Mean ± SE	n = 3 Mean ± SE	n = 3 Mean ± SE
Profile 1	87,5 ± 2,1	9,3 ± 1,1	0,8 ± 0,0	0,6 ± 0,2	0,8 ± 0,4	1,1 ± 0,0	0,7 ± 0,0	0,7 ± 0,0	0,7 ± 0,0
Profile 2	79,6 ± 4,9	15,4 ± 4,3	1,0 ± 0,2	0,8 ± 0,3	0,5 ± 0,1	1,2 ± 0,1	0,8 ± 0,3	0,9 ± 0,2	0,7 ± 0,0
Profile 3	87,7 ± 2,2	9,4 ± 1,5	0,3 ± 0,0	0,6 ± 0,2	0,4 ± 0,2	1,0 ± 0,3	0,7 ± 0,2		

The chemistry of the tailings' bioavailable fraction (Table 9.3) shows high aluminium concentrations in all the samples. Unlike aluminium, iron was only detected in high concentrations in profiles 1 and 3. Potentially toxic elements such as chromite, zinc

and nickel were detected only in the Profile 2, while lead was only present in the bioavailable fraction of profile 3.

Table 9.3: The bioavailable chemical analysis results obtained from ICP-OES analysis.

	Bioavailable fraction											
Units	Al ($g.kg^{-1}$)	Fe ($g.kg^{-1}$)	Li ($g.kg^{-1}$)	In ($g.kg^{-1}$)	Ni ($g.kg^{-1}$)	Zn ($g.kg^{-1}$)	Co ($g.kg^{-1}$)	Pb ($g.kg^{-1}$)	Ga ($g.kg^{-1}$)	V ($g.kg^{-1}$)	Cr ($g.kg^{-1}$)	Bi ($g.kg^{-1}$)
	n = 3 Mean ± SE	n = 3 Mean ± SE	n = 3 Mean ± SE	n = 3 Mean ± SE	n = 3 Mean ± SE	n = 3 Mean ± SE	n = 3 Mean ± SE	n = 3 Mean ± SE	n = 3 Mean ± SE	n = 3 Mean ± SE	n = 3 Mean ± SE	n = 3 Mean ± SE
Profile 1	28,15 ± 11,77	15,64 ± 14,00	7,96 ± 2,33	6,25 ± 0,86	1,03 ± 1,12				0,11 ± 0,20			0,037 ± 0,064
Profile 2	19,63 ± 10,08		3,32 ± 1,31	5,68 ± 0,95	3,49 ± 1,41	2,94 ± 5,09	2,46 ± 4,26				0,17 ± 0,012	
Profile 3	31,97 ± 21,78	22,11 ± 15,78	1,82 ± 0,36	7,89 ± 2,82	0,90 ± 0,71			1,67 ± 2,90	1,29 ± 0,59	0,41 ± 0,48		0,007 ± 0,012

9.3.2 Taxonomy assignment

Metagenomics analysis and binning involved a total of 326439 raw reads generated on average per Profile. The bins with more than 80% completeness were chosen. Taxa with relative abundance above 1% are represented in Figure 9.2. The taxonomy classification indicated that the phyla *Proteobacteria* and *Firmicutes* dominated the profiles. These phyla are known to colonize acid tailings with high concentrations of heavy metals thanks to their chemoautotrophic or chemoheterotrophic metabolisms (Fashola et al., 2020). *Acidiphilium* > *Paenibacillus* > *Bordetella* > *Acinetobacter* were the most predominant genera in Profile 1. In Profile 2, while the representation of *Acidiphilium* decreases, the relative abundance of members of the genus *Paenibacillus* increases followed by *Klebsiella, Bordetella, Achromobacter,* among others*. Paenibacillus* is the most abundant genera present in the Profile 3 followed by *Bordetella, Cutibacterium and Acidiphilium*, among others*.*

Thermoplasma (2.35 %) was also identified in the Profile 3. A member of the *Thermoplasma* genus, namely *Thermoplasma* (Tp.) *acidophilum*, a chemolithotrophic acidophilic archaeon, is commonly found as part of the microbial community in tailings, along with *Acidophilum* and *Paenibacillus* (Sibanda et al., 2018). On the other hand, *Bordetella*, *Acinetobacter*, *Klebsiella*, *Achromobacter* and *Cutibacterium* might come from external sources. Some of those opportunistic pathogens can oxidize inorganic

sources (e.g., Fe^{2+}, H_2S, S^0, among others) to obtain energy, helping them to thrive in the tailings environment (Johnson et al., 2012). The slightly acid conditions (pH 4) in the system might also facilitate the proliferation and establishment of these communities.

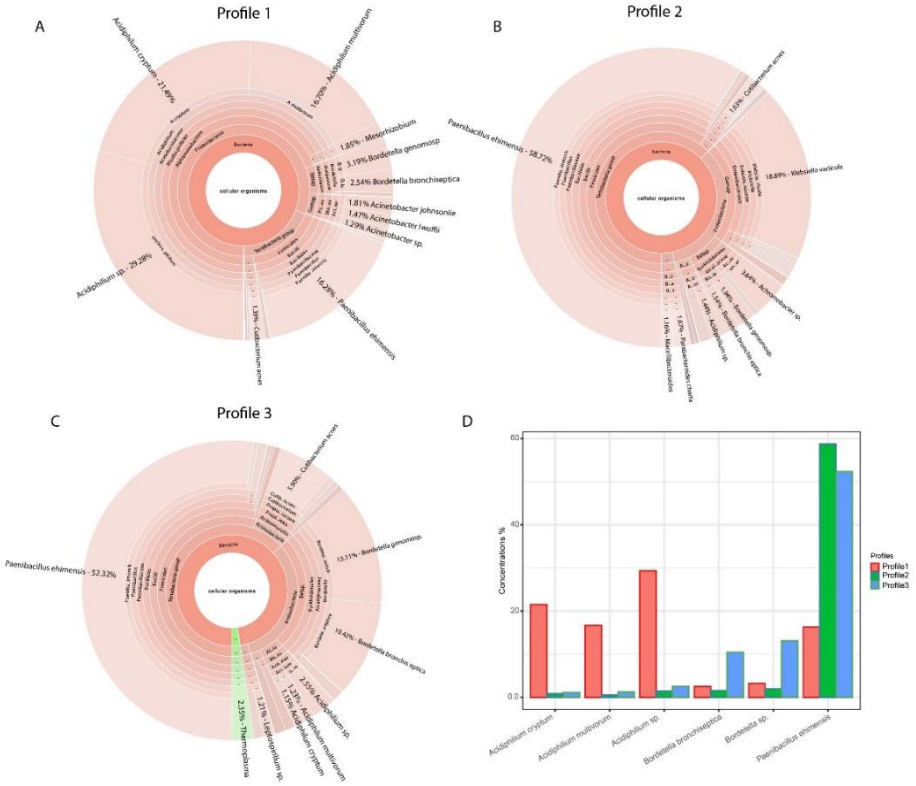

Figure 9.2: Depiction of the diversity and abundance of the microbes in each of the Profiles (their Phyla, Class, Order, Family, Genus and Species). The proportions are a representation of microbes with a relative abundance greater than 1 %.

9.3.3 Main metabolisms in the tailings

In the three metagenomes, genes associated with the biogeochemical cycles of carbon (Figure 9.3A), sulphur (Figure 9.3B), and nitrogen (Figure 9.3C) were detected. Heatmaps of these pathways can be seen in Figure S9.10. Genes and pathways associated with the carbon cycling were the most abundant in the three metagenomes. Anaplerotic reactions > TCA > gluconeogenesis > fermentation to succinate > glycolysis pathways represent 50.27 % of the functional annotations in the metagenomes. The presence of genes and pathways associated with the carbon cycle corresponded with the total carbon content across the tailings that might include the

cyanide concentrations, as well as the presence of bacteria capable of oxidizing inorganic carbon sources (e.g., *Acidophilum*, *Bordetella*, *Acinetobacter*).

Most of these bacteria also play a crucial role in the sulfur biogeochemical cycle as some members of these genera can perform sulfur (*fccAB*), thiosulfate (*SOX*, *doxAD* and *tsdA*), sulfite (*sorB*, *SUOX* and *soeABC*), and sulfide oxidation (*sat* and *aprAB*), representing 5.9 % of the 10.2 % of the functional annotations identified in this cycle (Figure 9.3B). The genes involved in assimilatory sulfate reduction (3.5%) and the disproportionation of elemental sulfur and thiosulfate (0.7%) also form part of the sulfur biogeochemical cycle. It seems that the disproportionation of elemental sulfur and thiosulfate in this system fuel the bacterial sulfur oxidation pathways with sulfur reduced species. It has been documented that the catalysis of the chemolithotrophic process by the disproportionation of inorganic sulfur intermediates at moderate temperatures (Finster, 2008; Amend et al., 2020; Rameez et al., 2020; Santana et al., 2021; among others). Indeed, *Sulfobacillus acidophilus*, a bacterium identified in all the profiles with abundance below 1 %, is able to carry out disproportionation of inorganic sulfur intermediates (Finster, 2008). Despite the oxidative conditions in the outermost layer of the tailing, the presence of the dsrAB gene in profile 1 suggests that the dissimilatory sulfate reduction cannot be ruled out in this environment as another source of sulfur-reduced species.

The nitrogen biogeochemical cycle seems to be driven mainly by nitrogen fixation (*nif*KDH), nitrification (*nxr*AB), denitrification (*nar*GHI/*nap*AB, *nir*K or *nir*S, *nor*BC, *nos*Z), and dissimilatory nitrate reduction to ammonium (nirBD/nrfAH). Nitrogen fixation and complete denitrification seem to be only achieved in the Profile 2. The members of the genera *Paenibacillus* and *Acinetobacter* have the capability to fix atmosphere nitrogen and to carry out complete denitrification as they host the *nif*KDH and *nos*Z genes (Shelly et al., 2020). *Paenibacillus* is abundant in Profile 2, but is also one of the more abundant bacteria in Profile 1 and 3. Therefore, the presence of those pathways in Profile 1 and 3 cannot be ruled out and their absence might be associated to the quality of the metagenome.

The dissimilatory reduction of the arsenic pathway was also well represented in the tailing (7.7 %). Arsenic is often found in arsenopyrite or in trace amounts in pyrite in gold deposits (Agangi et al., 2014). Mineral extraction and cyanidation process leads

to the mobilization of arsenic that could be immobilized again into the mineral structure of iron oxyhydroxide when deposited in the tailings dams. For instance, As^{3+} can be sorbed onto schwertmannite (Burton et al., 2009). This reiterates the concept mentioned that the absence of arsenic in the bioavailable fraction is due to arsenic bonding to the fraction associated with iron oxyhydroxide minerals. It is well known that As^{3+} is used as an energy source by chemolithotrophic bacteria (Akerman et al., 2011) and may be an explanation for the overrepresentation of this pathway in the system. This concept will be explored in future studies.

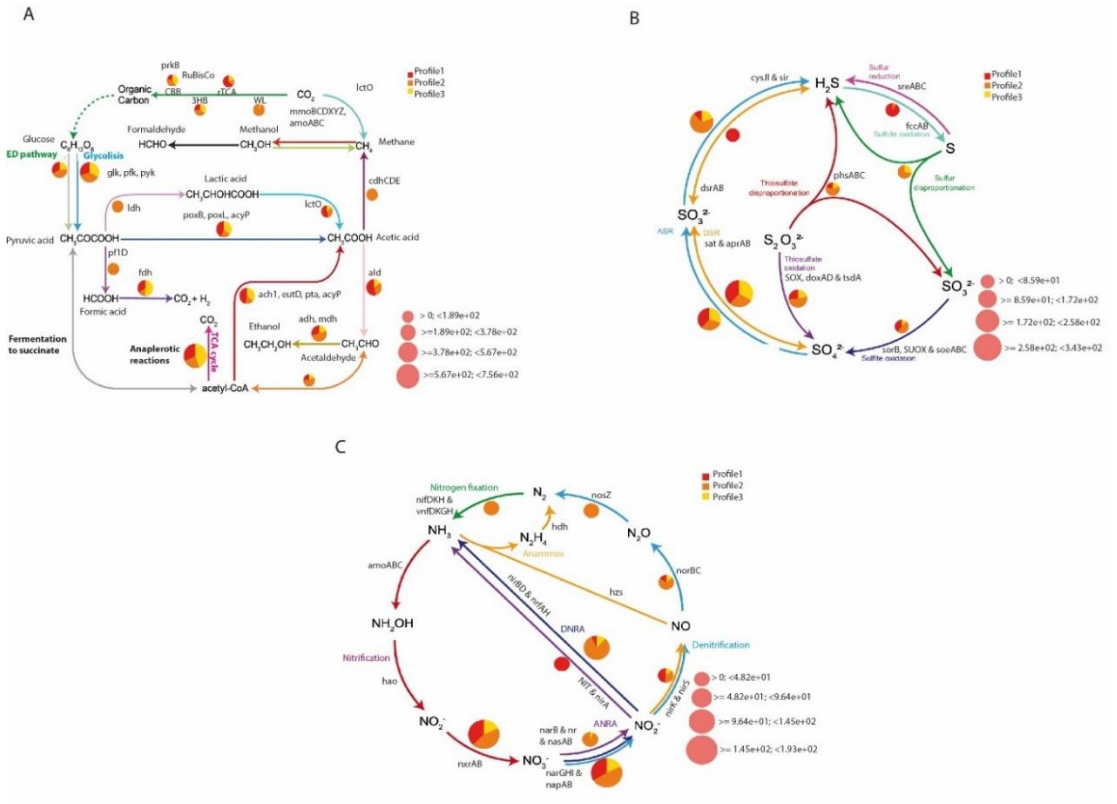

Figure 9.3: Diagrams displaying the metabolisms obtained from the metagenome results in Table S4. The pie charts represent relative abundances in each sample and the size of the charts represents the relative abundance of each pathway. A) A depiction of the pathways determined from the metagenomic samples analysed in this study of the carbon cycle (CBB – Calvin-Benson-Bassham cycle; rTCA – reductive citric acid cycle; WL – Wood-Ljungdahl pathway; 3HB – 3-hydroxypropionate bicycle; DHC – dicarboxylate-hydroxybutyrate cycle). B) A representation of the sulphur cycle pathways observed in the metagenomic results of the samples in this study (ASR – assimilatory sulfate reduction; DSR – dissimilatory sulfate reduction). C) Diagrammatic representation of the pathways in the nitrogen cycle in each of the metagenomic samples in this study (ANRA – assimilatory nitrate reduction to ammonium; DNRA – Dissimilatory nitrate reduction to ammonium; Anammox – anaerobic ammonium oxidation).

9.3.4 Enzymes and pathways associated with the cyanide degradation

Genes encoding enzymes to carry out hydrolytic, reductive, and substitution/transfer pathways were identified in the three profiles. Despite the oxidative conditions, no functional annotations for oxidative pathways were identified in the metagenomes analysed by MGRAST. The analysis suggests that cyanide assimilation (substitution/transfer) controls the detoxification process in the system. The mercaptopyruvate sulfurtransferase that catalyses this process represents 72.3 % (on average) of the functional annotations associated with cyanide detoxification in the profile's metagenomes. Annotating enzymes such as nitrile hydratase (NHase) and nitrilase trigger hydrolytic degradation (Table 9.4). The NHase has specific substrate and can directly hydrolyse and cleave to the carbon-nitrogen triple bond of cyanide, forming formamide. The nitrilase converts cyanide to ammonia and carboxylic acid, which are utilized in their metabolism activity (Gupta et al., 2010). The hydrolytic pathway represents, on average, 27 % of the functional annotations associated with cyanide degradation.

Nitrogenase such as *nifH*, annotated in the metagenomes, might serve to detoxify cyanides (Mehta et al., 2003). This enzyme degrades (in the reductive pathway) the carbon-nitrogen triple bond species of HCN, nitriles and isonitriles to methane and ammonia (Luque-Almagro et al., 2018). Nitrogenase is oxygen-sensitive (Seefeldt et al., 2004); thus, its inactivity under oxidative conditions present in the outermost layer of tailing might be expected.

Table 9.4: The different functions of the metabolisms related to cyanide degradation that were discovered in samples. Counts are displayed here as percentages.

Pathways	**Enzymes**	**Profile 1**		**Profile 2**		**Profile 3**	
		Hits	**%**	**Hits**	**%**	**Hits**	**%**
Hydrolytic pathway	Nitrilase	906	18.75	1500	23.11	1241	17.61
	Nitrile hydratase	330	6.83	635	9.78	328	4.65
Reductive pathway	Nitrogenase (nifH)	9	0.19	86	1.32	61	0.87

Substitution/transfer pathway	Mercaptopyruvate sulfurtransferase	3588	74.24	4270	65.78	5417	76.87

Indeed, in the metagenome-assembled genomes (MAGs), nitrogenases triggering the reductive pathway for cyanide degradation were not found. However, enzymes such as cyanase that drive oxidative cyanide degradation pathways were annotated in members of the genera *Alicyclobacillus* (bin 4) and *Achromobacter* (bin 19) thriving in the Profile 2 and *Alicyclobacillus* (bin 10) and *Chthonomona* (bin 14) colonizing the Profile 3 (Figure 9.4). All these bacteria have aerobic metabolisms (Bertrand et al., 2015). Interestingly, cyanase was not annotated in Profile 1; though, due to the completeness of the bins and the quality of the metagenomes (the lowest number of sequences between the profiles), its presence cannot be ruled out.

Hydrolysis and cyanide assimilation (substitution/transfer, and synthases – Figure 9.4) seem to be the main pathways controlling the degradation and detoxification of cyanide in most of the bins colonizing the profiles, which correspond with the results obtained by MGRAST. Hydrolytic degradation seems to be catalysed mainly by cyanidase (CynD) and nitrilase enzymes. CynD is known to convert cyanide to relatively nontoxic formate directly. This enzyme is commonly present in prokaryotes, while nitrilase is involved in the biosynthesis of proteins from cyanide in fungi and certain prokaryotes. The NHase was only annotated in members of the order *Actinomycetales* (genera unknown belongs to bins 9, 11 and 23).

The assimilatory cyanide pathways seem to be catalysed by rhodanese (rhdA), mercaptopyruvate sulfurtransferase (Mpst) and cyanoalanine nitrilase (Can) annotated in most bins assembled from the metagenome obtained from Profiles 1, 2, and 3 (Figure 9.4). The cyanide assimilation tends to increase the growth of the microorganism by providing an extra nitrogen source and preventing it from cyanide toxicity.

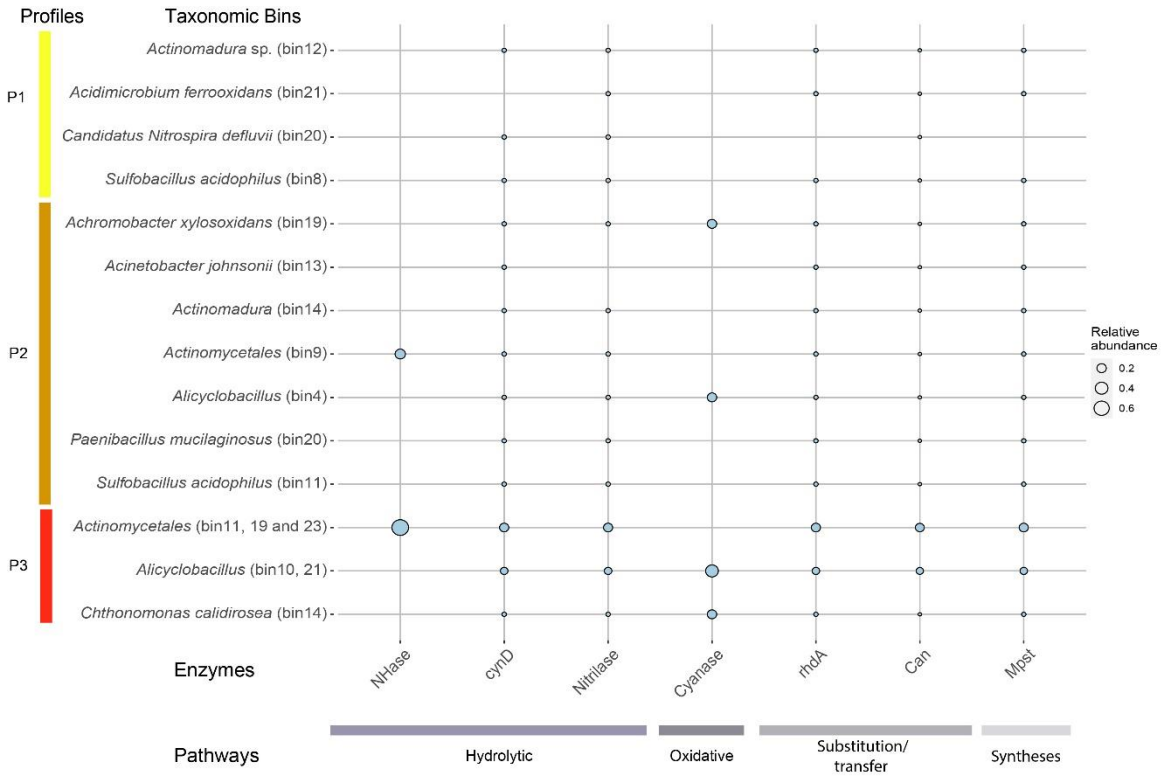

Figure 9.4: Bins, enzyme and pathways expressed from the metagenomic data obtained in this study.

Microorganisms identified and characterized genomically from Profiles 1, 2, and 3 represent the first barrier for the detoxification and degradation of cyanide in the outermost layer of the tailings. It seems that the oligotrophic conditions and lack of nitrogen sources (except for the atmospheric) induce the use of cyanide, which would contribute to its natural attenuation in those anthropogenic systems.

9.4 Conclusion

The disposal of cyanide and mining wastes dumped in tailings from gold extraction is a public concern in mining countries. The need to create eco-friendly and sustainable technologies has led to the development of biotechnologies based on microorganisms that are capable of degrading cyanide. Indigenous consortiums isolated from mining wastes containing cyanide have been used for these purposes. The performance of these consortium used in bioreactors has been dissected using omics tools. However, despite the advance in omics techniques, the understanding of cyanide's natural attention in gold tailings has been overlooked. Here, this study brings the first insight into bacterial cyanide degradation in situ and shows how bacteria degrade cyanide in complex environments such as gold tailings that contain cyanide. The hydrolytic and assimilatory cyanide pathways seem to be the pathways that control the system. Also,

it appears that most of the bacteria characterized in this system can perform cyanide degradation and assimilation through these processes suggesting that cyanide is an excellent source of carbon and energy sources in those oligotrophic systems. The identification of both the pathways and the bacteria that can carry out those processes will improve/are the stepping stone to developing a new generation of cyanide bioremediation technology that could be used in situ or ex situ.

9.5 References

Acera F, Carmona MI, Castillo F, Quesada A and Blasco R, 2017, A Cyanide-Induced 3-Cyanoalanine Nitrilase in the Cyanide-Assimilating Bacterium *Pseudomonas pseudoalcaligenes Strain CECT 5344*, Applied and Environmental Microbiology, v. 83, n. 9, p. 1-14.

Aczel MR, 2019, What Is the Nitrogen Cycle and Why Is It Key to Life?, Frontiers for Young Minds, v. 7, article number 41.

Agangi A, Hofmann A, Rollion-Bard C, Marin-Carbonne J, Cavalazzi B, Large R and Meffre S, 2014, Gold accumulation in the Archaean Witwatersrand Basin, South Africa — Evidence from concentrically laminated pyrite, Earth -Science Reviews, v. 140, p. 27-53.

Akcil A, 2003, Destruction of cyanide in gold mill effluents: biological versus chemical treatments, Biotechnology Advances, v. 21, n. 6, p. 501–511.

Akcil A and Mudder T, 2003, Microbial destruction of cyanide wastes in gold mining: process review, Biotechnology Letters, v. 25, p. 445–450.

Akerman NH, Price RE, Pichler T and Amend JP, 2011, Energy sources for chemolithotrophs in an arsenic- and iron-rich shallow-sea hydrothermal system, Geobiology, v. 9, p. 436–445.

Alvillo-Rivera A, Garrido-Hoyos S, Buitron G, Thangarasu-Sarasvathi P and Rosano-Ortega G, 2021, Biological treatment for the degradation of cyanide: A review, Journal of Materials Research and Technology, v. 12, p. 1418-1433.

Amend JP, Aronson HS, Macalady J and LaRowe DE, 2020, Another chemolithotrophic metabolism missing in nature: sulfur comproportionation, Environmental Microbiology, v. 22, n. 6, p. 1971–1976.

Aslıyüce S and Denizli A, 2017, Design of PHEMA Cryogel as Bioreactor for Biological Cyanide Degradation from Wastewater, J. Biol. & Chem., v. 45, n. 4, p. 639-645.

Asta MP, Cama J, Martinez M and Gimenez J, 2009, Arsenic removal by goethite and jarosite in acidic conditions and its environmental implications, Journal of Hazardous Material, v. 171, p. 965-972.

Bakatula EN and Tutu H, 2016, Characterization and speciation modelling of cyanide in effluent from an active slime dam, South African Journal of Chemistry, v. 69, p. 140-147.

Bankevich A, Nurk S, Antipov D, Gurevich AA, Dvorkin M, Kulikov AS, Lesin VM, Nikolenko SI, Pham S, Prjibelski AD, Pyshkin AV, Sirotkin AV, Vyahhi N, Tesler G, Alekseyev MA and Pevzner PA, SPAdes: a new genome assembly algorithm and its applications to single-cell sequencing, Journal of Computational Biology, v. 19, p. 455–477.

Baxter J and Cummings SP, 2006, The current and future applications of microorganism in the bioremediation of cyanide contamination, Antonie Van Leeuwenhoek, v. 90, n. 1, p. 1–17.

Bertrand JC, Caumette P, Lebaron P, Matheron R, Normand P and Sime-Ngando T, 2015, Environmental Microbiology: Fundamentals and Applications: Microbial Ecology, Springer, 933pp.

Bolger AM, Lohse M and Usadel B, 2014, Trimmomatic: a flexible trimmer for Illumina sequence data, Bioinformatics, v. 30, n. 15, p. 2114–2120.

Burton ED, Bush RT, Johnston SG, Watling KM, Hocking RK, Sullivan LA and Parker GK, 2009, Sorption of Arsenic(V) and Arsenic(III) to Schwertmannite, Environmental Science and Technology, v. 43, n. 24, p. 9202–9207.

Chung AP, Coimbra C, Farias P, Francisco R, Branco R, Simão FV, Gomes E, Pereira A, Vila MC, Fiúza A, Mortensen MS, Sørensen SJ and Morais PV, 2019, Tailings microbial community profile and prediction of its functionality in basins of tungsten mine, Scientific Reports, v. 9, article number 19596.

Dash RR, Gaur A and Balomajumder C, 2009, Cyanide in industrial wastewaters and its removal: A review on biotreatment, Journal of Hazardous Materials, v. 163, n. 1, p. 1–11.

Donato D, Ricci PF, Noller B, Moore M, Possingham H and Nichols O, 2008, The protection of wildlife from mortality: hypothesis and results for risk assessment, Environ. Int., v. 34, n. 6, p. 727-736. 10.1016/j.envint.2007.10.003

Ebbs S, 2004, Biological degradation of cyanide compounds, Current Opinion in Biotechnology, v. 15, n. 3, p. 231–236.

Eisler R and Wiemeyer SN, 2004, Cyanide hazards to plants and animals from gold mining and related water issues, Environ Contam Toxicol, v. 183, p. 21-54.

Evans DJ, Jones R, Woodley PR, Wilborn JR and Robson RL, 1991, Nucleotide sequence and genetic analysis of the *Azotobacter* chroococcum nifUSVWZM gene cluster, including a new gene (nifP) which encodes a serine acetyltransferase, Journal of Bacteriology, v. 173, p. 5457-5469.

Fashola MO, Ngole-Jeme VM and Babalola OO, 2020, Physicochemical properties, heavy metals, and metal-tolerant bacteria profiles of abandoned gold mine tailings in Krugersdorp, South Africa, Canadian Journal of Soil Science, v. 100, n. 3, p. 309-318.

Feng C, Aldricha C, Eksteena JJ and Arrigan DWM, 2018, Removal of arsenic from gold cyanidation process waters by use of cerium based magnetic adsorbents, Minerals Engineering, v. 122, p. 84-90.

Finster K, 2008, Microbiological disproportionation of inorganic sulfur compounds, Journal of Sulfur Chemistry, v. 29, n. 3-4, p. 281-292.

Fivaz, CE, 1988, Presidential Address: How the MacArthur-Forrest cyanidation process ensured South Africa's golden future, J. S. At,. Inst. Min. Metal., v. 88, n. 9.

Frimmel HE, Groves DI, Kirk J, Ruiz J, Chelsey J and Minter WEL, 2005, The Formation and Preservation of the Witwatersrand Goldfields, the World’s Largest Gold Province, Economic Geology 100th Anniversary Volume, p. 769–797.

Fuhrmann M and Hennecke H, 1984, Rhizobium japonicum nitrogenase Fe protein gene (nifH), Journal Bacteriology, v. 158, n. 3, p. 1005-1011.

Guerrero-Cruz S, Vaksmaa A, Horn MA, Niemann H, Pijuan M and Ho A, 2021, Methanotrophs: Discoveries, Environmental Relevance, and a Perspective on Current and Future Applications, Frontiers in Microbiology, v. 12, article number 678057.

Gschwendtner S, Mansfeldt T, Kublik S, Touliari E, Buegger F and Schloter M, 2016, Long-term ferrocyanide application via deicing salts promotes the establishment of *Actinomycetales* assimilating ferrocyanide-derived carbon in soil, Microbial Biotechnology, v. 9, n. 4, p. 502–513.

Gupta N, Balomajumder C and Agarwal VK, 2010, Enzymatic mechanism and biochemistry for cyanide degradation: a review, Journal of Hazardous Material, v. 176, n. 1-3, p. 1–13.

Hansen RN, 2018, Inter-comparison geochemical modelling approaches and implications for environmental risk assessments: A Witwatersrand gold tailings source term characterisation study, Applied Geochemistry, v. 95, p. 71-84.

Hasan N, Young B, Minard-Smith A, Saeed K, Li H, Heizer E, Mcmillan N, Isom R, Abdullah A, Bornman D, Faith S, Choi SY, Dickens M, Cebula T and Colwell R, 2014, Microbial Community Profiling of Human Saliva Using Shotgun Metagenomic Sequencing, PloS one, v. 9, article number e97699.

Hedley N and Tabachnick H, 1950, Chemistry of Cyanidation, Mineral Dressing Notes, n. 17. American Cyanamid Co.

Howden AJM, Harrison CJ and Preston GM, 2009, A conserved mechanism for nitrile metabolism in bacteria and plants, Plant Journal, v. 57, n. 2, p. 243–253.

Howden AJM and Preston GM, 2009, Nitrilase enzymes and their role in plant–microbe interactions, Microbial Biotechnology, v. 2, n. 4, p. 441–451.

Huertas MJ, Luque-Almagro VM, Martínez-Luque M, Blasco R, Moreno-Vivián C, Castillo F and Roldán MD, 2006, Cyanide metabolism of *Pseudomonas pseudoalcaligenes CECT5344*: role of siderophores, Biochemical Society Transactions, v. 34, n. 1, p. 152–155.

Hyatt D, Chen GL, LoCascio PF, Land ML, Larimer FW and Hauser LJ, 2010, Prodigal: prokaryotic gene recognition and translation initiation site identification, BMC Bioinformatics, v. 11, n. 1, article number 119.

Jacobson MR, Brigle KE, Bennett LT, Setterquist RA, Wilson MS, Cash VL, Beynon J, Newton WE and Dean DR, 1989, Physical and genetic map of the major nif gene cluster from *Azotobacter vinelandii*, Journal of Bacteriology, v. 171, p. 1017-1027.

Jaszczak E, Polkowska Z, Narkowicz S, Namieśnik J (2017) Cyanide in the environment – analysis – problems and challenges. Environ. Sci. Pollut. Res. Springer 24:15929-15948.

Johnson DB, Kanao T and Hedrich S, 2012, Redox Transformations of Iron at Extremely Low pH: Fundamental and Applied Aspects, Frontiers in Microbiology, v. 3, n. 96, p. 1-13.

Kang DD, Froula J, Egan R and Wang Z, 2015, MetaBAT, an efficient tool for accurately reconstructing single genomes from complex microbial communities, PeerJ, v. 3, article number e1165.

Kantor RS, van Zyl AW, van Hille RP, Thomas BC, Harrison STL and Banfield JF, 2015, Bioreactor microbial ecosystems for thiocyanate and cyanide degradation unravelled with genome-resolved metagenomics, Environmental Microbiology, v. 17, n. 12, p. 4929–4941.

Karamba KI, Ahmad SA, Zulkharnain A, Yasid NA, Ibrahim S and Shukor MY, 2018, Batch growth kinetic studies of locally isolated cyanide-degrading Serratia marcescens strain AQ07, Biotechnology, v. 8, n. 11, p. 4-9.

Khan A, Akhter G, Gabriel H and Shahid M, 2020, Anthropogenic effects of coal mining on ecological Resources of the central indus basin, Pakistan, Int. J. Environ. Res. Publ. Health, v. 17, n. 4, p. 1255. 10.3390/ijerph17041255

Kobayashi M and Shimizu S, 1998, Metalloenzyme nitrile hydratase: structure, regulation and application to biotechnology, Nature Biotechnology, v. 16, n. 8, p. 733–736.

Kobayashi M and Shimizu S, 2000, Nitrile hydrolases, Current Opinion in Chemical Biology, v. 4, n. 1, p. 95–102.

Kumar R, Saha S, Dhaka S, Kurade MB, Kang CU, Baek SH and Jeon BH, 2016, Remediation of cyanide-contaminated environments through microbes and plants: a review of current knowledge and future perspectives, Geosystem Engineering, v. 20, n. 1, p. 28–40.

Kyle JH, Breuer PL, Bunney KG, Pleysier R and May PM, 2011, Review of trace toxic elements (Pb, Cd, Hg, As, Sb, Bi, Se, Te) and their deportment in gold processing, Part 1: Mineralogy, aqueous chemistry and toxicity, Hydrometallurgy, v. 107, n. 3–4, p. 91-100.

Kyle JH, Breuer PL, Bunney KG, Pleysier R and May PM, 2012, Review of trace toxic elements (Pb, Cd, Hg, As, Sb, Bi, Se, Te) and their deportment in gold processing: Part II: Deportment in gold ore processing by cyanidation, Hydrometallurgy, v. 111–112, p. 10-21.

Lax S, Smith D, Hampton-Marcell J, Owens S, Handley K, Scott N, Gibbons S, Larsen P, Shogan B, Weiss S, Metcalf J, Ursell L, Vázquez-Baeza Y, Treuren W, Hasan N, Gibson M, Colwell R, Dantas G, Knight R and Jack G, 2014, Longitudinal analysis of microbial interaction between humans and the indoor environment, Science, v. 345, p. 1048-1052.

Luque-Almagro VM, Moreno-Vivián C and Roldán MD, 2016, Biodegradation of cyanide wastes from mining and jewellery industries, Current Opinion in Biotechnology, v. 38, p. 9–13.

Luque-Almagro VM, Cabello P, Sáez LP, Olaya-Abril A, Moreno-Vivián C and Roldán MD, 2018, Exploring anaerobic environments for cyanide and cyano-derivatives microbial degradation, Applied Microbiology and Biotechnology, v. 102, p. 1067–1074.

Manso CI, Ibáñez GMI, de la Peña MF, Sáez MLP, Luque-Almagro VM, Castillo RF, Roldán RMD, Prieto JMA and Moreno VC, 2015, *Pseudomonas pseudoalcaligenes CECT5344*, a cyanide-degrading bacterium with by-product (polyhydroxyalkanoates) formation capacity, Microbial Cell Factories, v. 14, n. 77, p. 1-12.

Marsden J and House I, 2006, The Chemistry of Gold Extraction, Society for Mining, Metallurgy, and Exploration, p. 503-651.

Martínková L, Veselá AB and Rinágelová A, 2015, Cyanide hydratases and cyanide dihydratases: emerging tools in the biodegradation and biodetection of cyanide, Applied Microbiology and Biotechnology, v. 99, n. 21, p. 8875–8882.

Mikheenko A, Saveliev V and Gurevich A, 2016, MetaQUAST: evaluation of metagenome assemblies, Bioinformatics, v. 32, n. 7, p. 1088-1090.

Mirizadeh S, Yaghmaei S and Nejad ZG, 2014, Biodegradation of cyanide by a new isolated strain under alkaline conditions and optimization by response surface methodology (RSM), Environ Health Sci Eng., v. 12, article number 85.

Moran R, 1998, Cyanide Uncertainties-Observations on the Chemistry, Toxicity, and Analysis of Cyanide in Mining-Related Waters, Mineral Policy Center, Issue 1.

Mudder TI, Botz MM and Smith A, 2001, Chemistry and Treatment of Cyanidation Wastes, Mining Journal Books Ltd.

Nallapan MM, Sjahrir F, Ibrahim A and Cass A, 2013, Biodegradation of cyanide by *Rhodococcus UKMP-5M*, Biologia, v. 68, n. 2, p. 177-185.

Nordstrom DK, 2000, Advances in the Hydrogeochemistry and Microbiology of Acid Mine Waters, International Geological Reviews, v. 42, issue 6, p. 499-515.

Nordstrom DK and Alpers CN, 1999, Geochemistry of Acid Mine Waters, Reviews in Economic Geology, v. 6A, p. 133-160.

Norman N and Whitfield G, 2006, Geological Journeys, Struik Publishers, Cape Town, pp. 38–49, 60–61.

Novak D, Franke-Whittle IH, Pirc ET, Jerman V, Insam H, Logar RM, Stres B, 2013, Biotic and abiotic processes contribute to successful anaerobic degradation of cyanide by UASB reactor biomass treating brewery waste water, Water Research, v. 47, n. 11, p. 3644–3653.

Nurk S, Meleshko D, Korobeynikov A and Pevzner PA, 2017, metaSPAdes: a new versatile metagenomic assembler, Genome Research, v. 27, n. 5, p. 824-834.

Ogata H, Goto S, Sato K, Fujibuchi W, Bono H and Kanehisa M, 1999, KEGG: Kyoto Encyclopedia of Genes and Genomes, Nucleic Acids Research, v. 27, n. 1, p. 29-34.

Ottesen A, Ramachandran P, Reed E, White J, Hasan N, Subramanian P, Ryan G, Jarvis K, Grim C, Daquiqan N, Hanes D, Allard M, Colwell R, Brown E and Chen Y, 2016, Enrichment dynamics of Listeria monocytogenes and the associated microbiome from naturally contaminated ice cream linked to a listeriosis outbreak, BMC Microbiology, v. 16, n. 1, article number 275.

Park JK, Sewell BT and Benedik MJ, 2017, Cyanide bioremediation: the potential of engineered nitrilases, Applied Microbiology and Biotechnology, v. 101, n. 8, p. 3029–3042.

Parks DH, Imelfort M, Skennerton CT, Hugenholtz P and Tyson GW, 2015, CheckM: assessing the quality of microbial genomes recovered from isolates, single cells, and metagenomes, Genome Research, v. 25, n. 7, p. 1043-1055.

Pepper I, Zerzghi H, Bengson S, Iker B, Banerjee M and Brooks J, 2012, Bacterial populations within copper mine tailings: long-term effects of amendment with class A biosolids, Journal of Applied Microbiology, v. 113, p. 569-577.

Ponnusamy D, Kozlova EV, Sha J, Erova TE, Azar SR, Fitts EC, Kirtley ML, Tiner BL, Andersson JA, Grim CJ, Isom RP, Hasan NA, Colwell RR and Chopra AK, 2016, Cross-talk among flesh-eating Aeromonas hydrophila strains in mixed infection leading to necrotizing fasciitis, Proceedings of the National Academy of Sciences of the United States of America, v. 113, n. 3, p. 722–727.

Qing HU, Hong-yan QI, Jing-hai Z and Hong-xun Z, 2007, Bacterial diversity in soils around a lead and zinc mine, Journal of Environmental Science, v. 19, p. 74-79.

Rameez MJ, Pyne P, Mandal S, Chatterjee S, Alam M, Bhattacharya S, Mondal N, Sarkar J and Ghosh W, 2020, Two pathways for thiosulfate oxidation in the alphaproteobacterial chemolithotroph *Paracoccus thiocyanatus SST*, Microbial research, v. 230, article number 126345.

Raybuck SA, 1992, Microbes and microbial enzymes for cyanide degradation, Biodegradation, v. 3, n. 1, p. 3–18.

Razanamahandry LC, Karoui H, Andrianisa HA and Yacouba H, 2017, Bioremediation of soil and water polluted by cyanide: a review, African Journal Environmental Science and Technology, v. 11, n. 6, p. 272-291.

Revey GF, 1996, Practical methods to control explosives losses and reduce ammonia and nitrate levels in mine water, Mineral Engineering, v. 48, n. 7, p. 61-64.

Sánchez-España J, 2007, The Behavior of Iron and Aluminum in Acid Mine Drainage: Speciation, Mineralogy, and Environmental Significance, Thermodynamics, Solubility and Environmental Issues, Chapter 7.

Santana MM, Dias T, Gonzalez JM and Cruz C, 2021, Transformation of organic and inorganic sulfur– adding perspectives to new players in soil and rhizosphere, Soil Biology and Biochemistry, v. 160, article number 108306.

Seefeldt LC, Yang ZY, Duval S and Dean DR, 2013, Nitrogenase reduction of carbon-containing compounds, Biochimica et Biophysica Acta (BBA) - Bioenergetics, v. 1827, n. 8-9, p.1102–1111.

Shelly Y, Kuc ME, Iasur-Kruh L, Azerrad S and Kurzbaum E, 2020, A New Acinetobacter Isolate Is an Extremely Efficient Biofilm-Formative Denitrifying Bacterium, Frontiers in Environmental Science, v. 8, article number 556226.

Sheoran V, Sheoran AS and Poonia P, 2010, Soil reclamation of abandoned mine land by revegetation: a review, International Journal of Soil, Sediment and Water, v. 3, p. 1-21.

Shin D, Park J, Park H, Lee JC, Kim MS and Lee J, 2019, Key Microbes and Metabolic Potentials Contributing to Cyanide Biodegradation in Stirred-Tank Bioreactors Treating Gold Mining Effluent, Mineral Processing and Extractive Metallurgy Review, v.41, i. 2, p. 85-95.

Sibanda T, Selvarajan R, Msagati T, Venkatachalam S and Meddows-Taylor S, 2019, Defunct gold mine tailings are natural reservoir for unique bacterial communities revealed by high-throughput sequencing analysis, Science of the Total Environment, v. 650, p. 2199-2209.

Singh U, Arora NK and Sachan P, 2018, Simultaneous biodegradation of phenol and cyanide present in coke-oven effluent using immobilized *Pseudomonas putida* and *Pseudomonas stutzeri*, Brazilian Journal of Microbiology, v. 49, n. 1, p. 38–44.

Terada A, Komatsu D, Ogawa T, Flamandita D, Sahlan M, Nishimura M and Masafumi Y, 2020, Isolation of cyanide-degrading bacteria and molecular characterization of its cyanide-degrading nitrilase, Biotechnology and Applied Biochemistry, p. 1-7.

Wei G, Fan L, Zhu W, Fu Y, Yu J and Tang M, 2009, Isolation and characterization of the heavy metal resistant bacteria CCNWRS33-2 isolated from the root nodule of Lespedeza cuneata in gold mine tailing in China, Journal of Hazardous Material, v. 162, p. 50-56.

Williamson MA and Rimstidt JD, 1994, The kinetics and electrochemical rate-determining step of aqueous pyrite oxidation, Geochimica Cosmochimica Acta, v. 58, p. 5443–5454.

Xue C, Lin H, Zhu X, Liu J, Zhang Y, Rowley G, Todd JD, Li M and Zhang X, 2021, DiTing: A Pipeline to Infer and Compare Biogeochemical Pathways From Metagenomic and Metatranscriptomic Data, Frontiers in Microbiology, v. 12, article number 698286.

Yibas B, Pulles W and Nengovhela C, 2010, Kinetic development of oxidation zones in tailings dams with specific reference to the Witwatersrand gold mine tailings dams. Water Research Commission Report 106 1554/1/10.

Zagury GJ, Oudjehani K and Deschênes L, 2004, Characterization and availability of cyanide in solid mine tailings from gold extraction plants, Science of the total environment, Science of The Total Environment, v. 320, p. 211-224.

Supplementary data

Table S9.1: Physicochemical results of the tailings samples.

Sample	Measured pH	Eh (mV)	T (ºC)	S (wt%)	Total C (wt%)	Total N (wt%)	Total cyanide ($mg.L^{-1}$)
Profile 1.1	4.89	221.1	24.0	0.84	0.17	bdl	2.1
Profile 1.2	4.87	299.2	24.2	0.67	0.17	bdl	2.4
Profile 1.3	5.00	239.0	23.9	0.79	0.16	bdl	1.3
Profile 2.1	4.57	397.2	23.8	0.58	0.18	bdl	10.0
Profile 2.2	4.56	294.3	23.9	0.95	0.16	bdl	6.3
Profile 2.3	4.71	293.9	24.1	0.98	0.16	bdl	0.6
Profile 3.1	4.67	258.0	24.2	0.84	0.17	bdl	2.9
Profile 3.2	4.70	207.0	24.0	0.82	0.17	bdl	3.3
Profile 3.3	4.36	326.1	24.3	0.98	0.17	bdl	2.8

Table S9.2: X-ray diffraction Rietveld results of the tailings samples.

wt%	Quartz	Pyrophyllite	Chlorite	Jarosite	Muscovite	Plagioclase	Microcline	Diopside	Siderite
Profile 1,1	89,4	8,2	0,8	0,4	0,5				0,7
Profile 1,2	85,2	10,4	0,8	0,5	0,6	1,1	0,7	0,7	
Profile 1,3	87,8	9,3	0,8	0,8	1,2				
Profile 2,1	85,2	10,4	0,8	0,5	0,6	1,1	0,7	0,7	
Profile 2,2	77,2	17,4	1,0	0,9	0,5	1,2	0,8	1,0	
Profile 2,3	76,3	18,3	1,1	1,0	0,5	1,2	0,8		0,7
Profile 3,1	87,9	9,1	0,3	0,4	0,3	1,2	0,8		
Profile 3,2	89,8	8,0	0,3	0,5	0,3	0,7	0,5		
Profile 3,3	85,4	11,0	0,3	0,8	0,6	1,1	0,8		

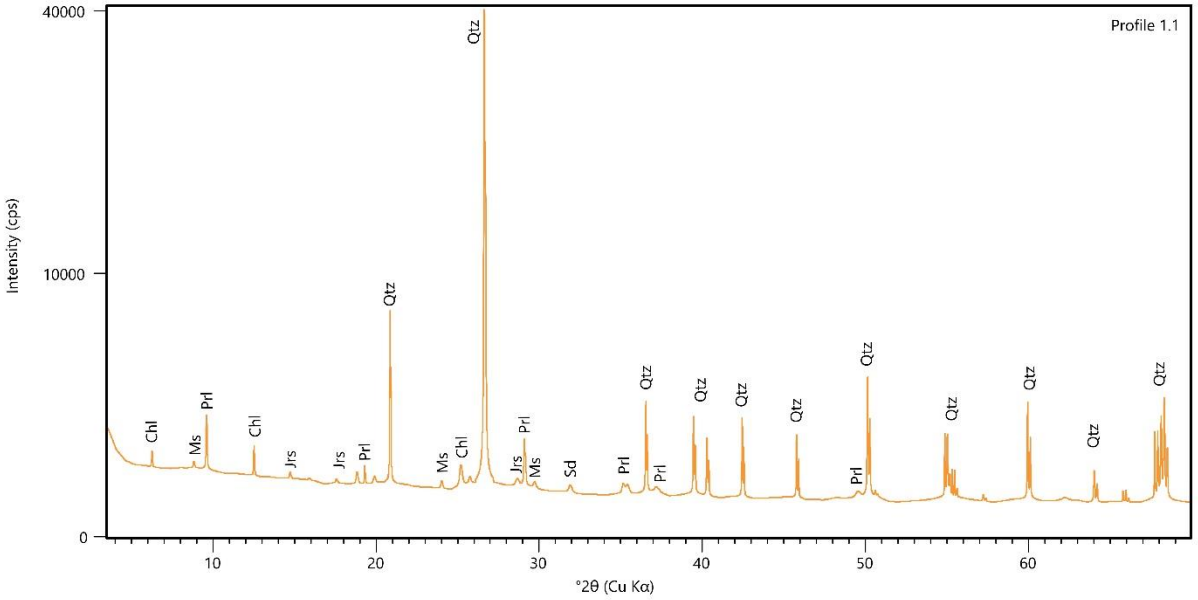

Figure S9.1: Diffractogram of the sample Profile 1.1. (Qtz – quartz, Jrs – jarosite, Sd – siderite, Chl – chlorite, Prl – pyrophyllite, Ms – muscovite)

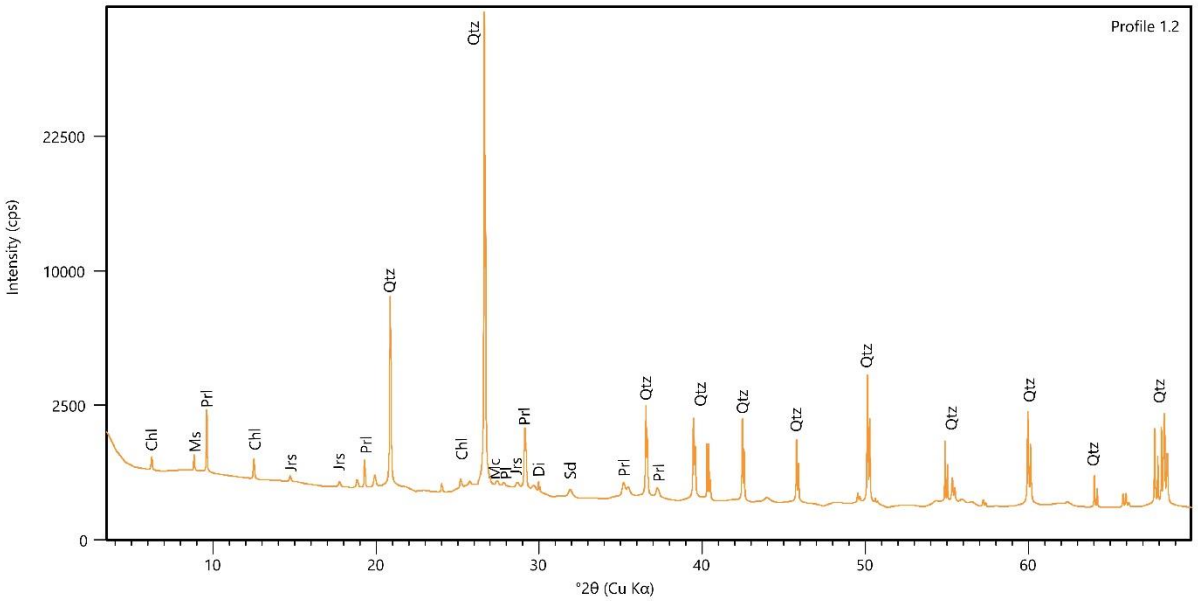

Figure S9.2: Labelled diffractogram of Profile 1.2. (Qtz – quartz, Jrs – jarosite, Sd – siderite, Chl – chlorite, Prl – pyrophyllite, Di – diopside, Ms – muscovite, Pl – plagioclase, Mc – microcline)

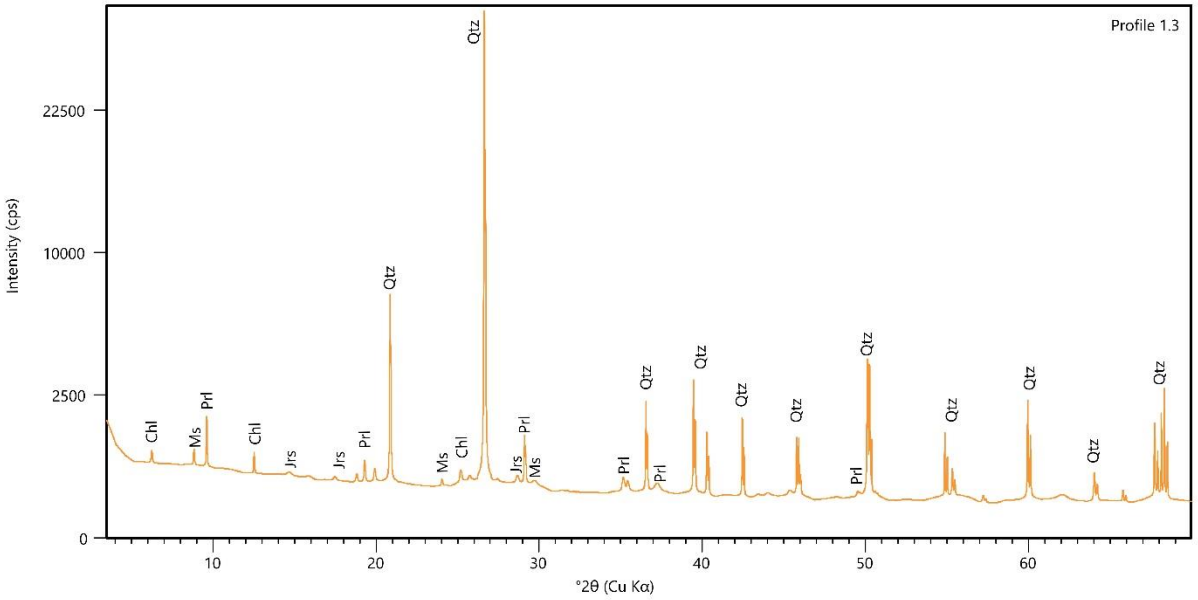

Figure S9.3: XRD diffractogram of the sample Profile 1.3. (Qtz – quartz, Jrs – jarosite, Chl – chlorite, Prl – pyrophyllite, Ms – muscovite)

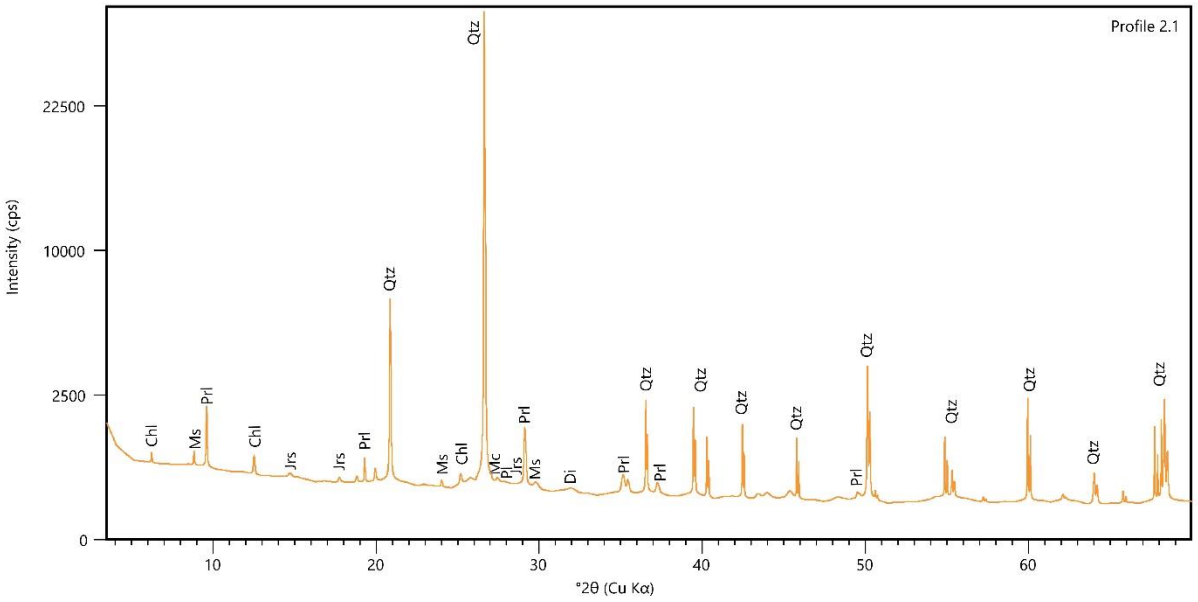

Figure S9.4: Sample Profile 2.1's diffractogram from the XRD analysis. (Qtz – quartz, Jrs – jarosite, Chl – chlorite, Prl – pyrophyllite, Di – diopside, Ms – muscovite, Pl – plagioclase, Mc – microcline)

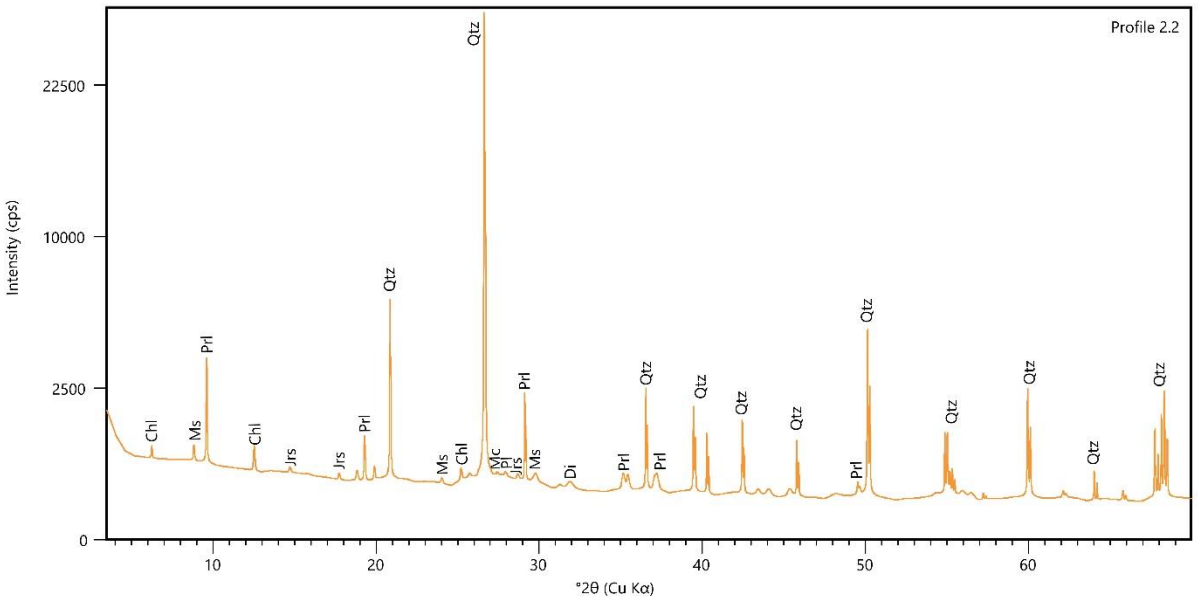

Figure S9.5: The diffractogram of the XRD results of Profile 2.3. (Qtz – quartz, Jrs – jarosite, Chl – chlorite, Prl – pyrophyllite, Di – diopside, Ms – muscovite, Pl – plagioclase, Mc – microcline)

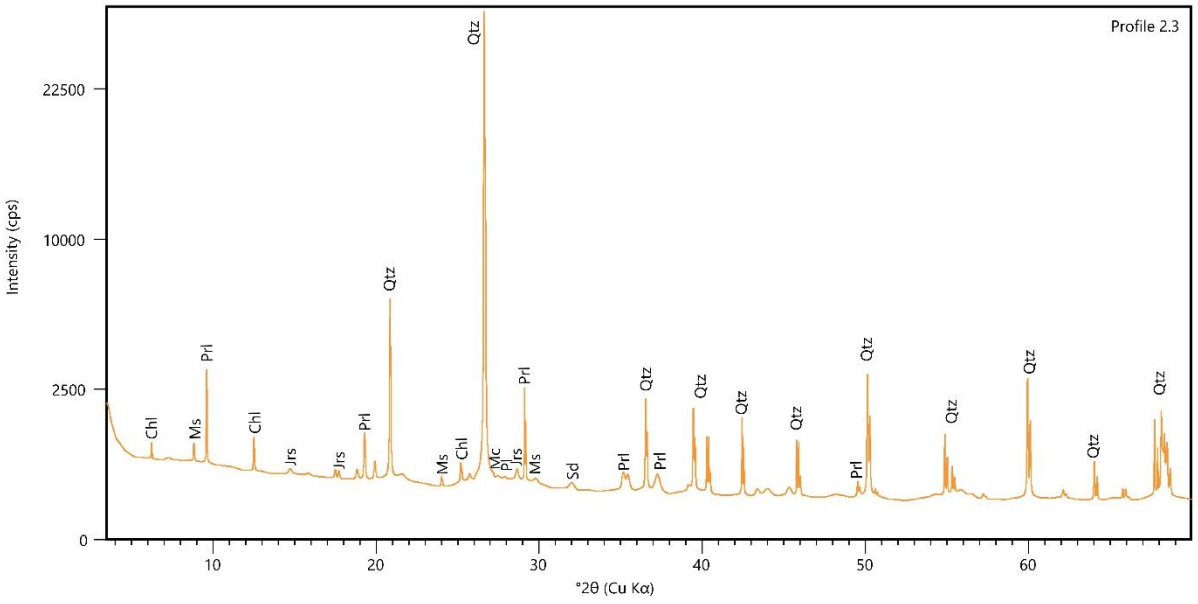

Figure S9.6: Display of the diffractogram of Profile 2.3. (Qtz – quartz, Jrs – jarosite, Sd – siderite, Chl – chlorite, Prl – pyrophyllite, Ms – muscovite, Pl – plagioclase, Mc – microcline)

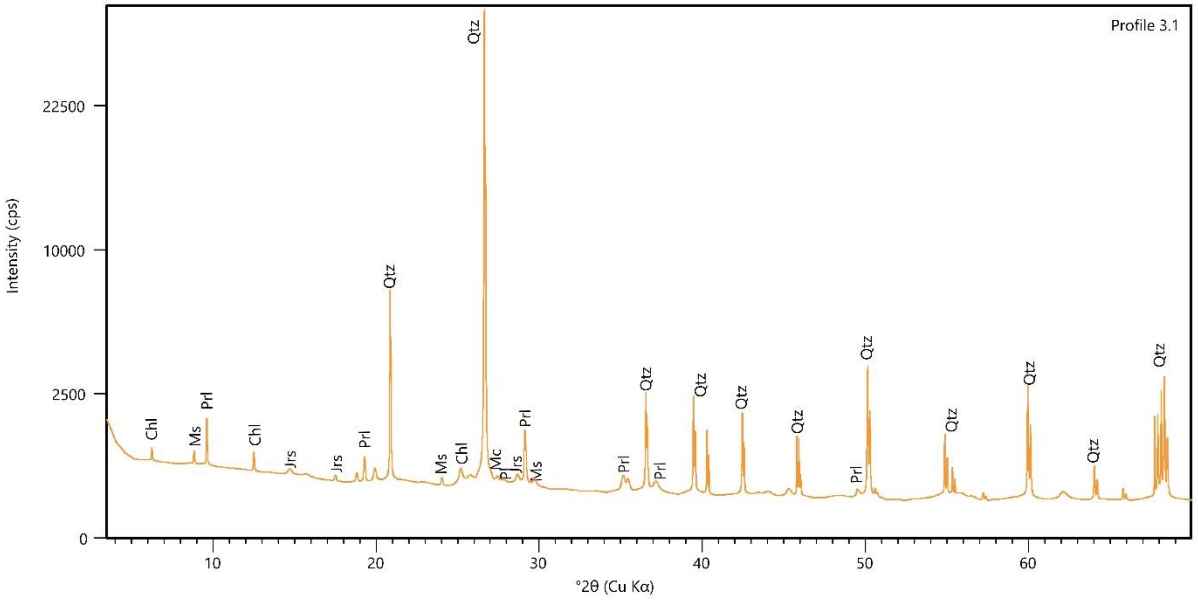

Figure S9.7: Diffractogram depicting the mineralogical results of Profile 3.1. (Qtz – quartz, Jrs – jarosite, Chl – chlorite, Prl – pyrophyllite, Ms – muscovite, Pl – plagioclase, Mc – microcline)

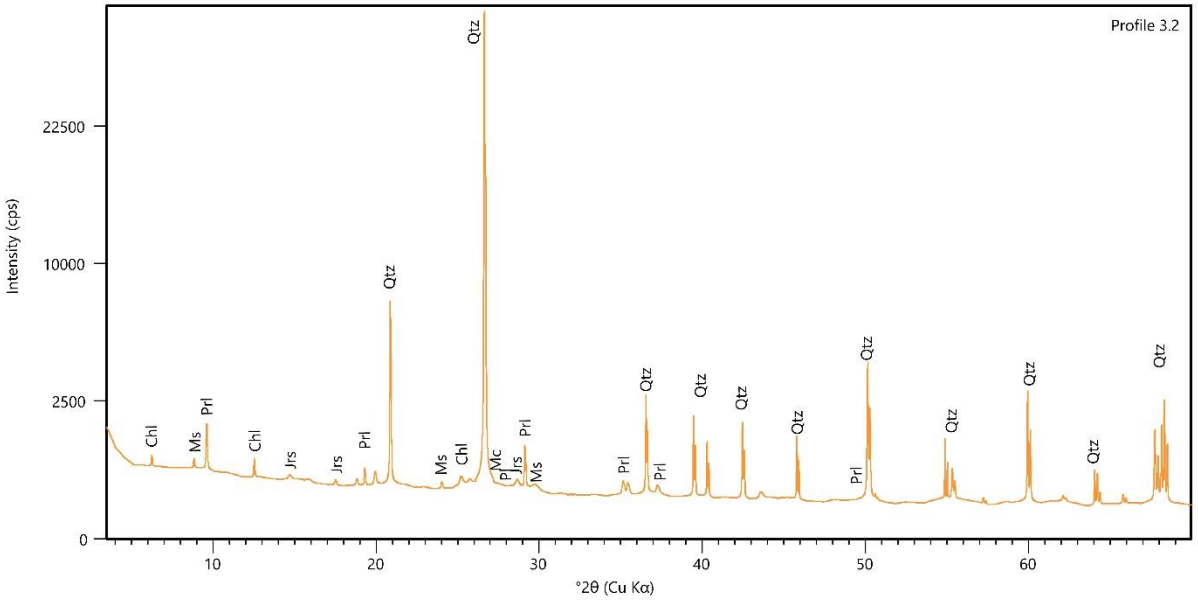

Figure S9.8: Diffractogram of the sample Profile 3.2. (Qtz – quartz, Jrs – jarosite, Chl – chlorite, Prl – pyrophyllite, Ms – muscovite, Pl – plagioclase, Mc – microcline)

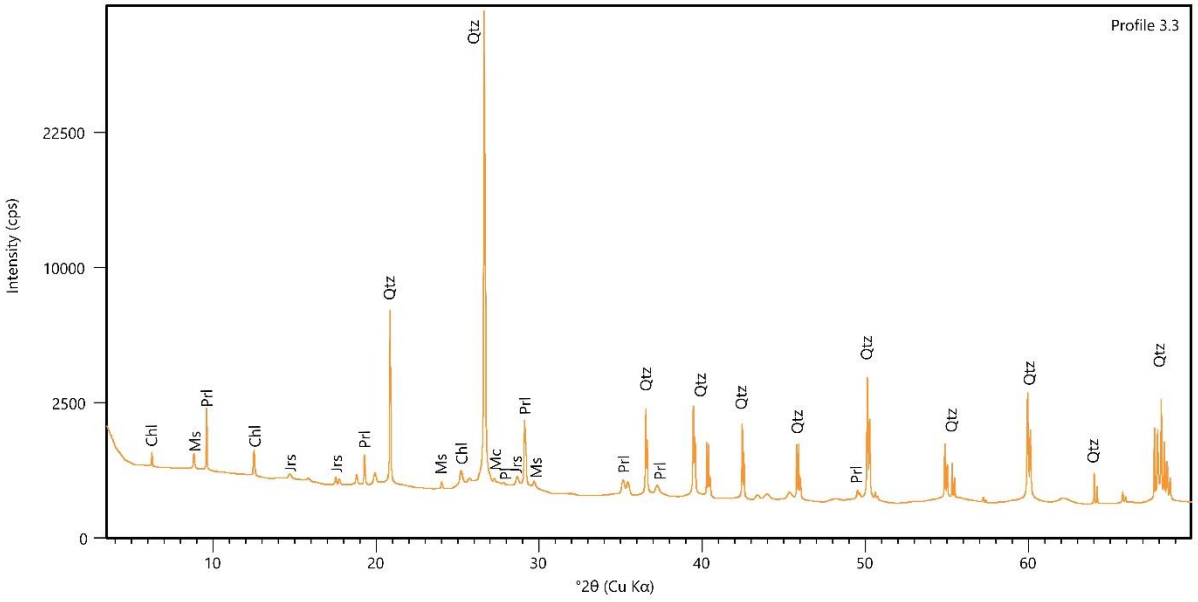

Figure S9.9: Profiles 3.3's diffractogram from the XRD results. (Qtz – quartz, Jrs – jarosite, Chl – chlorite, Prl – pyrophyllite, Ms – muscovite, Pl – plagioclase, Mc – microcline

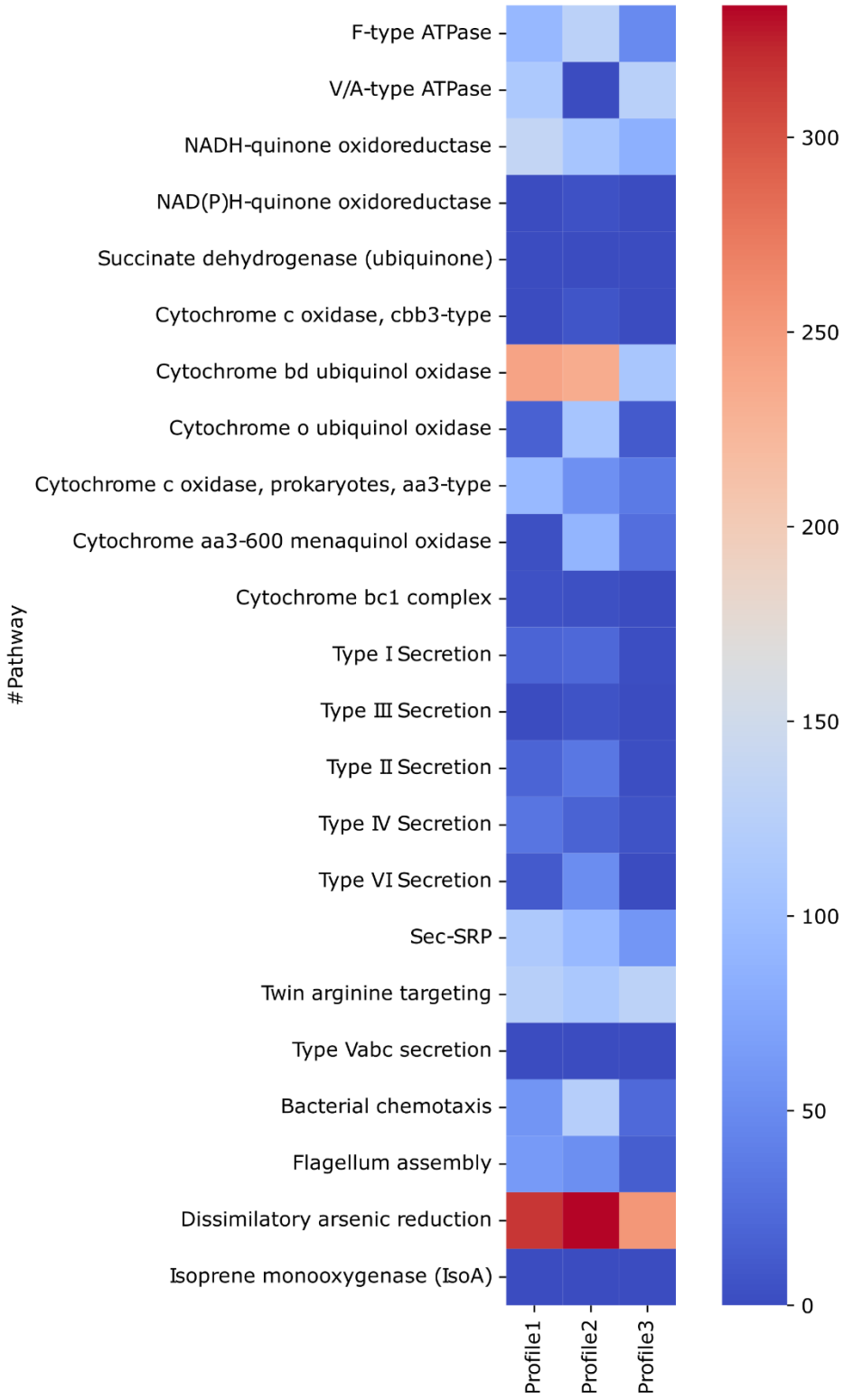

Figure S9.10: Heat map of the metabolic pathways.

Table S9.3: Bacteria and Archaea results of the bins for each of the profiles determined from the metagenomic results.

Sample	Domain	Phyla	Class	Order	Family	Genus	Species
Profile 1	Bacteria	Actinobacteria	Actinobacteria	Actinomycetales			
		Proteobacteria	Gammaproteobacteria	Xanthomonadales			
		Nitrospirae	Nitrospira	Nitrospiales	Nitrospiraceae		
		Firmicutes	Clostridia	Clostridiales	Clostridiales Family XVII. Incertae Sedis		
	Archaea	Euryarchaeota	Thermoplasmata	Thermoplasmatales	Thermoplasmataceae		
Profile 2	Bacteria	Firmicutes	Clostridia	Clostridiales	Clostridiales_Family_XVII._ Incertae_Sedis	Sulfobacillus	
		Proteobacteria	Gammaproteobacteria	Pseudomonadales	Moraxellaceae	Acinetobacter	Acinetobacter johnsonii
		Actinobacteria	Actinobacteria	Actinomycetales			
		Proteobacteria	Betaproteobacteria	Burkholderiales	Alcaligenaceae	Achromobacter	
		Firmicutes	Bacilli	Bacillales 2	Paenibacillaceae	Paenibacillus	
		Firmicutes	Bacilli	Bacillales 6	Alicyclobacillaceae	Alicyclobacillus	
		Proteobacteria	Gammaproteobacteria	Enterobacteriales	Enterobacteriaceae	Klebsiella	
Profile 3	Bacteria	Actinobacteria	Actinobacteria	Actinomycetales			
		Firmicutes	Bacilli	Bacillales 6	Alicyclobacillaceae	Alicyclobacillus	
	Archaea	Euryarchaeota	Thermoplasmata	Thermoplasmatales	Thermoplasmataceae		

Table S9.4: Display of the microbes in each sample set above the relative abundance of 0.01. They are displayed here as a percentage relative to other microbes relative in the sample. The most abundant microbes are Acidiphilium and Paenibacillus species.

Sample	Microbe	Relative abundance (%)
Profile 1	*Acidiphilium sp, PM*	30
	Acidiphilium cryptum JF-5	22
	Acidiphilium multivorum AIU301	17
	Paenibacillus ehimensis A2	17
	Bordetella genomosp, 6	3
	Bordetella bronchiseptica 99-R-0433	3
	unclassified Mesorhizobium	2
	Acinetobacter johnsonii SH046	2
	Acinetobacter lwoffii WJ10621	2
	Cutibacterium acnes	1
	Acinetobacter sp, MF4640	1
Profile 2	*Paenibacillus ehimensis A2*	65
	Klebsiella variicola	21
	Achromobacter sp, 2789STDY5608628	4
	Bordetella genomosp, 6	2
	Parabacteroides chartae	2
	Cutibacterium acnes HL025PA1	2
	Bordetella bronchiseptica 99-R-0433	2
	Acidiphilium sp, PM	2
	Macellibacteroides sp, HH-ZS	1
Profile 3	*Paenibacillus ehimensis A2*	60
	Bordetella genomosp, 6	15
	Bordetella bronchiseptica 99-R-0433	12
	Cutibacterium acnes SK187	7
	Acidiphilium sp, PM	3
	Acidiphilium multivorum AIU301	1
	Leptospirillum sp, Group II 'C75'	1
	Acidiphilium cryptum JF-5	1

Table S9.5: Metabolism results from the metagenome results.

Pathway	Profile1 (%)	Profile 2 (%)	Profile 3 (%)
Photosystem II (psbABCDEF)		0.003	
Cytochrome b6/f complex (petABCDGLMN)	0.015	0.003	0.010
Anoxygenic photosystem II (pufML)	0.149	0.024	
RuBisCo	0.970	1.464	2.528
CBB cycle (prkB)	0.884	1.512	2.104
rTCA cycle (aclAB, ccsAB, ccl)	0.117	0.026	0.044
Wood-Ljungdahl pathway (acsABCDE)		0.038	0.003
3-Hydroxypropionate Bicycle	0.075	0.090	0.118
Glycolysis (glk, pfk, pyk)	3.319	3.609	4.326
Entner-Doudoroff pathway, glucose-6P -> glyceraldehyde-3P + pyruvate	2.236	2.683	1.948
Gluconeogenesis (fbp, pck)	6.744	3.738	10.635
TCA cycle	6.719	4.287	11.253
Methanogenesis, acetate -> methane (cdhCDE)		0.011	
Fermentation to lactate, pyruvate -> lactate (LDH)		0.310	
Fermentation to formate, pyruvate -> formate (pf1D)	0.053	1.480	0.063
Fermentation to formate -> CO2 & H2 (fdh)	1.909	0.787	3.453
Fermentation to acetate, pyruvate -> acetate (poxB, poxL, acyP)	4.095	1.613	4.044
Fermentation to acetate, acetyl-CoA -> acetate (ach1, eutD, pta, acyP)	2.796	0.952	2.588
Fermentation to acetate, lactate -> acetate (EC:1,13,12,4)	0.601	0.313	0.195
Fermentation to ethanol, acetate to acetylaldehyde (ald)	4.698	2.299	1.629
Fermentation to ethanol, acetyl-CoA to acetylaldehyde (reversible)	1.061	2.617	0.893
Fermentation to ethanol, acetylaldehyde to ethanol (adh, mdh)	2.834	4.547	2.375
Fermentation to succinate (phosphoenolpyruvate to succinate via oxaloacetate, malate & fumarate)	4.656	4.354	5.899
Anaplerotic genes (pyruvate -> oxaloacetate)	12.735	14.032	16.014
Dissimilatory nitrate reduction, nitrate -> nitrite (narGHI or napAB)	1.820	2.249	1.149
Dissimilatory nitrate reduction, nitrite -> ammonia (nirBD or nrfAH)	0.267	2.843	0.557

Assimilatory nitrate reduction, nitrate -> nitrite (narB or NR or nasAB)		0.322	0.034
Assimilatory nitrate reduction, nitrite -> ammonia (NIT-6 or nirA)	0.444		
Denitrification, nitrite -> nitric oxide (nirK or nirS)	0.445	0.309	0.156
Denitrification, nitric oxide -> nitrous oxide (norBC)	0.197	0.753	0.207
Denitrification, nitrous oxide -> nitrogen (nosZ)		0.196	
Nitrogen fixation, nitrogen -> ammonia (nifKDH)		0.042	
Nitrification, nitrite -> nitrate (nxrAB)	1.942	1.976	1.124
Assimilatory sulfate reduction, sulfate -> sulfite	2.443	1.754	2.292
Assimilatory sulfate reduction, sulfite -> sulfide (cysJI or sir)	0.687	3.417	1.381
Dissimilatory sulfate reduction, sulfate -> sulfite (reversible) (sat and aprAB)	3.678	2.315	3.860
Dissimilatory sulfate reduction, sulfite -> sulfide (reversible) (dsrAB)	0.095		
Thiosulfate oxidation by SOX complex, thiosulfate -> sulfate	0.238	0.143	0.041
Alternative thiosulfate oxidation (doxAD)	0.254	0.955	0.666
Alternative thiosulfate oxidation (tsdA)	0.679	0.914	0.419
Thiosulfate oxidation (SOX, doxAD and tsdA)	1.172	2.012	1.126
Sulfur reduction, sulfur -> sulfide (sreABC)			
Thiosulfate disproportionation, thiosulfate -> sulfide & sulfite (phsABC)	0.057	0.153	0.065
Sulfhydrogenase, (sulfide)n -> (sulfide)n-1	0.697	0.081	0.771
Sulfur disproportionation, sulfur -> sulfide & sulfite		0.487	0.269
Sulfur dioxygenase	0.007	0.041	
Sulfite oxidation, sulfite -> sulfate (sorB, SUOX, soeABC)	0.681	0.750	0.233
Sulfide oxidation, sulfide -> sulfur (fccAB)	0.230	0.021	
DMSP demethylation, MMPA -> MeSH (dmdBCD or acuH)	5.910	5.172	7.013
DMSP cleavage, DMSP -> DMS (ddds or alma1)	0.232		0.038
DMSO reduction, DMSO -> DMS (dms or dorA)	0.020	1.913	0.102
MeSH oxidation, MeSH -> Formaldehyde (MTO)	0.841	0.230	0.776
F-type ATPase	2.899	3.067	1.942
V/A-type ATPase	3.129	0.009	6.484
NADH-quinone oxidoreductase	3.919	2.673	3.993
NAD(P)H-quinone oxidoreductase	0.007	0.094	0.034

Succinate dehydrogenase (ubiquinone)	0.037	0.005	
Cytochrome c oxidase, cbb3-type	0.018	0.207	0.009
Cytochrome bd ubiquinol oxidase	6.838	5.601	4.275
Cytochrome o ubiquinol oxidase	0.471	2.696	0.370
Cytochrome c oxidase, prokaryotes, aa3-type	2.638	1.303	1.922
Cytochrome aa3-600 menaquinol oxidase	0.037	2.124	1.016
Cytochrome bc1 complex	0.160	0.100	0.010
Type I Secretion	0.485	0.508	0.064
Type III Secretion	0.005	0.163	0.009
Type II Secretion	0.507	0.791	0.075
Type IV Secretion	1.002	0.411	0.235
Type VI Secretion	0.384	0.971	0.037
Sec-SRP	3.216	2.290	3.330
Twin arginine targeting	3.481	2.727	4.923
Bacterial chemotaxis	1.571	2.882	0.843
Flagellum assembly	1.811	1.274	0.507
Dissimilatory arsenic reduction	8.908	7.757	10.490

10 Conclusion

Cyanide that is still used in many countries to extract gold from deposits that have low grades. Numerous studies have found that, post gold extraction, cyanide is disposed of onto the tailings dam facilities. The cyanide is able to form different compounds and complexes, as difference metals are in abundance in such an environment. When cyanide interacts with iron, iron-cyanide compounds/complexes form such as Prussian and Turnbull's blue. In previous studies, blue samples have been found present in gold mine tailings samples, presumed to be iron-cyanide compounds. This study delved into understanding Prussian/Turnbull's blue, from a modelling aspect to creating them in a lab and then investigating the possibility for them to be bioremediated.

This study delved into the presence of different iron-cyanide compounds, their stability and their ability to form in the goldmine tailings dam environment. Initially the modelling used tailings dam mineralogical results to determine if Prussian or Turnbull's blue will form, followed by laboratory experimentation. Precipitating cyanide as an iron-cyanide solid will assist in the cyanide becoming immobile and preventing contamination of sources such as the groundwater. It was determined during the modelling that in an oxic environment, Prussian blue consumes 93 % of the 0.5 $mg.L^{-1}$ cyanide, which was added to the modelling. In an anoxic environment Turnbull's blue is the preferred cyanide compound, consuming 99 % of the 0.5 $mg.L^{-1}$ cyanide in the system. Both Prussian and Turnbull's blue are CN_{SAD}, which are stable unless exposed to low pH conditions or sunlight. Thus, buried samples have a higher probability to remain as precipitates.

The experimental section of this study delved into investigating the ability for Prussian/Turnbull's blue to form in different samples that are associated with gold mining. The samples included a pyrite sample, tailings sample, a Witwatersrand reference sample. A NaCN solution was added to the samples, where a blue layer formed in the pyrite sample and the Witwatersrand reference material. A blue sample was also found on a tailing dam, where the analyses revealed the that it is an iron-cyanide compound. FT-IR is a great method to determine the presence of an iron-cyanide compound and XPS be used to determine the Fe^{2+}:Fe^{3+} ratio, to determine the main compound present.

The pH vs. pE stability diagrams for iron and cyanide were also re-examined and compared to previous studies. According to the modelling, Prussian blue forms in an oxic environment and Turnbull's blue in both an oxic and anoxic environment. The stability fields in said models, are larger than initially thought and a combination of iron-cyanide compounds is believed to form.

Additional modelling revealed that the Prussian blue precipitation requires available Fe^{2+} and Fe^{3+} ions and an oxic environment. In an oxic environment Prussian blue forms initially but above a pH of 4 Turnbull's blue coprecipitates. In an anoxic environment, only Turnbull's blue forms. The concentration of Prussian blue decreases when $FeSO_4$, $Fe_2OH_2^{4+}$ and $FeOH^{2+}$ forms between a pH of 2 and 3. Above a pH 4, the formation of Turnbull's blue and $Fe(OH)_3$ decreases the concentration of Prussian blue forming.

The last section of this study investigated the indigenous consortiums isolated from mining wastes containing cyanide. The tailings environment is oligotrophic and as such does not have a large diversity of nutrients for microorganisms. The results revealed the first insight into bacterial cyanide degradation in situ. The hydrolytic and assimilatory cyanide pathways are the most prominent and it appears that most of the bacteria characterized in this system can perform cyanide degradation and assimilation. Cyanide is thus an excellent source of carbon and an energy source. Another observation was the presence of *Actinomycetales* and *Xanthomonadales*, which are able to degrade iron-cyanide compounds. It was also determined that there was a presence of the nitrilase enzyme in all of the samples, which is the best enzyme for cyanide degradation.

In conclusion, this study showed that Prussian/Turnbull's blue are able to form in the goldmine tailings environment that contain cyanide. Iron-cyanide compounds/complexes are relatively stable and if they are not exposed to photolysis, immobilizing cyanide and remain stable. This study then showed that the cyanide is able to be naturally biodegraded, according to the bacteria present. The implication that this study has, is an overall strategy for the immobilization and degradation of cyanide. Initially ensuring that there is enough iron in the environment for the cyanide to react with, followed by ensuring the presence of bacteria that are able to degrade or assimilate cyanide (Figure 10.1). Future geochemical risk assessments for mining

projects may need to include a microbiological aspect, which has not previously been considered.

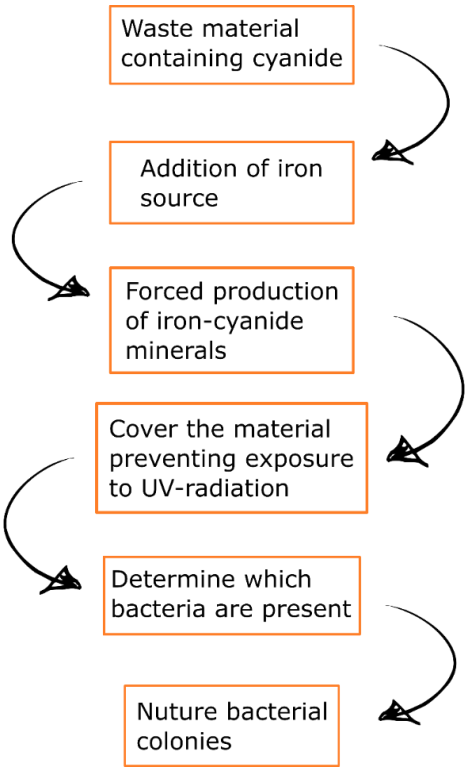

Figure 10.1: Flow diagram displaying the phases suggested in this study to bioremediate the cyanide contamination in in tailings dams.

11 Future studies

- Collect water samples from water sources surrounding the tailings dams in the Free State goldfields, determining the cyanide concentrations and speciation.
- Completing batch studies to determine if cyanide will leach from tailings after Fe_2SO_4 solution is added to them.
- Prussian/Turnbull's blue adsorption studies onto goethite.
- Adding geochemical data of other metal-cyanide compounds to the PHREEQC database and the effect that they may have on the production of Prussian and Turnbull's blue.
- Further investigate the redox conditions of tailings dams and the potential to produce HS as a by-product in order to remediate sulfur. This will include the actual soil redox condition analysis.
- Further investigation into determining the best microorganism to optimize the bioremediation of cyanide in a gold tailings environment.

12 References

Acheampong MA, Meulepas RJW and Lens PNL, 2010, Removal of heavy-metals and cyanide from gold mine wastewater, Journal of Chemical Technology and Biotechnology, v. 85, p. 590–613.

Adjei M and Ohta Y, 1999, Isolation and characterization of a cyanide-utilizing *Burkholderia cepacia* strain, World Journal of Microbiology and Biotechnology, v. 15, p. 699-704.

Akcil A, 2003, Destruction of cyanide in gold mill effluents: Biological versus chemical treatments, Biotechnology Advances, v. 21, p. 501–511.

Akcil A, Karahan A, Ciftci H, 2003, Biological treatment of cyanide by natural isolated bacteria (*Pseudomonas sp.*), Minerals Engineering, v. 16, p. 643–649.

Alvillo-Rivera A, Garrido-Hoyos S, Buitron G, Thangarasu-Sarasvathi P and Rosano-Ortega G, 2021, Biological treatment for the degradation of cyanide: A review, Journal of Materials Research and Technology, v. 12, p. 1418-1433.

Anning C, Wang J, Chen P, Batmunkh I and Lyu X, 2019, Determination and detoxification of cyanide in gold mine tailings: A review, Waster management and research, SAGE, v. 37, n. 11, p. 1117-1126.

Bakatula EN and Tutu H, 2016, Characterization and speciation modelling of cyanide in effluent from an active slime dam, South African Journal of Chemistry, v. 69, p. 140-147.

Barclay M and Day J, 2002, Substrate-regulated cyanide hydratase (chy) gene expression in *Fusarium solani*: The potential of a transcription-based assay for monitoring the biotransformation of cyanide complexes, Environmental Microbiology v. 4, n. 3, p. 183-189.

Bhalla TC, Kumar V and Kumar V, 2017, Microbial Remediation of Cyanides, In: Bioremediation Current Research and Applications, Chapter: 4, First edition, Publisher: IK International, p. 88-110.

Botz MM, 2001, Overview of cyanide treatment methods, Mining Environmental Management, Mining Journal Ltd, London, UK, p. 28–30.

Botz MM, Mudder TI and Akcil A, 2005, Cyanide treatment: Physical, chemical and biological processes, Advances in Gold Ore Processing, p. 672–702

Callender KL, Roy S, Khasa DP, Whyte LG and Greer CW, 2016, Actinorhizal alder phytostabilization alters microbial community dynamics in gold mine waste rock from northern Quebec: a greenhouse study, PLoS One, v. 11, p. 1–25.

Carillo-Pedroza FR and Soria-Aguilar MJ, 2001, Destruction of cyanide by ozone in two gas-liquid contacting systems, European Journal of Mineral Processing and Environmental Protection, v. 1, p. 55-63.

Chen CY, Kao CM and Chen SC, 2008, Application of *Klebsiella oxytoca* immobilized cells on the treatment of cyanide wastewater, Chemosphere, v. 71, p. 133–139.

Cipollone R, Ascenzi P, Frangipani E and Visca P, 2006, Cyanide detoxification by recombinant bacterial rhodanese, Chemosphere, v. 63, p. 942–949.

Cluness MJ, Turner PD, Clements E, Brown DT and O'Reilly C, 1993, Purification and properties of cyanide hydratase from *Fusarium lateritium* and analysis of the corresponding chy1 gene, Journal of General Microbiology, v. 139, p. 1807–1815.

Dash RR, Balomajumder C and Kumar A, 2009a, Removal of metal cyanides from aqueous solutions by suspended and immobilized cells of *Rhizopus oryzae* (MTCC 2541), Engineering in Life Sciences, v. 9, p. 53–59.

Dash RR, Gaur A and Balomajumder C, 2009, Cyanide in industrial wastewaters and its removal: a review on biotreatment, Journal of Hazardous Material, v. 163, p. 1-11.

Demopoulos G and Cheng T, 2004, A case study of CIP tails slurry treatment: Comparison of cyanide recovery to cyanide destruction, Mineral Processing and Environmental Protection, v. 4, p. 1–9.

De Wet JR, Hodgkinson G, Pistorius PC, Prinsloo LC and Sandenbergh, 1995, The influence of cyanide on the flotation of pyrite from Witwatersrand gold leach residues, Minerals Engineering, v. 8, n. 11, p. 1333-1345.

Dhal PK and Sar P, 2014, Microbial communities in uranium mine tailings and mine water sediment from Jaduguda U mine, India: a culture independent analysis, Journal

of Environmental Science and Health, Part A, Toxic/hazardous substances and environmental engineering, v. 49, p. 694–709.

Dold B, 2003, Speciation of the most soluble phases in a sequential extraction procedure adapted for geochemical studies of copper sulfide mine waste, Journal of Geochemical Exploration, v. 80, p. 55–68.

Donato DB, Madden-Hallett DM and Smith GB, 2017, Heap leach cyanide irrigation and risk to wildlife: Ramifications for the international cyanide management code, Ecotoxicology and Environmental Safety, v. 140, p. 271–278.

Donato DB, Nichols O, Possingham H, Moore M, Ricci RF and Noller BN, 2007, A critical review of the effects of gold cyanide-bearing tailings solutions on wildlife, Environment International, v. 33, p. 974–984.

Dong K, Xie F, Wang W, Chang Y, Lu D, Gu X and Chen C, 2021, The detoxification and utilization of cyanide tailings: A critical review, Journal of Cleaner Production, v. 302, article number 126946.

Dumestre AT, Chome J, Portal M, Gerard M and Berthelin J, 1997, Cyanide degradation under alkaline conditions by a strain of *Fusarium solani* isolated from contaminated soils, Applied Environmental Microbiology, v. 63, p. 2729–2734.

Dzombak DA, Ghosh RS and Wong-Chong GM, 2006, Cyanide in water and soil, CRC Press, Taylor and Francis Group, US, 602pp.

Eisler R, 1991, Cyanide hazards to fish, wildlife, and invertebrates: A synoptic review, Contaminant Hazard Reviews, v. 85, p. 58.

Eisler R, 2000, Handbook of Chemical Risk Assessment: Health Hazards to Humans, Plants, and Animals – three volume set, Boca Raton, US: CRC Press, p. 75–79.

Ezzi IM and Lynch JM, 2005, Biodegradation of cyanide by *Trichoderma spp.* and *Fusarium spp*, Enzyme Microbial Technology, v. 36, p. 849–954.

Frimmel HE, Groves DI, Kirk J, Ruiz J, Chelsey J and Minter WEL, 2005, The Formation and Preservation of the Witwatersrand Goldfields, the World's Largest Gold Province, Economic Geology, 100th Anniversary Volume, p. 769–797.

Fry WE and Miller RL, 1972, Cyanide degradation by an enzyme from *Stemphylium loti*, Archieves of Biochemistry and Biophysics, v. 151, p. 468–474.

Ghosh RS, Dzombak DA and Luthy RG, 1999a, Equilibrium Precipitation and Dissolution Behavior of Iron Cyanide Solids, Environmental Engineering Science, v. 16, n. 4, p. 293-313.

Ghosh RS, Dzombak DA, Luthy RG and Smith JR, 1999, In situ treatment of cyanide-contaminated groundwater by iron cyanide precipitation, Water Environment Research, v. 71, n. 6, p. 1272-1228.

Gschwendtner S, Mansfeldt T, Kublik S, Touliari E, Buegger F and Schloter M, 2016, Long-term ferrocyanide application via deicing salts promotes the establishment of *Actinomycetales* assimilating ferrocyanide-derived carbon in soil, Microbial Biotechnology, v. 9, n. 4, p. 502–513.

Gurbuz F, Ciftci H and Akcil A, 2009, Biodegradation of cyanide containing effluents by *Scenedesmus obliquus*, Hazardous Materials, v. 162, p. 74–79.

Gupta A, Dutta A, Sarkar J, Paul D, Panigrahi MK and Sar P, 2017, Metagenomic exploration of microbial community in mine tailings of Malanjkhand copper project, India, Genomics Data, v. 12, p. 11–13.

Hansen RN, 2018, Inter-comparison geochemical modelling approaches and implications for environmental risk assessments: A Witwatersrand gold tailings source term characterisation study, Applied Geochemistry, v. 95, p. 71-84.

Henny CJ, Hallock RJ and Hill EF, 1994, Cyanide and migratory birds at gold mines in Nevada, USA, Ecotoxicology, v. 3, p. 45–58.

Huang L, Baumgartl T and Mulligan D, 2012, Is rhizosphere remediation sufficient for sustainable revegetation of mine tailings? Annals of Botany, v. 110, p. 223–238.

Ibrahim K, Syed M, Shukor M and Ahmad S, 2015, Biological remediation of cyanide: a review, Buitrioua, v. 22, n. 2, p. 151-163.

Igwe JC and Abia AA, 2006, A bioseparation process for removing heavy metals from waste water using biosorbents, African Journal of Biotechnology, v. 5, n. 12, p. 1167–1179.

Jambor JL, Martin AJ and Gerits J, 2009, The post-depositional accumulation of metal-rich cyanide phases in submerged tailings deposits, Applied Geochemistry, v. 24, p. 2256-2265.

Jaszczak E, Polkowska Z, Narkowicz S and Namieśnik J, 2017, Cyanide in the environment – analysis – problems and challenges, Environmental Science and Pollution Research, Springer, v. 24, p. 15929-15948.

Kantor RS, van Zyl W, van Hille RP, Thomas BC, Harrison STL and Banfield JF, 2015, Bioreactor microbial ecosystems for thiocyanate and cyanide degradation unravelled with genome-resolved metagenomics, Environmental Microbiology, v. 17, n. 12, p. 4929–4941.

Keshri J, Mankazana BBJ and Momba MNB, 2015, Profile of bacterial communities in South African mine-water samples using Illumina next-generation sequencing platform, Applied Microbiology and Biotechnology, v. 99, p. 3233–3242.

Knowles CJ, 1976, Microorganisms and cyanide, Bacteriology, v. 40, p. 652–680.

Kumar V, Kumar V and Bhalla TC, 2013, In vitro cyanide degradation by *Serratia marcescens RL2b*, International Journal of Environmental Sciences, v. 3, p. 1985–1995.

Kunz DA, Nagappan O, Silva-Avalos J and Delong GT, 1992, Utilization of cyanide as a nitrogenous substrate by *Pseudomonas fluorescens NCIMB 11764*: evidence for multiple pathways of metabolic conversion, Applied Environmental Microbiology, v. 58, p. 2022–2029.

Kuyucak N and Akcil A, 2003, Cyanide and removal options from effluents in gold mining and metallurgical processes, Minerals Engineering, v. 50–51, p. 13-29.

Kyle JH, 1997, Stability of metal-cyanide and hydroxide complexes, World Gold ’97 Conference, p. 163-169.

Kyoseva V, Todorova E and Dombalov I, 2009, Comparative assessment of the methods for tdestruction of cyanides used in gold mining, Journal of the University of Chemical Technology and Metallurgy, v. 44, n. 4, p. 403-408.

Luque-Almagro VM, Blasco R, Martinez-Luque M, Moreno-Vivian C, Castillo F and Roldan MD, 2011, Bacterial cyanide degradation is under review: *Pseudomonas psedoalcaligenes CECT5344*, a case of an alkaliphilic cyanotroph, Biochemical Society Transactions, v. 39, n. 1, p. 269–274.

Luque-Almagro VM, Moreno-Vivián C and Roldán MD, 2016, Biodegradation of cyanide wastes from mining and jewellery industries, Current Opinion in Biotechnology, v. 38, p. 9–13.

Luque-Almagro VM, Cabello P, Sáez LP, Olaya-Abril A, Moreno-Vivián C and Roldán MD, 2018, Exploring anaerobic environments for cyanide and cyano-derivatives microbial degradation, Applied Microbiology and Biotechnology, v. 102, p. 1067–1074.

Mansfeldt T and Höhener P, 2016, Isotopic fingerprints of iron-cyanide complexes in the environment, Environmental Science and Technology, v. 50, p. 7382-7388.

Meyers PR, Gokool P, Rawlings DE and Woods DR, 1991, An efficient cyanide degrading *Bacillus pumilus* strain, Journal of General Microbiology, v. 137, p. 1397–1400.

Misra M, Priyadarshan G and Jena BK, 2003, Cyanide Detoxification Process: US Patent No. 6,551,514. Washington, DC: US Patent and Trademark Office.

Monsser L and Adhoum N, 2002, Modified activated carbon for the removal of copper, zinc, chromium and cyanide from wastewater, Separation and Purification Technology, v. 26, p.137–146.

Mudder TI and Botz MM, 2004, Cyanide and society: a critical review, European Journal of Mineral Processing and Environmental Protection, v. 4, n. 1, p. 62-74.

Muntasir M, Muhammad Z and Indah R, 2016, Elimination cyanide with hydrogen peroxide (H_2O_2) and calcium hypochlorite ($Ca(OCl)_2$) on gold mine waste from North Luwu, South Sulawesi, Environmental Protection, v. 5, p. 97–102.

Navarro-Noya YE, Jan-Roblero J, González-Chávez DC, Hernández-Gama R and Hernández-Rodríguez C, 2010, Bacterial communities associated with the rhizosphere of pioneer plants (*Bahia xylopoda* and *Viguiera linearis*) growing on heavy metals-contaminated soils, Antonie van Leeuwenhoek, v. 97, p. 335–349.

Norcross R, 1996, New developments in Caro's acid technology for cyanide destruction, Proceedings of Randol Gold Forum, p. 175-177.

Ngole-Jeme VM and Fantke P, 2017, Ecological and human health risks associated with abandoned gold mine tailings contaminated soil, PLoS One, v. 12, p. 1–24.

Nyirenda KK, 2020, Toxicity Potential of Cyanogenic Glycosides in Edible Plants, in P. Erkekoglu, T. Ogawa (eds.), Medical Toxicology, Intech Open, London.

Park D, Lee DS, Kim YM and Park JM, 2008, Bioaugmentation of cyanide degrading microorganisms in a full scale cokes wastewater treatment facility, Bioresource Technology, v. 99, p. 2092–2096.

Park J, Trevor B and Benedik M, 2017, Cyanide bioremediation: the potential of engineered nitrilases, Applied Microbiology and Biotechnology, v. 101, p. 3029-3042.

Parmar P, Soni A and Desai P, 2013, Enzymatic study of cyanide utilizing Pseudomonas species isolated from contaminated soil, Journal of Scientific and Innovative Research, v. 2, n. 6, p. 1058-1066.

Potivichayanon S and Kitleartpornpairoat R, 2010, Biodegradation of cyanide by a novel cyanide degrading bacterium, World Academy of Science, Engineering and Technology, v. 66, p. 1362-1365.

Quan ZX, Bae HS, Baek JH, Chen WF, Im WT and Lee ST, 2005, *Rhizobium daejeonense sp. nov.* isolated from a cyanide treatment bioreactor, International Journal Systematic and Evolutionary Microbiology, v. 55, p. 2543–2549.

Rastogi G, Osman S, Kukkadapu R, Engelhard M, Vaishampayan PA, Andersen GL and Sani RK, 2010, Microbial and mineralogical characterizations of soils collected from the deep biosphere of the former homestake gold mine, South Dakota, Microbial Ecology, v. 60, p. 539–550.

Razanamahandry LC, Karoui H, Andrianisa HA, Yacouba H, 2017, Bioremediation of soil and water polluted by cyanide: a review, African Journal Environmental Science and Technology, v. 11, n. 6, p. 272-291.

Rinagelova A, Kaplana O, Veseláa AB, Chmátala M, Krenkováa A, Plíhala O, Pasquarellia F, Cantarellad M and Martínková L, 2014, Cyanide hydratase from

Aspergillus niger K10: Overproduction in *Escherichia coli*, purification, characterization and use in continuous cyanide degradation, Process Biochemistry, v. 49, n. 3, p. 445-450.

Rodriguez JR and Ramirez-Lepe M, 2015, Purification and characterization of a cyanide-degrading nitrilase from *Trichoderma harzianum VSL291*, Turkish Journal of Biology, v. 39, n. 2, p. 248-257.

Rubec PJ and Soundararajan R, 1990, Chronic toxic effects of cyanide on tropical marine fish, In: Chapman et al. (eds.). Proceedings of the Seventeenth Annual Toxicity Workshop, Canadian Technical Report of Fisheries and Aquatic Sciences, v. 1774, n. 1, p. 243–251.

Sajjad W, Zheng G, Zhang G, Ma X, Xu W, Ali B and Rafiq M, 2018, Diversity of *prokaryotic* communities indigenous to acid mine drainage and related rocks from Baiyin open-pit copper mine stope, China, Geomicrobiological Journal, v. 35, p. 580–600.

Shete HG and Kapdnis BP, 2003, Cyanide hydratase production using acclimatized strain of *streptomyces phaeovride* and its characterization, International Journal of Bioassays, v. 8, p. 1098–1103.

Sibanda T, Selvarajan R, Msagati T, Venkatachalam S and Meddows-Taylor S, 2019, Defunct gold mine tailings are natural reservoir for unique bacterial communities revealed by high-throughput sequencing analysis, Science of the Total Environment, v. 650, p. 2199-2209.

Singh U, Arorab NK and Sachanc P, 2018, Simultaneous biodegradation of phenol and cyanide present in coke-oven effluent using immobilized *Pseudomonas putida* and *Pseudomonas stutzeri*, Brazilian Journal of Microbiology, v. 49, p. 38-44.

Smith A and Mudder T, 1991, The Chemistry and Treatment of cyanidation Wastes, Mining Journal Books Ltd., London.

Smith A and Struhsacker DW, 1988, Cyanide Geochemistry and Detoxification Regulations in Introduction to evaluation, design and operation of precious metal heap leaching projects, Society of mining engineers, Littleton, CO, p. 275-292.

williamTheis TL and West ML, 1986, Effects of cyanide complexation on the adsorption of trace metals at the surface of goethite, Environmental Technology Letters, v. 7, p. 309.

Tucker RF, Viljoen RP and Viljoen MJ, 2016, A Review of the Witwatersrand Basin - The World's Greatest Goldfield, IUGS, Journal of International Geosciences, Episodes v. 39, n. 2, p. 105-133.

Vermeulen NJ, Rust E and Clayton CRI, 2002, Variations in the composition on SA gold tailings dams, Tailings and Mine waste 2002, Proceedings of the 9th International Conference on Tailings and Mine Waste, p. 45-52.

Wang X and Forssberg KSE, 1990, The chemistry of cyanide-metal complexes in relation to hydrometallurgical processes of precious metals, Mineral Processing and Extractive Metallurgy Review, v. 6, p. 81-125.

Watanabe A, Yano K, Ikebukuro K and Karube I, 1998, Cyanide hydrolysis in a cyanide-degrading bacterium *Pseudomonas stutzeri AK61* by cyanidase, Microbiology, v. 144, p. 1677-1682.

White JM, Jones DD, Huang D and Gauthler JJ, 1988, Conversion of cyanide to formate and ammonia by a *Pseudomonad* from industrial wastewater, Journal of Industrial Microbiology, v. 3, p. 263–272.

Williamson MA and Rimstidt JD, 1994, The kinetics and electrochemical rate-determining step of aqueous pyrite oxidation, Geochimica Cosmochimica Acta, v. 58, p. 5443–5454.

Winch S, Mills HJ, Kostka JE, Fortin D and Lean DRS, 2009, Identification of sulfate reducing bacteria in methylmercury-contaminated mine tailings by analysis of SSU rRNA genes, FEMS Microbiology Ecology, v. 68, p. 94–107.

Wu CF, Feng AJ, Xu XM, Huang SH, Deng MC, Zheng XN, Wu XY, Peng J, Yuan JP and Wang JH, 2013, Construction of recombinant *Pichia strain GS115-Ch-Glu* expressing glucosidase and cyanide hydratase for cyanogenic glycosides detoxification, African Journal of Biotechnology, v. 11, p. 4424–4423.

Yang Y, Li Y and Sun QY, 2014, Archaeal and bacterial communities in acid mine drainage from metal-rich abandoned tailing ponds, Tongling, China, Transition Nonferrous Metals Society, v. 24, p. 3332–3342.

Yibas B, Pulles W and Nengovhela C, 2010, Kinetic development of oxidation zones in tailings dams with specific reference to the Witwatersrand gold mine tailings dams. Water Research Commission Report 106 1554/1/10.

Zagury GJ, Oudjehani K and Deschênes L, 2004, Characterization and availability of cyanide in solid mine tailings from gold extraction plants, Science of the total environment, v. 320, p. 211-224.